

High Resolution Time-of-Flight Neutron Spin-Echo Spectrometer for the SNS

Dieter Richter, Ferenc Mezei, Michael Ohl, Michael Monkenbusch, Catja Pappas, Thomas Krist, Klaus Lieutenant and Geza Zsigmond

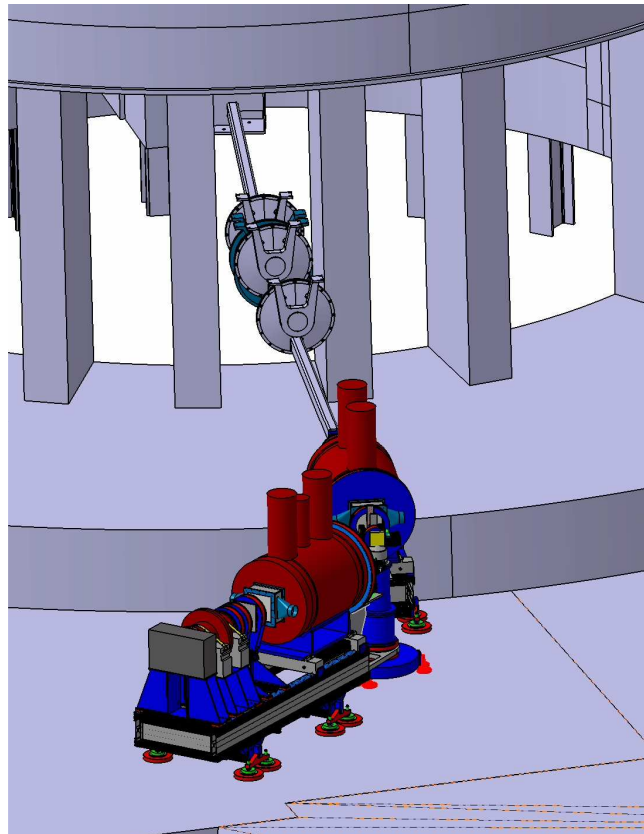


Table of Contents

1	Executive Summary	3
2	Introduction	5
2.1	General Overview	5
2.2	Principles	7
2.3	Highest Resolution Time - of - Flight NSE	9
3	Scientific Justification and Challenges.....	12
3.1	Soft and Complex Condensed Matter	12
3.1.1	Polymers Melts and Molecular Rheology	12
3.1.2	Worm like micelles	14
3.1.3	Complex Fluids	14
3.1.4	Rubbers and Molecular Networks	18
3.1.5	Gels and Polyelectrolytes	19
3.1.6	Polymeric electrolytes	20
3.2	Biophysics.....	20
3.2.1	Protein Dynamics	21
3.2.2	Membranes	21
3.3	Glasses	22
3.3.1	The structural relaxations	23
3.3.2	The secondary relaxations	24
3.3.3	Future challenges for NSE.....	24
3.4	Nanostructured materials	25
3.4.1	Introduction	25
3.4.2	Nanoparticles, suspension of nanoparticles.....	25
3.4.3	Ferro fluids, magnetofluids and electrorheological fluids.....	27
3.4.4	Complex fluids in porous media.....	28
3.5	Magnetism	29
3.5.1	Introduction	29
3.5.2	Spin Glasses	29
3.5.3	Superparamagnetic fluctuations in monodomain iron particles	31
3.5.4	Dynamical cross-over in Spin Ice $\text{Ho}_2\text{Ti}_2\text{O}_7$	32
3.5.5	Flux Line Motions in Superconductors	33
4	Instrument description	35
4.1	Introduction.....	35
4.2	Beam transport.....	37
4.2.1	Guide system and polarizers.....	37
4.2.2	Chopper system	41
4.3	Magnetic Layout.....	44
4.3.1	Solenoids and Fields.....	45
4.3.2	Superconducting Main Solenoids.....	48
4.3.3	Effect of hysteresis fields	49
4.3.4	Correction Elements	51

Executive Summary

4.3.5	Flippers	54
4.3.6	Analyzer	55
4.3.7	Add - on : Ferromagnetic and Intensity Modulated NSE	57
4.3.8	Add – on: “small - echo”	59
4.3.9	Magnetic shielding	60
4.4	Miscellaneous	61
4.4.1	Radiation Shielding	61
4.4.2	Detector	61
4.4.3	Mechanical Layout – Structural Support.....	62
4.5	Automatic Controlling	62
4.5.1	Hardware Interfacing.....	63
4.5.2	Data (pre-) treatment and User Interface.....	64
4.6	Sample Environment	64
4.7	Further Requirements	65
4.7.1	Space	65
4.7.2	Media.....	66
4.7.3	Magnetic and Radiation Shielding Interface	66
4.8	Summary.....	67
5	Estimated costs (unburdened).....	68
6	IDT Organization	69
7	References	70

1 Executive Summary

We propose to build an advanced neutron spin-echo spectrometer (NSE) at the high power target station of the SNS. This instrument will be the best of its class both with respect to resolution and dynamic range. Exploiting superconducting technology and developing novel field correction elements, the maximum achievable Fourier time – this qualifies the resolution – will be extended to $1\mu\text{s}$, a nearly one order of magnitude step compared to what is available now. Utilizing the time structure of the source an unprecedented dynamical range up to $1:10^6$ will be achieved. Optional easily accessible operation modes as ferromagnetic and intensity modulated NSE will enable the detailed investigation of magnetic samples and phenomena.

Flexibility and reliability will be the keys for the success of the proposed spectrometer. The design will allow for worldwide unique features, which will open up new experimental possibilities in soft matter research as well as in the field of magnetism. The design of the spectrometer will take full advantage of the recent progresses in neutron optics and polarizing supermirrors, and the resulting considerable gains in neutron flux will allow for routine operation in optional configurations, which have been tested but were never used on a permanent basis before. This is the case of the Intensity Modulated NSE, an extremely powerful technique, the realisation of which, however implies severe losses in neutron intensity.

The major role of the proposed instrument will be to create a unique facility to analyze the dynamics on mesoscopic scales and thereby to unravel molecular motions and mobility at the nanoscopic level. A feature which is of utmost relevance for “soft matter” problems that occur in research fields as molecular rheology of polymer melts, related phenomena in networks and rubbers, interface fluctuations in complex fluids, polyelectrolytes, transport in polymeric electrolytes and gel systems. In biophysics the molecular dynamics of proteins, phospholipid membranes and other biomolecules is about to gain in importance. In particular rapidly improving facilities of molecular dynamics calculations that meanwhile extend into the multi nanosecond time domain demand for their validation for a detailed comparison with neutron scattering results. On the other hand, the longest Fourier times of the proposed instrument will establish a direct link to the light scattering (DLS) domain, while maintaining all advantages and all the additional possibilities of the tool of contrast variation that is unique for neutrons. Moreover, the Intensity Modulated NSE option will allow for a straightforward and unambiguous separation of the coherent and incoherent contributions, leading to new experimental opportunities in the field of soft matter and biology.

Glasses and the evolution of structural and molecular relaxation dynamics on the path towards the glass transition is a very active research field, where neutron scattering can further substantially contribute because of the ability to resolve relaxation processes in space and time from mesoscopic to atomic length scales. Especially here the huge dynamic range of the proposed instrument together with a large momentum transfer (Q)- range is essential and should lead to significant new experimental findings relevant to the glass transition problem.

The long Fourier time in combination with very low Q scattering will allow to analyze motions in nanostructured materials at the main structural length. The topics range from the stability of nanoparticle suspensions to transport phenomena in porous media.

The unique combination of a huge dynamic range with a large momentum transfer (Q)-range offered by the new spectrometer is required in all studies of slow processes, in soft matter and biology as well as in solid state physics and magnetism. In fact, both kinematical (small Q) and dynamic slowing down remain important aspects in the study of spin dynamics and magnetic phase transitions. The high resolution NSE spectrometer will be ideal for investigating spin-glasses, ferromagnets as well as the phase transitions of new kinds, which steadily emerge in the forefront of magnetism, like the quantum phase transitions, which appeared most recently. Furthermore, the Intensity Modulated NSE option will make the spectrometer particularly attractive for systems, which depolarize the beam like ferromagnets and superconductors.

High resolution NSE instruments need a high flux especially at long wavelength. The Fourier time of $1\mu\text{s}$ requires the use of long wavelengths up to 2.0nm in combination with a large magnetic precession field

(1..1.5 Tm). This implies the placement of the instrument at a cold coupled moderator and the use of superconducting precession solenoids. The realization of large intensity gains at a pulsed source requires a short distance between moderator and detector, in order to utilize a large wavelength band in each pulse frame. On the other hand the magnetic layout requires a minimal length of the instrument which results in the selected 18m detector distance. Then each frame covers a $\Delta\lambda=0.366\text{nm}$ and the pulse gain in the second frame is about 7.

The short detector distance imposes geometrical restrictions on the maximum scattering angle, i.e. on the maximum achievable momentum transfer, Q . Depending on the assigned position the instrument is either restricted to an extended small angle regime or may cover a larger Q -range at the expense of some extra space from a neighboring sector.

The novel proposed NSE instrument will be unique and best-of-its class both in resolution and dynamic range. The time averaged intensity on the sample will be comparable or slightly higher than the flux at the high flux ILL instrument IN11. Compared to single detector NSE instruments it will accept a significantly larger solid angle. Therefore, the effective data rate will gain an additional factor of 5. As additional and important extra quality the wavelength distribution width at any time is well below 0.5%. Thereby the resolution in momentum transfer increases significantly compared to reactor instruments with 10% or more wavelength distribution width. Finally the huge range of used incoming wavelengths from about 0.30nm up to at least 2nm leads to an unprecedented dynamic range of six orders of magnitude. With the planned options the proposed instrument will be the most powerful and versatile NSE instrument worldwide.

2 Introduction

2.1 General Overview

This proposal for an advanced NSE spectrometer appears more than thirty years after neutron spin echo (NSE) was invented and the echo effect was experimentally first demonstrated in April 1972 at the Budapest Research Reactor on the forested hills around the city. The first realization of an NSE instrument was achieved with the spectrometer IN11 at the ILL in 1978. Today more than 10 NSE instruments serve a broad and well-established user community and more machines are being required. Current examples of research results obtained by NSE spectroscopy well illustrate the broad relevance of the method for the study of a variety of phenomena, including phase transitions, magnetism, superconductivity and the vast field of soft matter and biology with polymers, complex liquids, glasses and biological systems. Spin echo neutron spectroscopy e.g. has revealed the salient features of polymer chain dynamics covering simultaneously the proper length and time scales. In particular neutrons have provided direct evidence for the reptation mechanism proposed by Edwards and deGennes (Nobel Prize 1991).

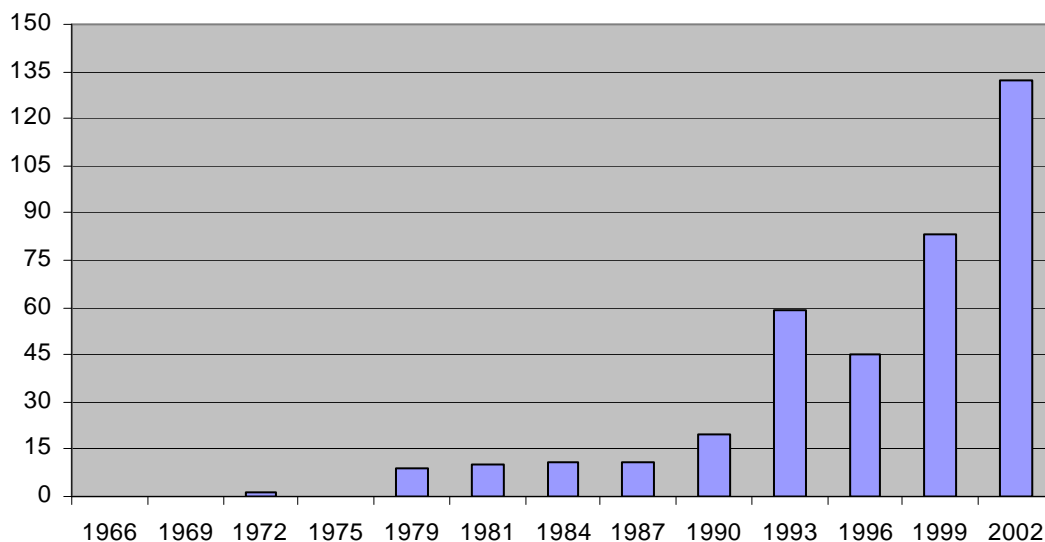


Fig. 1: The number NSE-related articles in 3-years periods from the invention of the method.

A wealth of innovations proposed in the past two decades have also been realized. The zero field (ZF) or resonance NSE (NRSE) variant was introduced some 15 years ago. At about the same time it was also realized and demonstrated that the NSE principle can also be efficiently used for neutron velocity dependent modulations of intensity. More recent years have seen a particular surge of new ideas for extending both the techniques and the field of applications to new domains such as to use the NSE principle in small angle scattering, reflectometry and to develop combinations of NSE and neutron optical phenomena such as nuclear refractive index and interference effects. On the other hand, the instrument performance in the “classical” applications in quasi-elastic scattering has also tremendously progressed. Resolutions available today reaches about 200ns (about 3 neV HWHM equivalent) compared to 10 ns 20 years ago. The technique of using large solid angles for detection has also been established with the actual capability of taking NSE data simultaneously in a high angular range if one can afford to acquire a vast collection of either supermirror analysers or polarized He³.

Since its birth in the early seventies a broad range of applications have been developed covering the study of a variety of phenomena in condensed matter research. The attractive features together with the increasing availability of NSE instruments at reactor sources leads to a rapidly increasing use and attention as can be

inferred from Fig 1. In this general frame we propose to build an ultra high resolution neutron spin - echo spectrometer (HR-NSE) at the Spallation Neutron Source (SNS).

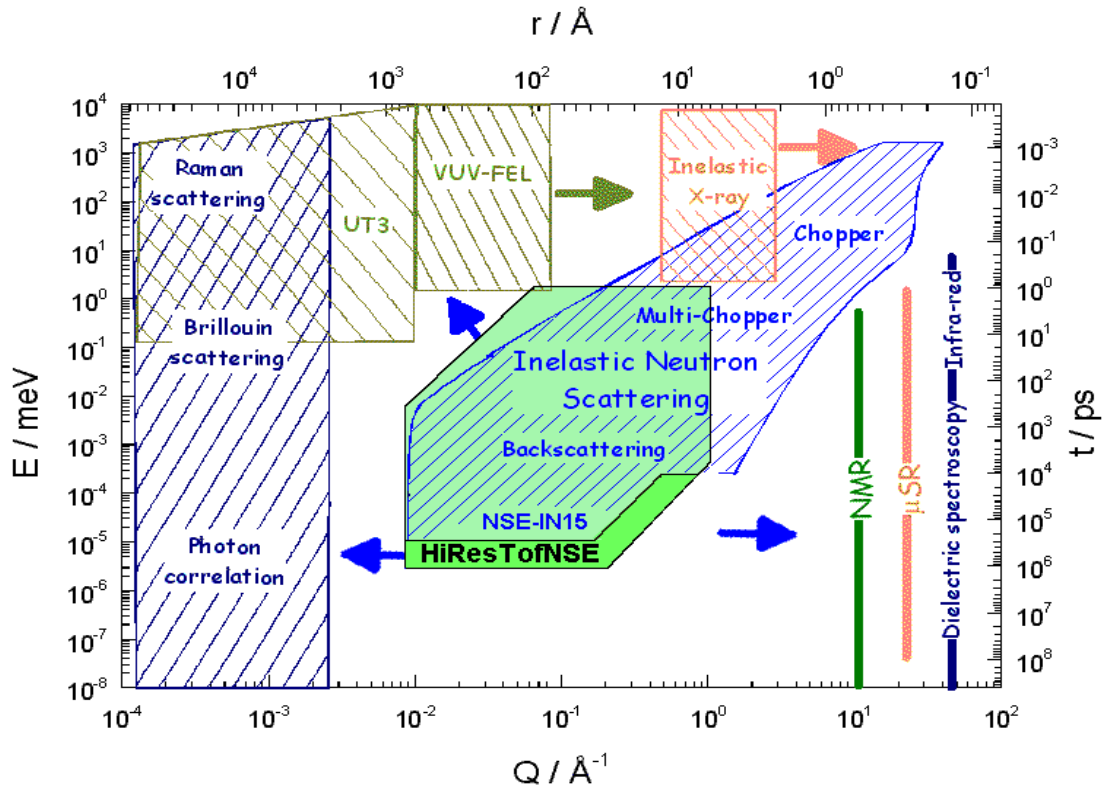


Fig. 2: The momentum transfer (Q)-time(t) region in which the Raman scattering, Brillouin scattering, Photon correlation, and further spectroscopic techniques are operating. In this landscape the new NSE will extend the neutron range by nearly one decade in maximum energy resolution (see area – HiResTofNSE - at the bottom of the neutron field). Polygon shaped green area describes the complete dynamic range in Q and t of the proposed NSE instrument

The high resolution neutron - spin - echo spectrometer will deserve to be among the first instruments around the first MW pulsed Spallation Neutron Source (SNS) in the United States. Furthermore, this spectrometer will mark a breakthrough in neutron spectroscopy, by reaching the highest resolution ever achieved with neutrons. The maximum Fourier time $\tau=1\mu\text{s}$, which is a factor of 6 better than the actual limit reached at the NSE spectrometer IN15 of the ILL. Fig.2 shows the Q - and τ - range of modern neutron scattering instruments including the proposed high resolution NSE spectrometer at SNS. This spectrometer will cover an unprecedented large dynamic range of 6 orders of magnitude and will be able to access to Fourier times $1\text{ps}<\tau<1\mu\text{s}$, i.e. from the microscopic to the mesoscopic time scale and beyond.

The high NSE resolution will be obtained by optimising the neutron optics of the instrument for usage of the highest possible wavelengths on one side and by increasing the magnetic field integral J of the precession coils up to what it seems to be the actual technological limit of $J\geq 1\text{Tm}$ on the other side.

The optimisation for using the highest wavelengths will not affect the performance of the spectrometer at low wavelengths because the source delivers a high neutron flux even at very low wavelengths. The guide system, polarizer/ analyser elements and all in beam devices like Fresnel coils and shifters will be optimised for a maximum transmission at the highest wavelengths. Modern and new developed polarizers and analyzers for the usage of a broad wavelength band 0.3nm to 2.0nm with excellent transmission and polarization will also significantly contribute to the outstanding performance of the spectrometer. To achieve the high magnetic field integral, a superconducting magnet system will be used offering excellent current carrying capability with optimised active shielding for an automatic, geometry independent operation.

Methods for the usage of flippers for broad wavelength bands, data acquisition and optimized data treatment have already been developed at IN15 in cooperation with the ILL, FZJ and HMI. High field integrals require also improved correction elements with high current carrying capabilities to correct for the inherent magnetic field inhomogeneities of the main precession coils. A complete magnetic shielding will surround the instrument and will assure an environment independent stable and reliable operation of the spectrometer. The profound theoretical understanding of the method and the capability to simulate the all in all more than 30 magnetic field sources at the instrument at different scattering angles and configurations guarantees the outstanding energy resolution of the instrument.

To summarize, this instrument will be equipped with the best and newest technologies conceivable and will be best of its class. It will provide at the same time the highest energy resolution and the broadest dynamic range ever reached in neutron scattering and will serve as a fascinating flagship and milestone in the field of modern neutron scattering techniques.

2.2 Principles

The neutron spin-echo technique is the only known neutron spectroscopic method to realize a neutron spectrometer that reaches an effective energy resolution of neV with an intensity and momentum transfer range suitable for practical use¹. The method codes minute neutron velocity changes into a polarisation difference. Thereby the use of a broad incoming wavelength band is possible, i.e. the resolution does not depend on the source pulse length. Another property of the method is that the scattering signal is proportional to the intermediate scattering function $S(Q, \tau)$ instead of $S(Q, \omega)$. This facilitates a simple resolution correction –especially for relaxation type quasielastic spectra. However, as other Fourier-methods low intensity spectral features may be masked by intensive other scattering contributions.

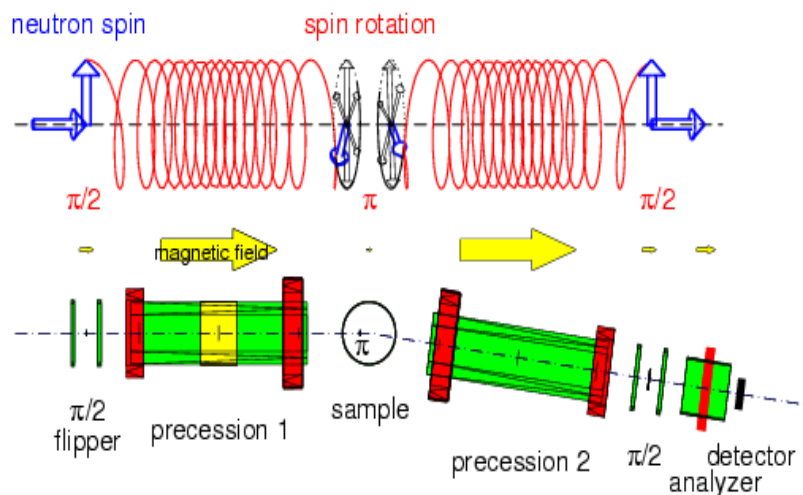


Fig. 3: Spin history leading to the formation of the spin-echo. Longitudinally polarized neutrons enter from the left. Upper part: spin motion. Lower part: NSE setup, $\pi/2$ -flipper between Helmholtz coils, primary main precession solenoid with symmetry scan windings in the middle and stray-field compensating loops -as used in the FZ-Jülich design- at both ends, π -flipper near the sample, symmetric arrangement on the secondary side followed by analyser and detector. The arrows indicate the strength of the longitudinal field.

The Fourier time- and Q-range as well as the direct accessibility of $S(Q, \tau)$ makes NSE spectrometers in particular well suited for “Soft Condensed Matter” and in the future possibly also for biological investigations. It may be considered as the dynamics window in the SANS regime. However, also scattering at large Q is important in order e.g. to understand the physics of relaxations in glasses. In spite of inherent

¹ Gravity spectrometry with ultracold neutrons could resolve neV energy, however, it is not suitable for normal scattering experiments.

technical difficulties (see below) incoherent inelastic scattering may be observed even down in the low Q-region.

The neutron spin echo technique allows for the detection of tiny ($1:10^6$) velocity changes which the neutrons acquire during the scattering process in spite of the fact that an incoming polarized beam of 10 to 20 percent velocity spread --and therefore reasonably intensely-- is used. From the broad wavelength band derives the high intensity at the instrument. All the basic physics of the instrument is explained in Ref. [3]. Only a short survey of the most important facts is given here. The essential idea is to employ the precessing neutron spin as a kind of individual clock for each neutron. The precession frequency is controlled by a magnetic field along a flight path from a so called $\pi/2$ -flipper to the sample, see Fig. [3].

Figure 3 shows a symmetric set up which is placed in the flight path from the sample to the detector. Close to the sample a π -flipper reverses the precession angle such that for an elastically scattered neutron there is no net spin turn observed at the second $\pi/2$ -flipper, irrespective of the starting velocity of the neutron. Only if the symmetry is distorted due to a velocity change at the sample the precession angles in the primary and secondary flight paths (arms) of the spectrometer differ and a polarization change after the second $\pi/2$ -flipper is observed. The polarization is detected by an analyzer in front of the detector that transmits only neutrons of one polarization direction. The signal at the detector is proportional to the cosine of the difference of the precession angles (phase= $\Delta\phi$) which is proportional to the difference in flight times in the primary and secondary precession fields due to the velocity change Δv during the scattering process. The distribution of these velocity changes corresponds to the spectral shape $S(Q,\omega)$ because for small ω there is a virtually linear dependence of ω on Δv , i.e. $\omega \sim \Delta v v_0 m_n h/2\pi$ where v_0 is the nominal velocity of the neutron and m_n its mass. The detector signal at the echo point results from the average over this distribution and therefore is proportional to the cosine Fourier transform of $S(Q,\omega)$, i.e. the intermediate scattering function $S(Q,\tau)$. Besides Δv , the acquired net precession angle, $\Delta\phi$ also depends on the precession field B and the dwell time of the neutron inside the field region. The variable to control the Fourier time t in a measurement of $S(Q,\tau)$ is the magnitude of the precession field. The dwell time is inversely proportional to v_0 ; linearizing yields:

$$\Delta\phi = \int_P |B| dl \gamma \left(\frac{m_n^2}{h^2} \right) \lambda^3 \omega = t \omega \quad (1)$$

therefore $\tau = \int_P |B| dl \gamma \left(\frac{m_n^2}{h^2} \right) \lambda^3$ is the time parameter where $J = \int_P |B| dl$ is the B-field integral over the flight path P from $\pi/2$ -flipper to the π -flipper, $\gamma = 2913.06598 \times 10^4 \text{ Hz/Tesla}$ the Larmor constant of the neutron and λ the nominal neutron wavelength. The remarkable λ^3 -dependence of the Fourier time may be used to efficiently expand the dynamical range.

NSE instruments enable the observation of slow motions (mm/sec - m/sec) in neutron scattering condensed matter samples. The NSE instruments are especially useful for the investigation of soft matter and questions connected with glass dynamics or other processes that slow down at all length scales. Usually the observed motions are relaxations. Especially the soft matter samples exhibit small angle scattering (SANS) intensity carrying the information on the system. By the NSE technique the SANS patterns may be investigated revealing to the dynamics of the scattering structures. For objects of mesoscopic size as observed in SANS immersed in liquids of usual viscosity (cPoise or more) the elastic and viscous forces are much larger than inertial forces. Therefore the motions are relaxative. Due to the property of the NSE spectrometers to yield the intermediate scattering function $S(Q,\tau)$ rather than the spectrum $S(Q,\omega)$ they are well adopted for the measurement of relaxation motions. By measuring a relaxational $S(Q,\tau)$ directly rather than $S(Q,\omega)$ the tedious deconvolution of a quasielastic line from the instrumental resolution necessary for instruments yielding $S(Q,\omega)$ is replaced by the simple division of the sample data by those obtained from an elastically scattering resolution sample. The large dynamic range of $1\text{ps} < \tau < 1\mu\text{s}$ is a further property supporting the investigation of relaxations. Unfortunately these positive properties are also accompanied by some restrictions. The Fourier transformation property means that virtually all scattered neutrons enter the analyser-detector combination and therefore only processes that contribute to more than about 5 percent to

the total scattering intensity at the chosen Q-value may be successfully analysed. Weak spectral features or inelastic lines are buried under the statistical noise. Also spin incoherent scattering is difficult to observe. First due to the low intensity compared to the coherent SANS because the scattered neutrons are spilled evenly over a solid angle of 4π . Secondly the spin flip suffered by two of three scattered neutrons converts two thirds of the scattering intensity to non polarized background. However, stable instruments with sufficient neutron flux open also the view into this regime. I.e. advanced NSE instruments offer an unique observation window for the dynamics of (soft) condensed matter in the mesoscopic length and time scale and on slow processes on mesoscopic and molecular length scales as e.g. in studies of the glass dynamics.

The options to adapt an intensity modulated ferromagnetic NSE for studies of systems in the ferromagnetic domain which in a normal NSE set – up destroy the encoding and decoding process of the neutrons spins will offer unique possibilities, too.

2.3 Highest Resolution Time - of - Flight NSE

Here we propose an advanced NSE spectrometer with the following unique properties:

- The routinely usable maximum Fourier time will be $> 1000\text{ns}$ (6x IN15) at reasonable $\Delta\Omega$.
- Due to the inherent pulsed operation a dynamic range $1:10^6$ will be easily accessible.

Compared to a normal time of flight instrument, the intensity gain of a broad band machine like NSE at a pulsed source is not as stringent. For a SANS or NSE instrument the band width $\Delta\lambda_R \cong 10\%$ which would be used at a reactor needs to be compared with the wavelength width of one time frame (see Fig. 4.). The effective intensity gain for a given frame is

$$g = \ln\left(\frac{\lambda_{\max}}{\lambda_{\min}}\right) / 0.1 \quad (2)$$

where λ_{\max} and λ_{\min} are the maximum and minimum wavelength in the frame and 0.1 is the wavelength resolution at the reactor instrument.

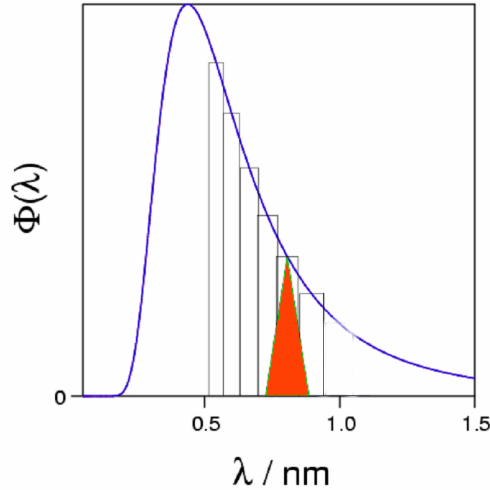


Fig. 4: Gain factor g compared to a reactor instrument: red triangle reactor wavelength band; histogram: wavelength bands in TOF operation.

Depending on the pulse frequency, distance and wavelength- gains up to 5-7 above the average intensity are obtainable. In order to be competitive to reactor based installations, NSE instruments suitable for efficient

use in actual and future state-of-the-art measurements require a MW spallation source. Therefore, up to now NSE spectrometers are not installed at one of the currently available sub - MW spallation sources.

Changing wavelength during one pulse requires a number of further measures for operation. Important functional elements, the flippers, that must impose a defined spin rotation on the neutrons that traverse them, are genuinely wavelength dependent. Therefore the adaption of NSE on a pulsed, time-coded, wideband neutron beam originating from a white pulsed source at some distance goes beyond the exploitation of the $\lambda(t-t_0)$ dependence, detection and data treatment. In addition flippers must cope with the rapid varying wavelength arriving at their position either by fast current ramping or intrinsically broad band design. A wide wavelength range also requires improvements of polarizers and analysers so that they have sufficient efficiency over the complete neutron bandwidth. Finally new data treatment procedures have to be developed. Some of these points also apply for the simpler SANS machines which thereby would also benefit.

Besides these generic pulsed source issues the current project also aims at the extension of the Fourier time range in combination with optimised beam usage and high detection solid angle. The approach -successful at the IN15- to use very long wavelengths and thereby exploit the proportionality $\tau \sim \lambda^3$ is limited by the steep decrease of flux with increasing λ in the region of interest. At spallation sources this limitation is even more severe due to additional problems of frame overlap. Therefore new techniques to cope with the field integral differences encountered for different neutron paths in a wide and divergent beam that currently limit the extension of the Fourier times by increase of the precession magnetic fields $\tau \sim B$ are a key issue to build an advanced NSE machine at a MW-spallation source that significantly surpasses the performance of the best reactor based machines. Development of field integral correctors is closely connected to design optimisation of the main precession fields which must be reconsidered and optimized. Especially the applicability of superconducting compounds needs a careful investigation.

The notion “high resolution” used in connection with NSE instruments means high achievable Fourier times τ . Eq. (1) shows that there are two parameters available to influence the Fourier time τ , the neutron wavelength and the field integral $J = \int |B| dl$. The latter is at the disposition for the design of the genuine NSE spectrometer whereas the range of λ depends on the neutron source characteristics as well as on the desired Q-range. J contains the magnitude of the precession field and the effective path length as factors. For a field generated by a resistive coil the power (effort and costs) increases quadratically with B , whereas the same factor may be achieved with a linear power increase by adding to the length² [5]. However additional length restricts the solid angle available for the illumination of the sample as well as for the detection of the scattered neutrons resulting in a severe overall intensity penalty. Achieving a high value of J by aiming at a high value of B at a given length --if not limited by the costs-- is restricted by the inhomogeneity of J , i.e. the differences of J along different neutron paths have to be small compared to the value corresponding to half a precession, i.e. to a phase variation of $\Delta\phi = \pi$. $\Delta J < 10^{-4} \text{Tm} / (\lambda/\text{\AA})$ is required. Here, this translates to $\Delta J/J_{\text{max}} \ll 2 \times 10^{-5}$. Because $\Delta\phi \sim \lambda$ while $\tau \sim \lambda^3$ the use of very large wavelengths is beneficial to achieve the highest possible resolution for a given magnetic design. Therefore an efficient, i.e. coupled cold moderator best meets the NSE requirements. Optimisation of the instrument has to observe the corresponding source parameters carefully.

The following measures will ensure the requirements mentioned above:

- Methods for broadband flippers to deal with the fast changing wavelength arriving at the instrument have been established in a joint effort of FZJ, HMI and ILL (Grenoble) [18]. By ramping the current in the flippers a pulsed broadband operation could be demonstrated.
- The associated data collections and evaluation procedures have been established
- Improved field integral correction elements have been computed and test pieces currently are under development at the FZJ. They are the key elements to extend the accessible Fourier time range.

² The design of the MESS instrument in Saclay followed this direction.

Introduction

- The use of superconducting main solenoids with high field integral and low stray field involve the second key technology. Simulation assisted layout of components and configurations delivered the start up for this layout.
- The use of a novel type of transmission polarizers/benders [118, 119, 120, 121] will facilitate the needed broad band polarization.
- An instrument incorporating the best of the thus developed and optimized components and procedures will be unique and take the lead in the field of NSE spectroscopy.

3 Scientific Justification and Challenges

The physics of condensed matter is in the process of a radical shift of emphasis. The main focus in the 20th century was the study of crystalline matter. This meant that the crucial issues were related to the structure on atomic scale and the dynamics of elementary excitations, i.e. they involved the exploration of time and length scales around 10^{-14} - 10^{-12} s and 0.1-1nm, respectively. Neutron scattering played a very important role in this endeavour, as for example emphasized by the citation of the 1994 Nobel prize to Brockhouse and Shull. The trends in recent years indicate a shift of paradigm in condensed matter research, both fundamental and applied, towards complex matter and mesoscopic time and length scales. For example the new programs of the US Department of Energy in the science of materials concentrate on “Complex and Collective Phenomena” and “Nanoscale Science” and after in the US Phys. Rev. E was started also in Europe in 2000 a dedicated European journal for soft matter³ has been founded. This implies the exploration of structures on the 1-100nm length scale in systems which do not support well defined elementary excitations and whose behaviour is strongly determined by dissipative, relaxation dynamical processes. Dynamics is expected to play a central role in understanding the nature and functionality of complex matter and the most relevant time scale associated with dissipative and nanoscale phenomena ranges from 10^{-12} s to macroscopic times. Neutron scattering has the unique capability to directly explore much of these nanoscopic time and length scale and the Neutron Spin Echo technique allows us to cover the largest ground in this space and time domain simultaneously, viz. from the atomic scales up to 100nm and up to 1000ns with the proposed instrument, respectively. This amounts to 3 orders of magnitude beyond other spectroscopic methods both in energy and momentum resolution. NSE SANS and reflectometry instruments form the backbone for the research with neutrons for a number of fields of growing interest.

3.1 Soft and Complex Condensed Matter

The NSE method is unique in supplying a means to measure dynamical processes in the SANS regime. For larger momentum transfers -as necessary for the study of glasses- it is complemented by backscattering spectrometers. Unlike classical spectroscopic methods as dielectric or mechanical response, which yield the temporal development of macroscopic averages, the neutron spectroscopic methods -especially in combination with selective labelling-have the potential to identify the spatio-temporal nature of specific relaxations on a molecular level.

Furthermore, neutron scattering, in combination with computer simulations, will have a very large impact on many future scientific endeavors to understand old and new soft matter systems. The high level of complementarity between the two techniques rests on a simple reason. From a model of atomic positions, possibly as a function of time, it is straightforward to calculate the expected neutron scattering spectrum and to compare it to experimental results, on an absolute scale. There are no unknown, or difficult to calculate, coupling functions. Neutron scattering therefore provides the best method for testing and benchmarking computational methods, e.g. Monte Carlo (MC) and molecular dynamics (MD) simulations.

Neutron scattering and in particular NSE, in combination with computer simulations, thus, will have a very large impact on the understanding of a huge class of soft matter problems and eventually also on molecular motion related to biological function. The need to simulate large systems over long times (many nanoseconds) was a reason that simulations ready to compare with NSE data started to emerge only recently. The rapid development in computing technology, however, leads to an increasing number of simulations on soft-matter and biological systems that today extend even to many tens of nanoseconds, see e.g. Ref. [160]. The ongoing development supports the expectation that in a few years the abilities of MD calculations and NSE match and in combination will be a powerful tool to infer atomic and molecular motions.

3.1.1 Polymers Melts and Molecular Rheology

Polymer melts exhibit a rich and complex rheological behaviour that sensitively depends on the molecular architecture, e.g. the nature and amount of branching [41,42]. The ultimate goal to relate the constitutive

³ European Journal of Physics E. Soft Matter.

equation to molecular properties is a major challenge for basic science as well as a matter of great practical importance for the processing of polymeric materials. De Gennes, Doi and Edwards made the first steps towards this goal with the proposition of the famous tube or reptation model [43]. The salient viscoelastic features of long linear polymers thereby could be principally understood. However, puzzles like the exact exponents for the dependence of e.g. viscosity on molecular weight as well as the relation of the new characteristic length (tube “diameter”) on molecular properties remained. A microscopic corroboration of the model assumptions on the tube diameter scale could only recently be fully established using the time range of 200ns of the IN15 instrument at the ILL [44] and the ability to perform background reduced stable long time observation of the single segment dynamics in terms of (spin)-incoherent scattering from protons at the Jülich NSE [45].

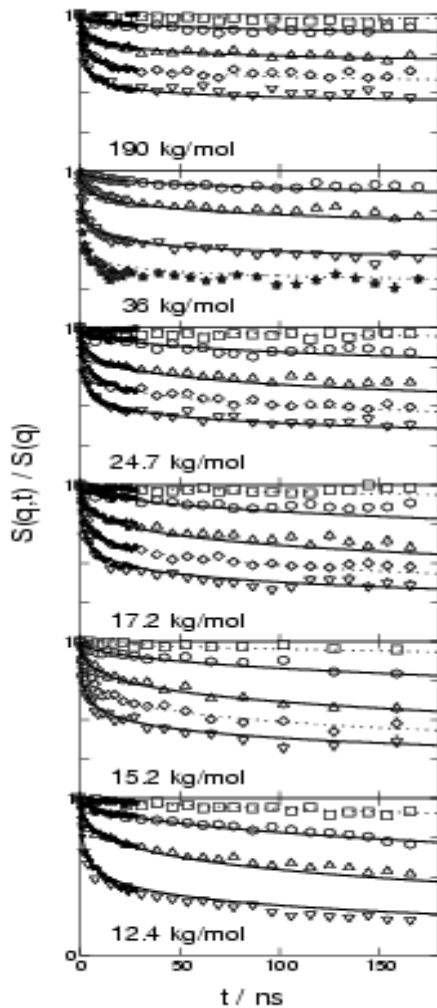


Fig. 5: NSE spectra from polyethylene (PE) melts with 10% hydrogen labelled material for different molecular weights. The Q -range spanned is 0.2 - 1.2nm^{-1} . From Ref. [48].

Thereby it was possible to directly establish the existence of the tube constraint and resulting features of the “reptation model” of deGennes [46] that predicts the behaviour of long polymer chains in a melt. On a macroscopic scale this model was the key to understand the dependence of the melt viscosity on the chain length and the shape of the viscoelastic response $G(\omega)$, especially the occurrence of the so-called “plateau modulus”, i.e. a rubber like behaviour of the melt at intermediate excitation frequency (times). NSE investigation could corroborate the existence of the postulated lateral restriction of the polymer chain on a tube around its contour axis and measure the diameter of this tube [44, 47]. The detailed comparison of the shapes of the measured intermediate scattering functions $S(Q,\tau)/S(Q)$ with the predictions of deGennes and with competing other models allowed for a clear decision in favour of the reptation picture. The latter was only possible after the IN15 NSE spectrometer at the ILL became operational and extended -due to the

availability of very long wavelength neutrons with sufficient intensity- the time range up to 200ns⁴. Series of experiments with varying polymer length (see Fig. 5 requiring extended and continuous access to appropriate instruments revealed the role of higher order effects, i.e. Contour Length Fluctuations (CLF), for the chain motions [48] which also explains some of the discrepancies between the viscoelastic behaviour and the predictions of the reptation theory [41].

Experiments with partially labelled chains yield closer insights into the role of tube restrictions at different positions of the chain. This opens the unique possibility to discriminate the motions of inner chain parts from motions of the ends or focus on the behaviour of branching points etc., compare e.g. Ref [50]. Also the effects in blends of chains with different lengths are to be investigated to model polydispersity and/or to focus on effects like (tube) constraint release CR [41,42]. Here contrast may be put to the long or the short chains. Further progress will result from detailed observation of the motions of constituents of polymer molecules with various architectures as e.g. n-arm stars, H-polymers, combs, dendrimers etc.. As first step into this fields centre-labelled 3-arm stars are currently under investigation by NSE in the Jülich group. For these type of investigations it will be vital to extend the time range in the SANS regime since the full expression of the tube constraint as seen in Fig. 5 is currently only obtained for a very limited number of polymers, mainly polyethylene PE, at the highest possible temperatures. For most other polymers the tube diameter d is larger and the molecular friction coefficient is larger, which leads to the request for an extension of the time range by the factor $f=(d/d_{PE})^4 \times \zeta(T)/\zeta_{PE}(T_{PE})$.

Multi-component systems like block-copolymers with differently labelled blocks or partially labelled blocks are used to study the interaction of different polymers at close contact [49] and the dynamical properties of the inner interfaces [50]. Future experiments on oriented samples (e.g. by shear) and systems with more sophisticated block-sequences promise new insights. On shorter, intermediate length-scales the universal Rouse dynamic of single chains is modified by effects of local chemical structure [96].

On even shorter length scales the glass dynamics (phenomenologically classified as α, β, \dots -relaxations) also determines the dynamics observed in many polymers (and other glassy materials including window glass) which also influence mechanical properties as e.g. the impact strength.

3.1.2 Worm like micelles

Worm-like micelles [143] are another example of linear chains that become entangled beyond a sufficient length. However, in these self-aggregating micellar systems the length is not static but results from an equilibrium of breaking and reforming. Their viscoelastic behavior may be described by a plateau modulus G_0 and a characteristic time τ_R the challenge is to understand the values of G_0 and τ_R from molecular properties. Due to their intrinsic stiffness these micelles may also be considered as model systems to study the physics of (electro statically stiffened) polyelectrolytes. Due to the much larger scattering intensity of micelles experiments would be much easier. In addition by mixing different types of surfactants, e.g. cationic and anionic [144], the properties of the micelles may be tuned. The dynamics of these systems is interesting because external influences as counterion concentration and composition changes considerably modify the flexibility, structure and interaction and consequently also the rheological behavior. Also an increasing number of applications rely on the controlled viscosity introduced by these types of micelles in (complex) fluids.

Finally we like to mention that the NSE method and in particular the proposed instrument may be employed to extend the tracer microrheology [145] (using light to follow tracer particles in a viscoelastic medium) into a range which might be called tracer nanorheology by following the time depended mean squared displacement of small particles with huge contrast.

3.1.3 Complex Fluids

Complex fluids containing mesoscopic structures, i.e. polymers in solution, molecular aggregates like micelles or microemulsion structures, interact with the structures of comparable size in porous media or with added objects (polymer molecules, nanoparticles ...) in a non trivial way. On mesoscopic scale there are

⁴ For very strong scatterers 400ns may be reached by use of 2nm neutrons. In analogy the proposed NSE instrument would reach a $t_{max}=2\mu s$ if the scattering intensity allows the use of very long wavelength neutrons ($\lambda > 2nm$).

hydrodynamic, electrostatic and osmotic pressure related interactions besides the purely geometrical restrictions. These determine the physical chemistry of polymer solutions, surfactant systems or aggregates covered with polymeric brushes in solution. The interactions are important for the stabilization of such colloidal systems that are found in a huge variety of applications ranging from cosmetics and pharmaceuticals, foodstuffs, paints, agrochemicals, firefighting, oil recovery to fuel additives [69].

Polymer solutions

Linear non-charged polymers in solution exhibit centre-of-mass diffusion and universal Zimm behaviour⁵ at low and intermediate Q and low concentrations. In the semidilute and concentrated regime collective concentration relaxations driven by the osmotic pressure of the segments is observed. Two new length scales emerge, the “blob”-size, i.e. the correlation length of concentration fluctuations and the “entanglement-length” that can dynamically be discriminated using NSE [68].

More complex geometries in the form of chemically bound aggregates in solution are e.g. stars and dendrimers which receive growing interest. The influence of their connectivity and overall shape yields specific dynamic properties which can be probed by NSE [71,70]. By different labelling collective density fluctuations can be discriminated from caging effects, as has been demonstrated for a star-polymer solution[72], see Fig.6.

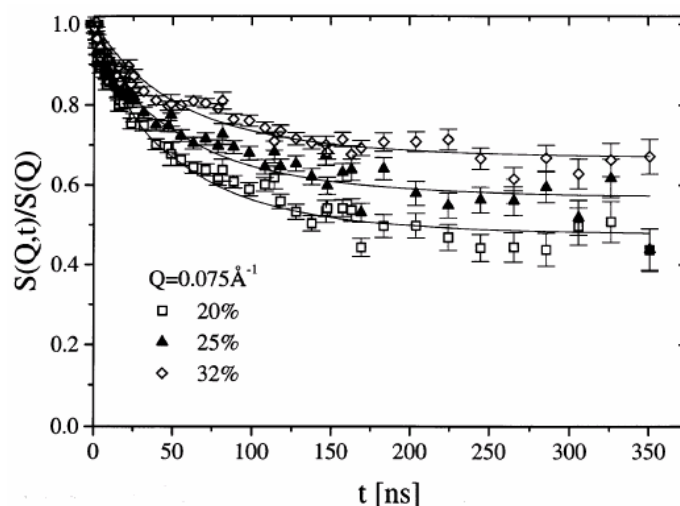


Fig. 6: IN15 spectra from a star-polymer solution showing a plateau indicating a caging effect, from Ref [72]. Due to the high scattering intensity it was possible to extend the time range of IN15 to the record value of 350 ns.

Block copolymers form aggregates in selective solvents. The huge possible variation of architectures will lead to new yet unknown effects. The (more) soluble polymer blocks form brushes or coronae on the periphery of the aggregates. First attempts to characterize the physical properties of these brushes include also NSE experiments on their collective dynamics [75,76] which yield information on their (local) viscoelastic properties.

Finally also the role of fluctuations and flexibility in molecular recognition, protein folding and association are topics for which we expect valuable contribution from advanced use of NSE in the future.

⁵ The balance of entropic springs in a Gaussian chain with hydrodynamic interaction of chain segments leads to a universal behaviour: $S(Q,\tau)/S(Q)=F(Q^3/\eta \tau)$ where η is the solvent viscosity, see e.g. M. Doi, S.F. Edwards, “The Theory of Polymer Dynamics”, Clarendon Press Oxford (1986).

Jamming and reentrant glasses

A wide variety of systems including granular media, colloidal suspensions and molecular systems, exhibit non-equilibrium transitions from a fluid like to a solid-like state, characterized solely by the sudden arrest of their dynamics which may be probed by NSE spectroscopy. Crowding or jamming of the constituent particles traps them kinetically, precluding further exploration of the phase space [131]. The disordered fluid like structure remains in principle unchanged near the transition. The jammed solid can be refluidized by thermalization, through temperature or vibration, or by an applied stress. The generality of the jamming transition led to the proposal of a unifying description [133], based on a jamming phase diagram. It was further postulated that attractive interactions might have the same effect in jamming the system as a confining pressure, and thus could be incorporated into the generalized description. Recent experiments support the concept of a jamming phase diagram for attractive colloidal particles [132] providing a unifying link between the glass transition [134], gelation [135] and aggregation [136]. The jamming concept is further supported by application of mode coupling theory (MCT) to attractive colloidal systems [138, 139], which identifies colloidal gels as special types of glasses, namely *attractive* glasses.

Dynamic light scattering or photon correlation spectroscopy (PCS) is most frequently applied for investigating the slowing down of colloid dynamics when approaching the jammed state [140]. Its Q - and time range, *i.e.* $Q \approx 10^{-3} \text{ \AA}^{-1}$ and $10^{-8} \leq \tau \leq 10 \text{ s}$, cover the length and time scales of classical colloidal systems with $R \approx 1000 \text{ \AA}$. Unfortunately, there are often severe experimental limitations due to multiple scattering effects. In addition, due to the recent developments in nanotechnology smaller and smaller colloidal systems have been synthesised and now there exists an urgent need for experimental techniques which covers smaller length *and* time scales. More recently, X-ray photon correlation spectroscopy (X-PCS) has extended the accessible Q -range up to $Q \approx 10^{-1} \text{ \AA}^{-1}$, but with this technique only relatively slow processes can be resolved, $10^{-6} \leq \tau \leq 100 \text{ s}$ [141]. Therefore, extending the time range of NSE $1 \text{ ps} < \tau < 1 \text{ \mu s}$ would perfectly close the gap to existing correlation techniques and would certainly attract a new user community from colloid science.

Microemulsions, soaps and membranes

Functional complex fluids often are based on the aggregation behaviour of amphiphilic molecules, which may have a wide variety of sizes and of chemical constituents. The largest class of these systems is based on a water-amphiphilic (=surfactant)-oil mixture which may also contain cosurfactants or other additives. These systems exhibit extremely rich phase diagrams with zones of droplet, wormlike, bicontinuous and lamellar aggregation. An example for a bicontinuous structure is displayed in Fig. 7. Their sensitivity on temperature or external forces -like shear- is high [52]. Applications of surfactant formulations are abundant and still rapidly growing, from the bulk use as washing agent in many contexts they are also used in fields ranging from emulsion polymerisation, oil recovery, waste water treatment to firefighting and pharmaceutical use.

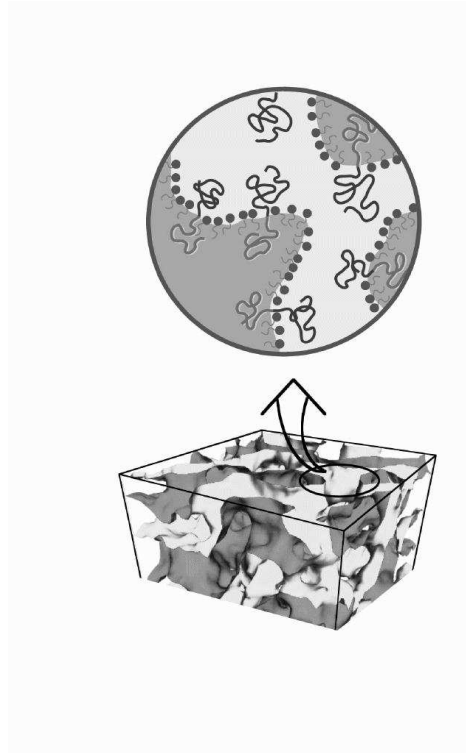


Fig. 7: Bicontinuous microemulsion phase decorated by amphiphilic diblock copolymers, see Refs. [54,55].

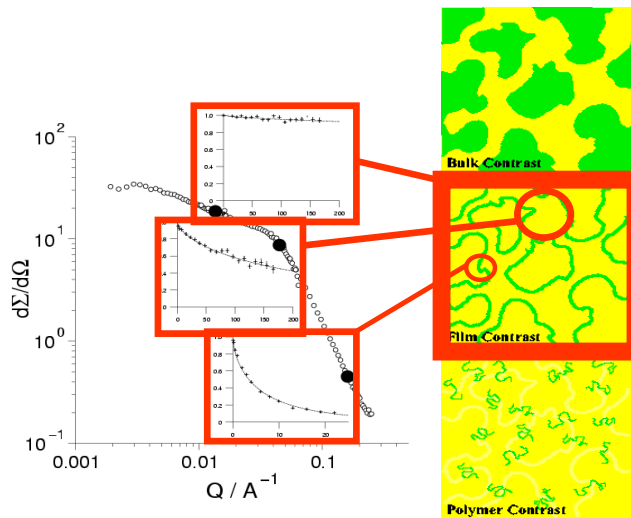


Fig. 8: SANS intensity and (inserts) NSE spectra of a bicontinuous microemulsion. Note the strong slowing down of the relaxation towards low Q .

Typical structural dimension of microemulsions are in the 10nm range. Only SANS and NSE are able to resolve structural and dynamical details in the transition region between average macroscopic (continuum) material properties and the basic molecular aggregates down to single molecules, which is the key region to understand the relation between the structural chemistry of the building blocks and the macroscopic functionality of the complex fluid (micro emulsion). The role of the viscoelastic properties of surfactant membranes separating the incompatible oil and water phases as well as the structural influences on the

hydrodynamic forces have to be studied and are within the scope of NSE. Again various contrasts by combining D/H-oil+D/H-surfactant+D/H-water (+D/H-cotenside) are vital to identify contributions from different relaxation modes or different structural units. Applications range from just washing to the exploitation of tertiary oil fields, from cosmetics to food additives, from nano-polymerization to nano-crystallization in micro droplets. Basically any water based (and therefore environmentally favourable) functional fluid will most probably rely on properties mediated by amphiphilic molecule systems, NSE results yield information on the elastic membrane properties in relation to the (viscous) friction forces. Early NSE experiments were performed on droplet phases to extract the surfactant membrane bending moduli [61,63,64] establishing a method of continued interest [62,60].

A recent example is the discovery that the addition of a small fraction of a block-copolymer, i.e. a macromolecular analog of a surfactant, to the water-oil-surfactant system enhances the ability to solubilize oil in water considerably -as expressed in the largely reduced total amount of amphiphilics needed for a homogeneous bicontinuous phase from a 50:50 water oil mixture. The structure and dynamics of the interfaces involved and the influence and structure of the macro surfactant are investigated by SANS and NSE [54,55] (see Fig. 8 Lamellar phases may often be macroscopically oriented and exhibit a rich fluctuation dynamics. NSE opens the view to local membrane dynamics and even internal dynamics of double layers [65]. Membrane dynamics [58,59] and the effects of polymers that differently anchor in the membranes may thus be investigated [56,57]. Also mixtures of homopolymers can lead to lyotropic single phases where the polymer can be localized completely in the membrane or in the solvent or in both [91]. Open questions concerning the stabilization of those phases –especially if membrane fluctuations are involved- may be addressed by NSE.

New surfactants and applications are emerging, like silicone-based surfactants [67]. Microemulsions with supercritical fluids, e.g. CO₂ under pressure, as constituents will offer new experimental control parameters, i.e. the fluid density and viscosity, as well as new applications. The restriction of configuration space due to connectivity or external obstruction, i.e. in porous media or close to interfaces, changes the entropy and may shift the subtle balance between entropy and enthalpy controlling much of the rich behaviour of complex soft matter systems. Such effects together with eventual absorption and the topology of the porous network control the percolation and flow properties in these media. To understand these properties is important for many fields of chemical processing or environmental issues. Extraction of oil from porous rock, catalytic activities of zeolites and the diffusion of pollutants in soils are only a few examples [66]. Neutron scattering allows for the observation of the structural (SANS) and dynamical (NSE) changes in the fluid within a pore size. Local energy terms and viscosities may be extracted and used to develop or improve thermodynamical theories that enable the prediction of confinement effects.

3.1.4 Rubbers and Molecular Networks

Rubbers of various kinds are indispensable in daily life, transportation relies on tires, shock-absorbing elements are ubiquitous in small to large machines and buildings, flexible protective enclosures and seals are further applications. Applications need tailored properties, e.g. rubber in tires contains small particles, fillers to achieve the right combination of elasticity, damping, friction and wear resistance. Neutron scattering (SANS) contributes significantly to the understanding of the underlying physics of the molecular networks, NSE will augment this by dynamical information as e.g. local mobility or moduli. Molecular structures with network connectivity show rubber elasticity, which implies mobility of the chains between crosslinks. By macroscopic mechanical deformation orientation and environment of the chains may be influenced. Fillers are essential to modify the elastic properties in the desired direction. Early exploratory NSE experiments [77] showed the restriction of crosslink mobility in crosslink labelled PDMS model networks. Like high molecular weight polymer melts the chains between crosslinks in a rubber exhibit a tube confinement which in this case depends anisotropically on the stretching. This can be inferred from SANS experiments by application of models, however, NSE yields the tube diameters model free [90].

Fillers are vital for the application of rubbers, they interact by space filling, adsorption of the network chains, chemical binding and possibly modification of hydrodynamic interaction. All of these interactions will leave a fingerprint on the dynamics of polymer chain (segments) in the time and space domain of the NSE instrument.

One of the scientific challenges that polymer physics had to cope with in the last few decades was to improve the understanding of basic mechanisms and structure-property relationships between mechanical performance and molecular details under external load. The so-called quenched disorder in a melt of polymers through covalent crosslinking or equivalently the thermal quenching of non-equilibrium melt structures of linear and branched polymers basically yield the same observation that the entanglement topology of chains is a key component. The NSE technique provides a unique means to independently probe the fluctuation range of both crosslinks and polymer segments in the presence of an uniaxial deformation field. Other than the evaluation of SANS results which need to be based on models, NSE probes confinements model free. Present NSE capabilities, however, are too limited in the times domain, in order to access the important asymptotic regime.

The NSE technique could, however, equally be used in the clarification and separation of mechanisms in the reinforcement process which is typical for filled elastomers. The presence of fillers must definitely affect the dynamics of chains at the filler surface or due to local confinement effects in between filler particulates. These ‘nanocomposites’ allow at proper labeling and contrast matching a separation of hydrodynamic contributions, filler-chain interactions, bound rubber and filler-filler interactions which add up to the total time/strain/filler degree-dependent shear modulus of the composite blend as schematically shown in Fig. 9. The unfilled contribution is obtained from the analysis of unfilled elastomers. The correlation with dynamical mechanical analysis is highly important and will lead to a molecular understanding of complex filled elastomers and polymer nanocomposites.

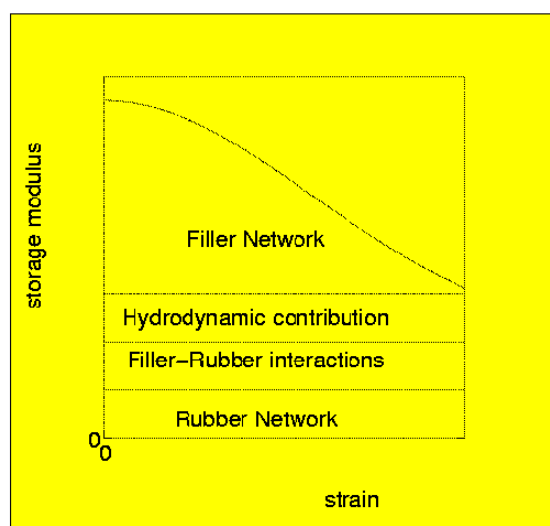


Fig. 9: The rubber elastic modulus as a function of strain at constant filler content and frequency. At the shown strain level of 10% the contribution of the filler network approaches zero. For large nonlinear strains in the order of 100%-500% only the other contributions are of importance.

3.1.5 Gels and Polyelectrolytes

Gels are very soft solids that share properties with swollen networks and –on short length scales- with semidilute or concentrated solutions. The network forming crosslinks may be chemical bonds or reversible physical associations. The dependence of the latter on external parameters as temperature, pH, ion-concentration etc. lead to a number of applications as functional materials [80]. Similar the sensitivity of swelling on thermodynamical parameters leads to huge volume changes. Diffusion of mesoscopic objects, e.g. protein molecules, may be controlled by the mesh size. Such diffusive motions and the influence of the presence of solvent with or without other solutes on the local and global mesh dynamics are accessible by NSE and DLS. One of the still very few examples of an NSE experiment probing gel properties in terms of collective diffusion on top of the frozen heterogeneity scattering intensity clearly shows the need of large Fourier times at low Q (today only available at the IN15) to separate the intensity from the different contributions [89].

Charged molecules, i.e. polyelectrolytes, exhibit properties that are quite different from non-ionic systems. Electrostatic forces change the conformation, are responsible for anomalous effects in the reduced viscosity and determine the intermolecular interactions. By variation of the ion composition in the solutions properties may be modified. Gels of polyelectrolytes show large response of the swelling on electrolyte quality or external “forces”, e.g. chemo-mechanical electrodrives can be made [80]. Applications range from diapers, drug delivery [79] to the biopolymers in mucus and their role in diseases [78] cholesterol control [81], paper making [82], sludge flocculation [83] (i.e. waste water treatment) and as electrolyte system for batteries [85]. Polyelectrolyte that form the corona of micelles offer new opportunities for experiments on charged brushes [84].

Yet no inelastic neutron experiments on polyelectrolytes in solution are known to us. However, it is expected that the specific electrostatic interactions contribute to the restoring forces of fluctuations and thereby may be analyzed by NSE experiments and the intensity restriction become alleviated by the new instrumentation.

3.1.6 Polymeric electrolytes

Polymeric electrolytes are of considerable interest for electrochemical devices such as solid state batteries. They yield a high energy density, are non-toxic and exhibit sufficient ionic conductivity if salts, e.g. LiClO_4 are dissolved. The mechanism of the ionic conduction must be fundamentally different from the one in usual solvents, its investigation is of considerable practical and fundamental interest. High resolution quasielastic scattering is a powerful tool to analyse ion- and molecular mobilities and their role in the ion conduction mechanism.

The structure of the polymeric model electrolytes poly(ethylene oxide) (PEO and PEO- $\text{LiSO}_3\text{-CF}_3$) has recently been studied with spin polarised neutrons [86], thereby coherent and spin-incoherent scattering contributions from hydrogen can be discriminated. The intensity modulated NSE option foreseen for the proposed instrument will enable such a discrimination also for the inelastic contributions, which will enable the distinction of Li-ion mobility from polymer motion. Related studies which currently need the combination of H- and D-labels aim at the coupling of the “invisible” Li-ions to the polymer dynamics and use different QENS and NSE instruments to cover a large dynamic range [87,88] which will be covered to a large extent by the proposed NSE alone.

3.2 Biophysics

Using similar methods as employed for the investigation of microemulsions the properties of biological model membranes and the influence and behaviour of incorporated protein molecules may be studied by NSE in combination with SANS and reflectometry. Quasielastic Neutron scattering (QENS) that is performed mainly with normal time-of-flight instruments yields information on the ps-motions in protein molecules that can be compared to the results of computer simulations. Thereby important information on the interactions between molecular constituents could be retrieved. With the rapidly developing computing techniques (hard and software) the time range of simulation is expected to reach ns in the foreseeable future. Then NSE experiments will become necessary to compare and adjust computer simulations for longer times to study more subtle and cooperative structural motions that are closer related to the biological function than the ps-vibrations of small molecular units or single atoms.

New opportunities to gain new insights in the function of biological molecules by NSE spectroscopy will thus be boosted by the “explosive” increase in number, size, time range and realism of computer simulations that are needed to guide the experiments and to interpret the results. Further the ability to produce sufficient amounts of a specific protein by genetic engineering will increase the power of such “sample amount demanding” techniques as NSE. Together with the enhanced instrument capabilities these facts foster the expectation that biophysics with NSE will strongly develop from the currently still marginal activities to a flourishing branch.

3.2.1 Protein Dynamics

Proteins are of particular importance in biology. They serve as catalysts of special chemical reactions, as transport molecules and in many other functions. After the detection of their three dimensional structure with a high density of atoms inside, the picture of a solid structure arose. Later investigations showed that the dynamics of proteins are essential for their functions, e.g. a O_2 molecule would not be able to bind to (or leave) a myoglobin (or hemoglobin) molecule without fluctuations of the protein [100]. And practically all catalytic reaction are accompanied by drastic conformational changes.

Below 200 K a protein behaves very much like solid; the mean square displacement raises proportional to temperature with values comparable to solids. But above this temperature the protein gets much more flexible. This was found in many investigations using different measurements techniques. The theory is that proteins undergo conformational changes with rising frequency and/or amplitude. These conformational changes seem to be the functional important fluctuations of the protein.

Inelastic and quasielastic neutron scattering measurements were performed on proteins in aqueous solution (e.g. [101]) and in membranes (e.g. [102]) to study protein dynamics and gave new insights into the problem. But the functionally important fluctuations are slow. Typical frequencies are 10^7 to 10^{11} Hz at room temperature [103], but also much lower frequencies are found [104]. Therefore, most neutron scattering methods are only sensible to the fast conformational changes. NSE could become the most important neutron measurement technique to study the functional dynamics of proteins, as it is sensitive to slower motions.

Until now, the dynamics of only a few proteins were studied with neutron spin echo measurements, pig anti-Dnp-immunoglobulin [106], hydrated soluble C-phycoyanin [107]. The results were compared to molecular dynamics simulations and gave good agreement [107,109]. But the relaxation times examined were still quite short compared to those of the functionally important conformational changes. With long Fourier times as planned for this instrument, it would be possible to approach the main frequency range of conformational changes with NSE measurements. However, the flexibility connected to the “nanomechanics” of protein substructures that may be involved in the biological function will have sizes of some nanometers. Therefore quasielastic scattering intensity may be expected in a range between $2\text{nm}^{-1} < Q < 10\text{nm}^{-1}$. At present the window of opportunity for such experiments has been hardly opened. The ultra high resolution NSE instrument at SNS together with extended simulation may reveal essential information on the relation between biological function and motion.

Some spin echo measurements were performed to study the diffusive translation of proteins (using low Q -values). From the diffusion constants it can be decided, whether the proteins are monomeric, dimeric etc. [108]. Furthermore, forces between proteins may be inferred. In addition the change of dynamics on aggregation can be studied. But already the study of haemoglobin in solution and in red cells gave diffusion constants at the limit of the resolution of IN11. Therefore, it is not possible to investigate proteins significantly larger than haemoglobin or to study the aggregation process itself with existing NSE instruments. To do that, higher Fourier times are required which will be provided by the proposal instrument.

3.2.2 Membranes

Biomembranes play a significant role for the function of cells. They control the transport of molecules into the cell, out of the cell and between compartments of the cell. Any transport of molecules through the membrane must be actively supported by membrane proteins. Membranes are bilayers consisting of lipids with its hydrophobic ends to the inner side of the membrane. As a consequence, biomembranes have exceptional elastic and dynamic properties [111]. One question of interest is the mobility of lipids or proteins within the membrane. Neutron scattering investigations have contributed to access such questions [112], but we still wait for decisive NSE results.

Neutron spin - echo measurements in this matter are still rare, though first examinations were already performed. Pfeiffer et al. investigated the mobility of a lipid bilayer by quasielastic neutron scattering using ultracold neutrons (UCN) and neutron spin echo measurements. In this way the lateral lipid diffusion

constant could be measured [113]. The UCN measurements (which suffer from low beam intensities) were necessary, because the low energy region down to about 2neV could not be reached otherwise. With the planned Fourier time of 1 μ s, e.g. lateral diffusion phenomena of membrane proteins could be investigated.

A study of the relaxation undulations of stacks of bilayers with neutron spin echo spectroscopy revealed unexpectedly low relaxation frequencies, which seem to be caused by friction between the two layers [114]. To check theories describing the elastic properties of bilayers, measurements with higher Q values ($Q \geq 5\text{nm}^{-1}$) and (at the same time) low τ values are necessary. They would be possible with the NSE instrument described here, especially if the maximal scattering angle were 40° or more.

For both types of investigations, we can expect new studies, e.g. on natural membranes or on the influence of membrane proteins and hydration. Again a long spin echo time, which allows to study slow processes, would be important to study the slow, functionally important processes and promises new insight in this part of biology. For lamellar stacks as investigated in [114] the improved Q-resolution (<1% instead of >10% for a normal reactor NSE) of a pulsed source instrument will be extremely helpful to analyze the intensity close to lamellar (pseudo)Bragg-peaks.

Understanding the formation and stability of vesicles may help to get further insights into the processes connected to some diseases [116,117]. NSE can contribute by the investigation of local viscoelastic membrane properties as derived from the observation of Brownian fluctuations respectively undulations in different environments. The effect of decoration with other molecules, e.g. membrane proteins will be an important issue. Whereas light scattering and videomicroscopy contribute to the understanding of vesicle membranes on length scales beyond a μm , NSE may serve as a more local probe (1-100nm), H/D-labelling allowing to focus on different constituents of a complex membrane system.

3.3 Glasses

Our life would be difficult to imagine without the ubiquitous presence of glass forming polymers. They are important from their technical point of view and also with respect to their physical properties. Despite the long history of research with classical spectroscopic methods, the molecular nature of the glass transition and the associated relaxation processes is still not well understood. Investigations using neutrons are able to reveal the underlying molecular motions. Since relaxations influence the form stability, the ductility and the impact strength of materials, their understanding will be the basis to design new materials with corresponding properties. Also transport processes in polymers above the glass transition, e.g. ion mobility in rubber like polyelectrolytes, are closely connected to these molecular relaxations.

Aside of the simultaneous resolution of spatial and temporal processes on an atomistic scale neutron scattering offers the additional opportunity of labelling. In particular for organic and polymeric substances synthetic chemistry allows judicious replacement of hydrogens by deuterium. Fully hydrogenated samples will yield the single particle (segment) motion as obtained from the dominant spin-incoherent H-scattering. Fully deuterated samples reveal the collective response due to structural relaxation. More sophisticated chemistry may put labels to specific positions in the molecule and thereby enhance the intensity from specific correlations. Finally the (dynamic) single chain form factor of a polymer is obtained by mixing deuterated and protonated chains. In blends this may be used to focus on one component only. NSE and eventually backscattering spectroscopy covers the relaxation time range found for a typical glass forming system some 10K above T_g . Closer approach to T_g requires extension of the maximum NSE Fourier time to match the slowing down of the relaxation rate.

Glasses belong to the class of "soft-matter-systems" only insofar as on the one hand among polymers there are many easy-to-handle examples that do not crystallize at all and that exhibit glass-transitions at convenient temperatures --not to far from ambient temperature. Their glass-transition which is characterized by a steep increase of viscosity and a calorimetric signature is the boundary between elastic or rubbery and hard and brittle mechanical behaviour. There are also some low molecular organic molecular glass formers like glycerol and orthoterphenyl that have been investigated by NSE [149, 150] - beside other methods. Generally the currently available NSE instruments are only able to resolve dynamics of the liquid phase of

the glass-formers usually several 10K above the glass-transition temperature, where the dynamics has slowed down far beyond the scope of accessible Fourier-times.

3.3.1 The structural relaxations

The glass process is driven by the freezing of the structural relaxation which connects to the macroscopic flow. These structural relaxations have been studied by high resolution neutron techniques – neutron spin echo and backscattering – both investigating the pair - as well as the self correlation function. Fig.10 displays NSE results on the pair correlation function of polybutadiene studied at the first and second peak of the static structure factor. The first structure factor maximum relates to the interchain correlations – it moves strongly with temperature. Its time dependence measured by NSE could be shown to scale with the characteristic relaxation time of viscosity (Fig. 1010a). At the second peak relating to intrachain correlations such a scaling does not hold (Fig.10c) and the different relaxation functions cannot be scaled with the viscosity relaxation time τ_η . Here different physics is observed – as it turns out the relaxations at the second structure factor maximum are determined by the dielectric β process.

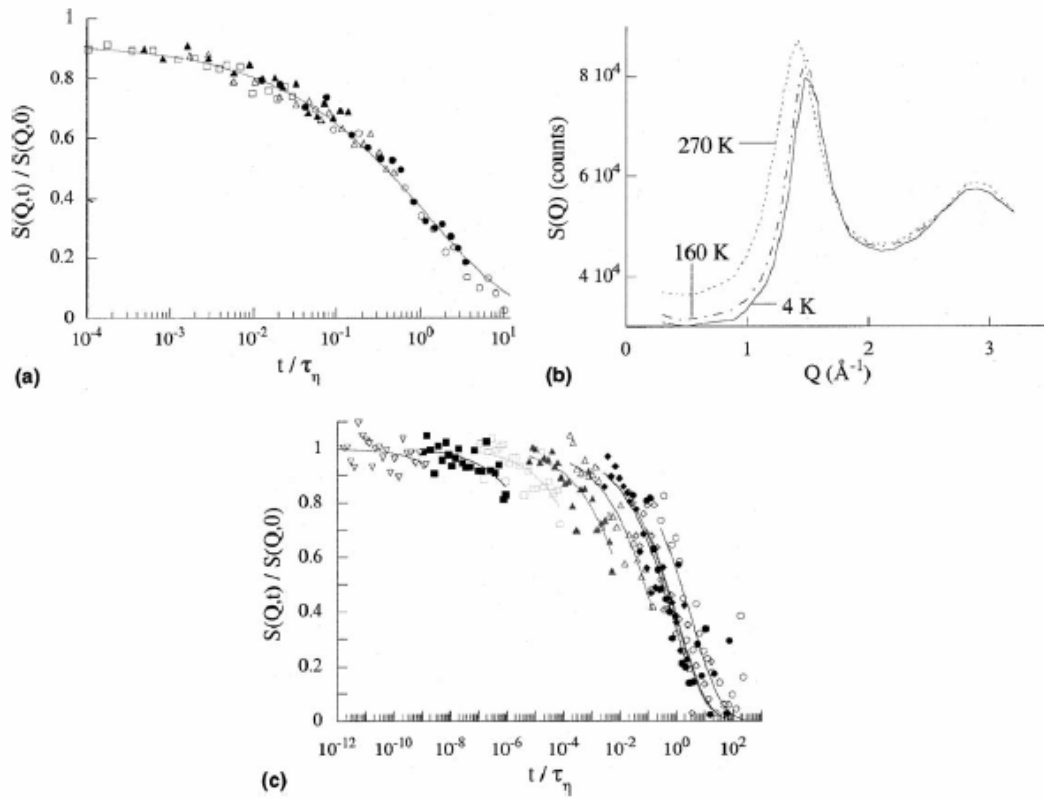


Fig. 10: (b) The static structure factor peak $S(Q)$ obtained for deuterated polybutadiene at different temperatures $T=4\text{K}$, 160K and 270K . NSE spectra are taken at the first (a) and the second (c) structure factor peak [97]. The NSE data has been fitted with a Kohlrausch - Williams - Watts - function (KWW) $(S(Q,t) \sim \exp(-(t/\tau)^\beta))$, where β is the stretching exponent and where subsequently shifted by the temperature shift factor for the viscosity relaxation.

Studying the self correlation function a strong dispersion of the characteristic relaxation time $\tau(Q) \approx Q^{-2/\beta}$, where β is the stretching exponent of the Kohlrausch-William-Watts relaxation function of the α process, is found in many polymers. This relation between dispersion and shape shows the Gaussianity of the relaxation process and was used in order to identify the α process as a sublinear diffusion process [10,96].

A rich variety of theories exists in order to describe the glass transition. One of the most prominent among those is the mode coupling theory (MCT) [146, 147]. Among others the MCT predicts of a cusp like anomaly of the α relaxation dynamic structure factor amplitude that should occur at the MCT glass

temperature T_c . For the several glass forming polymers this cusp temperature has been identified and it was found that it is close to the temperature where the α and the β relaxations appear to merge [161].

3.3.2 The secondary relaxations

The role of the secondary β - or Johari Goldstein process for the glass transitions is not well understood and it is generally assumed that this process is spatially localized. NSE and backscattering results have identified the associated jump lengths of typically 1 or 2 Å. Since most of these experiments have been performed at the resolution limit employing a limited dynamic range, the interpretation of such investigations requires the combination with other spectroscopic techniques like dielectric spectroscopy. The β process merges with the α process at temperatures close to the MCT T_c .

A very important unsolved question relates to the merging process itself. Investigations on polybutadiene are the only example where in depth NSE experiments were performed [148]. They were interpreted in terms of statistically independent primary and secondary relaxations. However, again these experiments were performed at the resolution limit and the statistical significance should be highly improved. Thus, the merging process is still wide open for further investigations on different polymers with better resolution employing a larger dynamic range.

The investigation of the α - β merging has the potential to lead to a better understanding of the nature of the β relaxation and its relation to the α process. Is the β process a frustrated α relaxation, meaning that possibly both processes are of similar molecular signature. However, the one leads to flow while the other remains localized? Such questions cannot be properly addressed today, because the time scale of the merging process are close to the resolution limit of existing instruments. The proposed instrument will lead to significant progress provided that space requirements, in order to reach larger Q values will be fulfilled.

3.3.3 Future challenges for NSE

There are a number of future challenges for the NSE investigations of the glass transition in polymers to be solved in the future.

- One of the most important problems relates to the much invoked possible length scale of the α process. Recently in polyisobutylene it has been found [162] that the mean square displacement needed, in order to relax the short range order at the structure factor maximum, increases with decreasing temperature. However, present capabilities are insufficient in order to come to conclusive results.
- Partial labelling of polymeric systems such as the hydrogenation of the methylgroup in otherwise deuterated polyisoprene has the potential to access to different partial structure factors and to elucidate the detailed molecular mechanisms. In order to be conclusive the separation of coherent and incoherent scattering will be highly important, a task waiting for the intensity modulated NSE options.
- At intermediate scales the collective dynamics is determined by the stress relaxation in the material. Recently it was found in polyisobutylene that temperature dependence of the intermediate scale dynamics appears to be different from the structural relaxation observed at the structure factor maximum [162]. An understanding of this observation which contradicts e.g. all MCT theories (they are based on the existence of one relevant scale only) would require measurements in a larger temperature frame which are hampered at present by the available resolution.
- In the same intermediate length scale regime (in front of the first structure factor peak), the new NSE instrument could address the suggested correlated string like motions which according to computer simulation should underly the α process [163]. Their signature in scattering experiments up to now remains very vague.
- Finally, it is not known how local relaxations couple to the stress relaxations determining the low Q collective dynamics. Again an access to this problem requires high resolution in order to allow measurements in a temperature regime, where the α process is already frozen out.

- A detailed measurement of the coherent form factor of the β process may reveal information about its collectivity. Is the β process a single uncorrelated event or does it extend over a number of monomers along the chain?
- Polymer blends have been addressed so far only once by high resolution neutron spectroscopy [164]. At present the dynamical miscibility of blends is a highly discussed topic. One of the important question relates to the length scale of the dynamic heterogeneity. Is there a dynamical mixing length or a cooperative volume for relaxation? This problem could be investigated up to now in one singular case at high temperatures and was strongly limited by available resolution.

With the exception of the intermediate scale dynamics, most of the glass problems relate to molecular motions on a relatively local scale. Therefore, its full access needs an NSE instrument covering a large range in Q . Therefore, this part of the science case demands an instrument which can operate at high scattering angles. This in turn needs sufficient amount of space in the instrument hall as discussed later in chapter 4.

3.4 Nanostructured materials

3.4.1 Introduction

Nanotechnology is based on specific properties of materials which are determined by their structure on a nanometer scale. Such nanosized objects determine our life in the form of protein complexes, as viruses, as colloidal particles in water and as aerosols, etc. Designing and controlling composite materials on the nanoscale is promoted by self-assembly and self-organization of compartmented macromolecules.

Nanostructuring of materials by non-equilibrium preparation or by self-organization is a new means to combine or to create new material properties. Many of those new materials contain soft components the dynamics of which is accessible for NSE. Functional micro gels, filled rubbers, magnetic fluids and block copolymers are a few examples. In these cases the soft interphase leads to forces and frictions that cause fluctuation dynamics in the NSE regime. NSE in combination with SANS allows for the extraction of the structural parameters and the elastic and viscous contributions that determine the microscopic dynamics as well as macroscopic properties. Most experiments we can envisage are at the limit of present day capabilities or they are just impossible. Thus the future development strongly demands high flux sources.

Some of the challenges in nanoscale science and technology which could be solved by the new capabilities provided by a new high-flux NSE spectrometer are: dynamics, magnetization kinetics and spin dependent transport in magnetic nanosystems, measurements of dynamic correlation length, identification of molecular-level processes occurring at liquid-solid interfaces, identification of the difference between activated and inactivated states of catalysts using monolayer-sensitivity inelastic neutron scattering.

NSE spectroscopy is needed to probe the wide time domain from 10^{-13} to 10^{-6} s, in order to reveal dynamic processes as different as binding in catalysts or displacements of nanoscale particles [51]. Here we only discuss some subjects of importance involving possibilities of using the main advantages of NSE spectroscopy at a new generation neutron source as SNS.

3.4.2 Nanoparticles, suspension of nanoparticles

Nanoparticles i.e. particles in the range of about 10 nm to a few hundred nm determine our life (protein complexes, colloidal particles, etc.) play an important role in the industry (formulation of pigments, production of catalysts, pharmaceutically active compounds, quantum dots in electronic components).

But it is also necessary to understand at a molecular level how a nanoparticulate system is formed. For example, many active organic compounds and organic effect materials are poorly soluble in water, or even insoluble. Aqueous forms of application thus require special formulation techniques to utilize or optimize the physiological (pharmaceuticals, cosmetics, plant protection, nutrition) or technical (varnishes, printing inks, toners) action [27]. NSE will inform on their mesoscopic diffusion properties and their mutual interactions.

Phenomena connected to suspension of nanoparticles represent an interesting research field. For example Loppinet et al [30] recently presented an experimental description of the dynamics of a dense colloidal suspension of model hairy nanoparticles using dynamic light scattering. Because of their small size and the small spacing of their liquid-like structure, as detected with small-angle neutron scattering, these particles enable the systematic investigation of the low-scattering wavevector (Q) fraction of the dynamic structure factor ($S(Q,\tau)$) away from the peak, which relates to the osmotic modulus of the suspension. The two relaxation processes contributing to $S(Q,\tau)$ are the fast cooperative diffusion of the concentration fluctuations (hair interactions) and the self-diffusion of the slightly polydisperse cores (incoherent contribution). The study of these hairy particles contributes to the overall picture of the dynamic response of concentrated colloidal suspensions sterically stabilized by grafted macromolecules.

Other examples of nanostructures are nanocomposites i.e. nanoparticle reinforced polymers, which are a new class of lightweight materials with stiffness and strength approaching that of metals. Particle displacements and interactions during deformation may be followed by SANS and NSE.

Molecular clusters of paramagnetic metal ions have already been widely investigated as model for magnetism at the nanoscale, especially for quantum effects like the tunneling of the magnetic moment. In the last decade molecular chemistry has had a large impact in the field of nanoscale magnetism by providing new magnetic clusters, whose superparamagnetic behavior resembles that of conventional nanomagnetic particles. Molecular clusters are relatively small objects with small spin compared to usual fine magnetic particles and quantum effects are more likely to reveal in these systems. The field dependence of the relaxation time is not monotone but shows a periodic structure due to the possibility of an underbarrier tunneling process, which can occur between thermally excited states within the ground state manifold [31].

NSE measurements of the dynamic susceptibility performed in parallel to magnetic susceptibility measurements (dynamics of magnetization) in the typical relaxation time range 50-600 ns to study magnetism and quantum effects of low symmetry-clusters (e.g. Fe8) will lead to a better understanding of the phenomena. Further fundamental research in the field of the structure dynamics in molecular magnetic clusters can provide precious information to transfer to chemists to design novel materials.

Understanding the magnetic properties of nanometer scale particles is a central issue in the field of magnetic materials. Magnetic nanoparticles themselves are used as active component of ferrofluids, recording tape, flexible disk recording media, as well as biomedical materials and catalysts. Spin wave spectrum of nanoparticles can, in principle, be measured directly by inelastic neutron scattering. Contributions to the elastic scattering can be measured, due to 'longitudinal' fluctuations of the particle moment over the anisotropy energy barrier, and due to a quasielastic component attributed to 'transverse' fluctuations, i.e. precessions of the particle moment. Also thermally activated and quantum tunneling relaxation can be investigated in the context of ideal single-domain particles, as well as particles with surface spin disorder [32].

An other example is the work started by F. Gazeau et al. [33] who have studied magnetodynamics of ferrofluid γ -Fe₂O₃ nanoparticles by quasi-elastic neutron scattering between 10 K and 250 K in the frequency range 10^{10} - 10^{12} Hz. They probed independently the precession of the core magnetic moment and surface spins fluctuations observed in a dissipative regime. These fluctuations slow down at low temperature leading to a frozen disorder of the surface layer. However, the available results calls for further investigations with a higher resolution technique (preferably NSE) at lower Q and lower energies to get rid of the surface contamination of the data in order to be able to correlate $\Gamma(T)$ to the temperature dependence of magnetisation.

We conclude this topic with the example of the very successful experiments of Casalta et al [34]. Using the technique of neutron spin-echo spectroscopy, they have conducted a direct measurement of the superparamagnetic relaxation of nanoscale, magnetic monodomain iron particles in the time range between 0.01 and 160 ns and for momentum transfers q between 0.035 and 0.15 \AA^{-1} . Using a phenomenological model, which includes the effect of a particle size distribution, it was possible to determine the temperature T and Q dependence of the longitudinal superspin relaxation time spanning 4 orders of magnitude.

Below about 40 K, the popular single-particle picture of Néel and Brown breaks down, and the interparticle correlations begin to influence the relaxation by introducing a more pronounced slowing down as the temperature is decreased. For T smaller than or approximately 40 K, interparticle correlations affect the longitudinal superspin fluctuations. The SNS NSE would allow larger relaxation times and more intensity. Thus the time range could be extended up to 1000 ns in order to study the intermediate structure factor at lower temperatures ($T < 20$ K).

The examples above illustrated that the application of new NSE studies at new generation spallation sources as SNS by using high flux, and a widely extended dynamic range $10^{-3} - 10^3$ ns and $3 \times 10^{-3} - 2 \text{ \AA}^{-1}$ i.e. corresponding lengths of 3 – 1000 Å would strongly widen our understanding on the dynamics of nanoscale systems. Here some concluding remarks.

As described above, the progress in synthesis of novel nanoclusters and derivatives (fullerenes, nanotubes), other nano-scale composites such as polymers, magnetic fluids, membranes and layered structures demand neutron scattering studies of their unique structural and dynamical properties.

These very different material are principally dynamical nano-systems which functional properties are revealed in the time range $\tau \sim 10^{-12} - 10^{-6}$ s covering the diapason of atomic and molecular motions. The most essential common feature of these small statistical systems is their quasi-classical behavior. Its investigation seems to be more adequate in the real "molecular" time. Indeed, the NSE-method enables to recognize the dynamical properties of nano-systems assuming the different NSE-modes [142]:

- Conventional measurement of dynamic scattering function $S(Q, \tau)$ in short time $\tau_s \sim 10^{-12} - 10^{-9}$ s and long time $\tau_s \sim 10^{-9} - 10^{-6}$ s ranges to evaluate both the local molecular motions (e.g. molecular groups rotations, β -relaxation in polymers, rotational diffusion of C_{60} , coil-globule transitions) and relatively slow dynamics like e.g. the structural relaxation in gels or the large scale motions in concentrated solutions or the dynamics of nano-defects at surfaces and interfaces);
- Ferromagnetic and spectrum modulation modes for the separation of magnetic and nuclear scattering to study the properties of magnetic and nuclear subsystems (e.g. vibrations and creep of vertices in superconductors, magnetic correlations and particles diffusion in ferrofluids).

It can be concluded that the nanoscale science case strongly underlines the importance of the planning of the proposed NSE instrument at SNS. As described above, the progress in synthesis of novel nanoclusters and derivatives (fullerenes, nanotubes), other nano-scale composites such as polymer aggregates, magnetic fluids, membranes and layered structures will raise new questions. Understanding their dynamical properties will certainly help to find answers and new insights.

3.4.3 Ferro fluids, magnetofluids and electrorheological fluids

The nanophase liquid systems known as ferrofluids (FF) consist of magnetic particles covered with a surfactant layer and is dispersed in a liquid. In the study of ferrofluid dynamics the separation of self and pair correlation is the essential problem at both intermediate and high concentrations of the magnetic phase.

Dynamics of concentrated ferrofluid with labeled particles has been investigated by Lebedev et al. [35]. In this system a moderate external field $H \leq 8000 \text{ A/m}$ can initiate structure formation through self-organization. On the other hand, the magnetic fluctuations inside the particles (fast and intense near T_c of the magnetic phase) influence the particles' diffusion rate, which decreases strongly near the critical point. Thus dipole-dipole interaction makes this colloidal solution extremely strongly correlated with and without external field.

Another subject of high technical interest is the electrorheological behaviour of nanostructured systems. Some aspects of structural dynamics are accessible for neutron scattering investigations as was shown by Aliotta et al [36].

They investigated the role played by the solvation water molecules on the macroscopically observed sol-gel transition in lecithin/cyclohexane/water reverse micelles. The self-diffusion properties of both the surfactant and the water molecules entrapped in the micellar cores were measured by quasi-elastic neutron scattering,

while dielectric relaxation and conductivity measurements furnished complementary information on the structural relaxation processes taking place in the system. The data from lecithin-based systems can be interpreted only by assuming that, the water molecules are entrapped at the interfaces without coalescing into an inner water pool. Also, the charge transport mechanisms look very different. In particular, in the case of lecithin, it was shown how the conductivity appears mainly due to inter-micellar bond percolation: it was suggested that the solvated water molecules can induce a change of the surface curvature, in such a way promoting the formation of branch points. The idea of the existence of a percolated network of branched cylindrical micelles agrees with the observed temperature dependence of the system conductivity. The study of the electrorheologic behavior of the system under electric field confirms the existence of a percolated transient network in the gel phase. The high resolution NSE spectrometer will reveal the microscopic dynamics underlying the rheological behavior.

3.4.4 Complex fluids in porous media

Understanding the behaviour of complex liquids in porous media is a particular challenge for the science of soft matter. By complex liquids we mean multicomponent systems of polymers, colloids, micelles and surfactants, whose characteristic length scales are frequently identical to those of porous materials. Complex liquids in porous media are of great practical significance. They are found in oil production where water comes up against petroliferous rocks, in processes separating materials through membranes, in remediating contaminated soils, in cleaning powders and pastes, and even in cosmetics.

The coincidence of the characteristic length scales of the liquid and the geometrical constraints due to the pores has a profound influence on the thermodynamics, the phase behaviour and the transport properties of the complex liquid. For example, a network of small pipes could be partially plugged by oil droplets of a microemulsion. The ability to predict the behaviour of oil/surfactant, polymer/surfactant, polymer/protein or protein/surfactant systems in microenvironments based on a scientific understanding would enable effective control of many industrial processes.

QENS is a unique technique in that it provides otherwise unobtainable information about liquid flow through porous media. This is a current topic of fundamental interest and also has practical significance. NSE informs about the dynamical behaviour of the complex fluid in the material, its flow, its plugging behaviour its collective fluctuations, etc. Using simple test fluids such experiment also inform about the network structure of the porous materials. While no experiment of the first kind is available, experiments on the interconnectivity of a network structure through a determination of $\langle r^2(t) \rangle$ in the appropriate range have been reported.

In their experiments, Li et al [38] demonstrate that the tracer diffusion of a liquid in a porous media can be well studied using the neutron spin echo technique. The samples used consisted of porous Vycor glass saturated with a mixture of D₂O-H₂O (64/36) water to match out the coherent small-angle scattering component due to the neutron scattering density contrast between water and the Vycor matrix, in order to reduce the small-angle neutron scattering and the chemical diffusion contribution to the quasi-elastic scattering. A series of measurements has been made in the Q range 0.07-0.14 Å⁻¹ using the spin echo spectrometer IN11 at the ILL. These experiments enabled to measure the tracer diffusion coefficient of the liquid within a pore and through the local pore network and hence to investigate the interconnectivity of these pores through a determination of $\langle r^2(t) \rangle$ over length scales to about 100 Å.

Experiments reveal a complicated exponential decay in $S(Q, \tau)$, implying that they result from a mixture of tracer diffusion and chemical diffusion, which cannot be separated one from another. Using matched water mixture, the chemical diffusion could be removed, however, the near cancellation of the echo at the contrast matching point and unexpected double relaxation process and low count rates on IN11 made the evaluation of the tracer diffusion difficult. The problem has to be overcome with multi-angle detectors, and higher flux.

3.5 Magnetism

3.5.1 Introduction

As in the case of atomic dynamics, the motion of spin magnetic moments in matter can tremendously slow down compared to single spin motion or the exchange energies, if many spins act in a collective fashion, i.e. when correlations involve a large number of atoms. Best known magnetic phenomena of this type are the “critical slowing down” (de Gennes) of magnetic fluctuations in the vicinity of second order phase transitions, the glassy dynamics in spin glasses with extremely disordered or frustrated structure and the superparamagnetic behaviour of nanoscale clusters of spins. Collective, correlated dynamics in all of these cases manifests itself by a slowing down of the spin relaxation processes by several orders of magnitude compared to the frequency (energy) characterizing the interaction between spins, which can vary from a fraction of a meV to a few hundred meV. NSE is a prime tool for the study of these slow processes in the time domain 0.01 to some 100ns(1000ns), i.e. for energies ranging from μeV down to some 10neV (1neV). A particular feature of NSE in the study of magnetic phenomena is that polarized neutrons are used both for the purpose of the energy analysis of the scattering process and for identifying various kinds of magnetic contributions by polarization analysis. In most of the cases the polarization characteristics of the scattering process leads to a unique, unambiguous signature of the magnetic effects compared to non-magnetic contributions. In other cases, the NSE spectra represent an algebraic sum of various magnetic and eventually non-magnetic contributions, which cannot be unambiguously singled out one by one by making use of the inherent polarization analysis feature of NSE.

Combining NSE with full polarization analysis capability is a new challenge, the principle of which has been tested on IN11 at ILL. Underlying it implies close to an order of magnitude loss in neutron intensity. Thus, this powerful new combination of NSE and full polarization analysis will really become feasible at the next generation of more intense neutron sources like the SNS. The study of the magnetic aspects of the conductor-insulator phase transition in CMR materials is one particularly promising area of applications of Polarimetric NSE in particular with respect to the lattice distortion induced local anisotropy and its role in the phase transition. More generally, NSE with or without 3D polarization analysis will be an important tool in the quest of understanding of an increasing variety of magnetic phase transitions in new materials, e.g. quantum phase transitions.

Another recent field of successful application of NSE is the study of vortex dynamics in conventional superconductors in magnetic fields. The behaviour of vortices determines the current carrying capabilities of superconductors, in particular resistive losses and the critical current, two parameters crucial in applied superconductivity. Due to the presence of a large density of lattice defects, the vortex properties are particularly complex in high T_c -superconductors, and on the basis of transport properties several new vortex phases have been identified: such as Bragg glass, vortex glass, vortex liquid. To understand the structural and dynamic behaviour of the vortices is one of the key challenges in the physics of high T_c -superconductors for the years to come, and access to very small momentum transfers together with the high energy resolution of NSE are of paramount importance in this work.

Already the current problems require wider Fourier time ranges to extend the experiments into the low- Q SANS regime to resolve the dynamics of larger structures. Also for the high-Q glass regime larger Fourier times are needed to get a closer approach to the glass transition.

3.5.2 Spin Glasses

Spin glasses are magnetic systems, which combine disorder and frustration, i.e. in these systems the magnetic interactions are randomly distributed and in conflict with each other. The disorder in the magnetic interactions is typically related to structural disorder and to a random distribution of the atoms, which bear the magnetic moments in a non-magnetic crystalline or amorphous matrix. Spin glasses can be metallic like Cu(Mn) and (Au)Fe or insulating like $\text{Eu}_x\text{Sr}_{1-x}\text{S}$ etc [6]. In spite of the strong differences in the nature of the samples, all these systems show characteristic common patterns in the high temperature paramagnetic phase as well as in the low temperature spin glass phase.

Between the spin glass freezing temperature T_g and some 3-10 times T_g the dynamics is largely wavenumber independent with a slowing down of the spin relaxation compatible with an Arrhenius behaviour assuming a large distribution of activation energies between 0 and about $10kT_g$ [123]. With certain legitimacy it can be argued that this phase can be identified by the predicted famous Griffiths phase, which has never been unambiguously put to evidence in any system yet. There is a strong change of the relaxation lineshape from the ordinary exponential decay to a more or less well born out Kohlrausch form $\exp(-(t/\tau)^\beta)$. Non-exponential relaxation is one of the qualitative predictions of the Griffiths theory and it has also been suggested by a number of sophisticated theoretical approaches of phase transitions in strongly disordered systems. Since the relaxation times are still too short for macroscopic observations the NSE results actually provide the only evidence available for the dynamic anomalies in this temperature range,. Thus, this anomalous paramagnetic phase appears to be normal in all other measurements and it is an equilibrium state showing no hysteresis effects, which only appear at T_g and below.

In in the intermediate vicinity of T_g the Arrhenius type slowing down of the relaxation breaks down. Close to T_g a more dramatic slowing down sets in, which can be interpreted as the footprint of a phase transition with a critical region of usual extent.

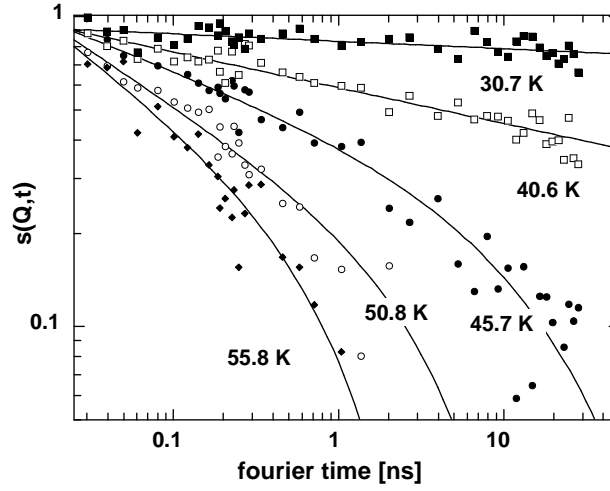


Fig. 11: Temperature dependence of the intermediate scattering function $S(Q, \tau)$ of $\text{Au}_{0.86}\text{Fe}_{0.14}$. The spectra were collected at $Q = 0.4 \text{ nm}^{-1}$ with the Neutron Spin Echo spectrometer IN15 (ILL) for $T=30.7 \text{ K}$, 40.6 K ($\sim T_g$), 45.7 K , 50.8 K and 55.8 K respectively. The continuous lines are the best fits to the data of a power law decay below T_g ($\sim 41 \text{ K}$) and of the Ogielski function $t^{-x} \exp(-(t/\tau)^\beta)$ above T_g .

For the data analysis in the low temperature phase, it is of particular importance to obtain data in a most broad dynamic range. Only recently, high accuracy data collected on the NSE spectrometer IN15 at the ILL gave the clue to understand the relaxation close to and in the spin glass phase (Fig. 11). These spectra span a large dynamic range and show that, as T_g is approached from above the strongly non-exponential decay of $S(Q, \tau)$ is well described by the empirical form $t^{-x} \exp(-(t/\tau)^\beta)$ whereas at and below T_g $S(Q, \tau)$ follows a simple power law $S(Q, \tau) \propto t^{-x}$. Exactly at T_g x is related to the standard static and dynamic critical exponents through the dynamic scaling relation $x = (d - 2 + \eta)/2z$, where d is the system dimensionality, η the static Fisher exponent and z the dynamic exponent [122].

These NSE results constitute the most direct evidence for a phase transition in spin glasses, which in turn implies that the non-exponential temporal relaxation we observe at T_g is an intrinsic, homogeneous feature of the phase transition. This compelling evidence for a transition with a non-conventional order parameter and for homogeneous non-exponential relaxation is particularly important in view of the understanding of glasses and of the vast category of non-crystalline systems.

On a more general level, the exploration of glassy behaviour induced by strong disorder is a subject of great actuality since over two decades, including both magnetic and structural glasses. Although considerable progress has been achieved, there are many open questions and new ones are emerging. The extended, very broad time domain accessible by the SNS NSE instrument will offer new perspectives for the study of all glassy systems. The nature of the glass transition and the non-exponential relaxation observed near glass transitions are open questions of particularly great theoretical and experimental interest. More precise observation of relaxation line shapes in an extended dynamic range (a particular inherent strength of the NSE method directly operating in the time domain) and the new potential of testing dynamic scaling features with enhanced accuracy will provide us with new understanding of glassy phenomena in magnetic systems.

3.5.3 Superparamagnetic fluctuations in monodomain iron particles

An experiment that pushed the experimentally accessed Fourier time to its technical limit was reported by the recent work of Casalta and co-workers [124, 125]. They investigated the spin dynamics of mono-domain iron clusters embedded in an insulating matrix of Al_2O_3 . By transmission electron microscopy (TEM) the sample was shown to possess a mean Fe particle diameter of 20 \AA (standard deviation of 4 \AA) and a body-centered cubic structure. Due to the lack of domain walls the clusters behave as single-domain particles, leading to the formation of a “superspin” associated with the entire particle. Inelastic neutron scattering showed the existence of two distinct magnetic fluctuation components both associated with the whole spin of the particle (superparamagnetic fluctuations). The faster relaxing component appeared in the time domain accessible by triple-axis and time-of-flight spectroscopy (timescale $0.1 - 100 \text{ ps}$) and was attributed to transverse fluctuations. The slow component (timescale $0.1 - 1000 \text{ ns}$) was identified with longitudinal superspin fluctuations and could only be resolved using the ultra-high energy resolution of the spin echo technique (Fig. 12). For comparison: the measurement at a correlation time of 200 ns in this experiment is about equivalent to a measurement at an energy transfer below 10 neV .

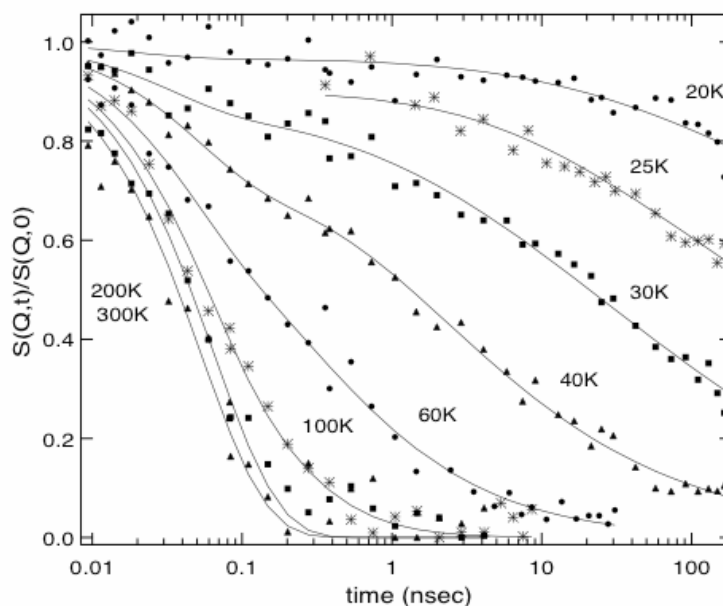


Fig. 12: Normalized intermediate scattering function from magnetic nanoclusters at $Q = 0.07 \text{ \AA}^{-1}$ for various temperatures. Below 200 K a specially derived model function is used to fit the data (higher temperature: single exponential relaxation) describing a distribution of relaxation times due to the spread in particle size.

At high temperature above $\sim 100 \text{ K}$ one essentially observes weakly Q -dependent isotropic single particle fluctuations. At temperatures below $\sim 40 \text{ K}$ interparticle correlations become important and manifest themselves in a modified Q dependence and line shape of the spin relaxation function.

A wide dynamic range is of the crucial importance for tracking down the form of a relaxation. Detailed relaxation studies are required not only for superparamagnetic systems but also for frustrated systems,

disordered antiferromagnets etc. In these systems, however, NSE experiments are scarce because of the lack of intensity. The proposed new generation NSE spectrometer will open up new possibilities and bring new ground-breaking results in the field of disordered magnetism.

3.5.4 Dynamical cross-over in Spin Ice $\text{Ho}_2\text{Ti}_2\text{O}_7$

The ‘‘Spin Ice’’ $\text{Ho}_2\text{Ti}_2\text{O}_7$ and $\text{Dy}_2\text{Ti}_2\text{O}_7$ compounds belong to the class of *geometrically frustrated* magnets. An introduction into the subject can be found in recent reviews [128, 129]. Here the spin echo measurement has proven particularly useful because, when combined with ac-susceptibility results different contributions to the spin dynamics could be separated, which otherwise would have been indistinguishable.

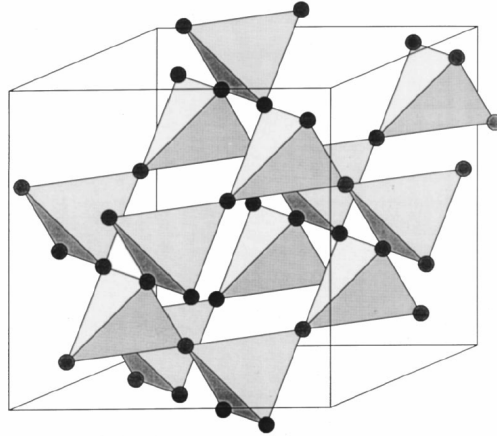


Fig. 13: The pyrochlore lattice. In cubic pyrochlores of chemical composition $\text{A}_2\text{B}_2\text{O}_7$ both the A and B atom sublattices independently form this network of corner-sharing tetrahedra.

The magnetic ions (Ho^{3+} or Dy^{3+}) occupy a cubic pyrochlore lattice (space group $Fd\bar{3}m$) of corner-linked tetrahedral (Fig. 13). At low temperature the magnetic moments are constrained by the crystal electric field (CEF) to local $\langle 111 \rangle$ axes. This frustrates the dominant (effectively ferromagnetic) dipolar interactions in the system and leads to frozen, non-collinear, spin disorder below $\sim 1\text{K}$. The spin ice state is in a way analogous to the Pauling hydrogen disorder of water ice (H_2O), with each spin equivalent to a hydrogen displacement vector situated on the mid-point of an oxygen-oxygen line of contact [28]. The NSE experiment was performed on the Ho compound, since natural Dy is opaque to neutrons which makes scattering experiments with cold neutrons very difficult. The single ion ground state of the Ho^{3+} ion is an almost pure $|J, M_J\rangle = |8, \pm 8\rangle$ doublet with $\langle 111 \rangle$ quantization axis, separated by over 200K from the first excited state. In the Dy compound the situation is similar.

At all temperatures between 0.05 K and 200 K the spin relaxation function $s(Q, \tau) = S(Q, \tau) / S(Q)$ measured by NSE is a single exponential and Q-independent, as shown in Fig. 14 [127]. Towards low times ($\sim 10^{-12}$ s) the limit is less than one, which means that fast relaxation processes at short timescales beyond the resolution of the NSE technique exist, which may be attributed to small incoherent oscillations of the spins about their $\langle 111 \rangle$ easy axes. The attempt frequency (inverse relaxation time) follows an Arrhenius law with attempt frequency $\tau_0 = 1.1 \pm 0.2 \times 10^{11} \text{Hz}$ and activation energy $E_a = 293 \pm 12 \text{K}$. The Q-independent relaxation and E_a being close to the energy of the first group of CEF levels establishes that the dynamics observed by NSE is due to a single-ion spin flip between the two states of the ground state doublet. Extrapolating this process into the ac-susceptibility frequency window ($\tau < 10^5 \text{Hz}$) shows that an ac-susceptibility peak should be observed at $\sim 15\text{K}$, as the process freezes out at lower temperature.

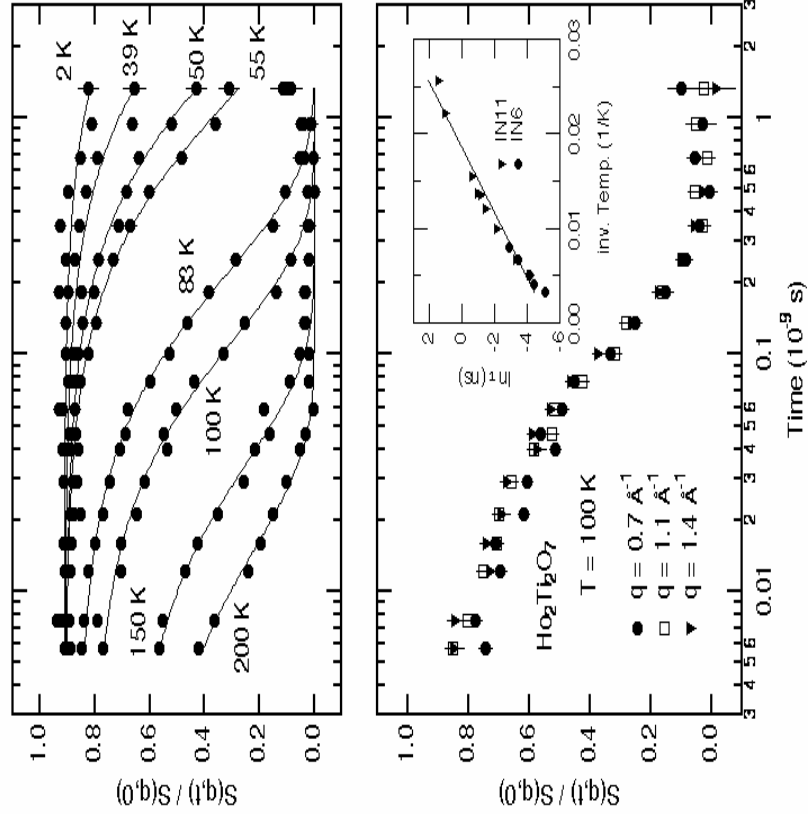


Fig. 14: The intermediate scattering function measured for a polycrystalline sample of $\text{Ho}_2\text{Ti}_2\text{O}_7$ at the IN11 spectrometer (ILL). Top panel: at different temperatures showing the speed-up when temperature is increased. Lower panel: at different Q 's showing the Q -independence of the dynamics.

Comparison to real ac-susceptibility data, which show the peak but increase again significantly towards lower temperature, giving a second peak at $\sim 1\text{K}$ let the authors conclude that in the temperature range of 4–15K the spin relaxation observed in ac-susceptibility must be due to *quantum tunnelling*. They suggested that the most likely origin for tunneling at this unusually high temperature is the strong intrinsic slowly fluctuating dipolar field arising from neighbouring spins fixed at angles of 109.5° deg. The gradual spin ice freezing below 4 K in their interpretation corresponds to development of a mean field, which splits the Ho^{3+} ground state doublet and thus extinguishes the tunneling process.

The interplay between NSE and macroscopic susceptibility (χ) is crucial for understanding not only spin glasses but also disordered and frustrated magnets. At this point we have to stress that neutrons deliver both $S(Q)$ and χ and thus give more information than susceptibility measurements. The comparison between NSE and susceptibility, however, naturally asks for long Fourier times, to minimize the gap in time between the two methods.

3.5.5 Flux Line Motions in Superconductors

By making use of the possibilities available on IN15 to combine polarised neutron techniques with small-angle neutron scattering, experiments on the vortex motion in superconductors have been able to push forward the frontiers of what can be measured.

In fact, despite intense activity in the last few years, only a few experimental methods allow to measure directly the dynamical properties of moving flux line lattices (FLL's) in superconductors and NSE is one of these. Recording of I - V curves is of course a most important one, but it provides only global information. On the other hand, neutron diffraction provides a very important contribution by measuring flux line arrangements but is normally used only in static situations. NSE can measure directly the neutron energy change on diffraction by a moving FLL, which corresponds to reflection by a moving “mirror,” which represents the flux-lattice planes, leading to a Doppler effect. The average speed of flux motion may be

related to the induction B and driving electric field E via $v = E/B$. For typical values of $v < 1$ m/s, the neutron energy change is very small and can only be detected by the neutron spin-echo technique in its 'ferromagnetic' variant. In this arrangement, the usual flipper, which reverses the precession angles of the neutrons at the sample, is replaced by two $\pi/2$ flippers on either side of the sample. These allow the neutrons to pass, without precessing, through the field associated with the flux-lines in the sample. The energy change in the scattered neutrons shows up as a phase shift in the spin echo, which is proportional to the 'Fourier time' of the measurement (which in turn is proportional to the magnetic field in which the neutrons precess). For these experiments on IN15 it was necessary to use the longer Fourier times available.

Typical results are given in Fig. 15:, on a $\text{Nb}_{87}\text{Ta}_{13}$ alloy, which was chosen because it provides both a very low critical current and a high normal state resistivity, in order to obtain a vortex velocity as large as possible for a given current. Using a cryomagnet, a uniform horizontal field of 0.2 or 0.3 T was applied perpendicular to the face of the sample, which was cooled to 2.2 K, and surrounded by liquid helium to provide efficient cooling. Currents were applied along the bar in the vertical direction; hence the flux lines experienced a force in a horizontal direction in the plane of the sample. The neutron beam was incident nearly parallel to the field. The results show that the average speed v of the flux lines may be measured NSE. This quantity is more easily and cheaply obtained with a voltmeter to measure the electric field, but NSE was also able to measure the distribution of vortex speeds in a specimen, which affects the amplitude as well as the phase of the spin echo [126].

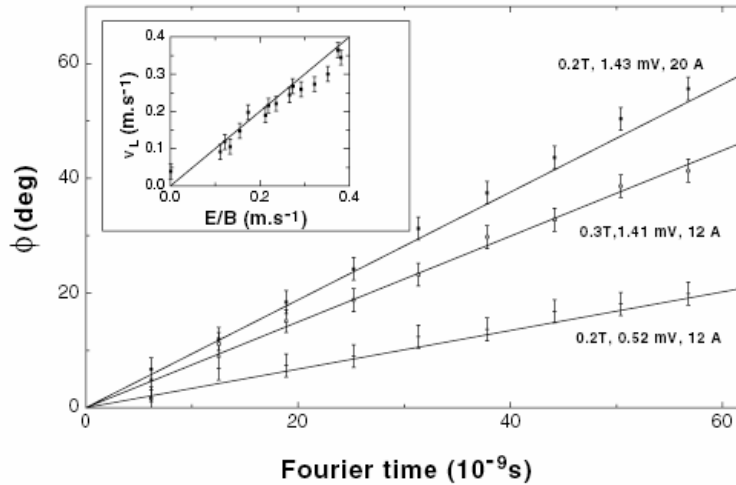


Fig. 15: The phase of the echo Φ as a function of the Fourier time at temperatures 2.2–2.5 K for different experimental conditions of magnetic field and of voltage. The lines are the calculated values of ϕ if v_L and E/B are equal. (To obtain the correct calibration of the Fourier time and hence the value of the slope of a line, one has to allow for the distribution of 15% of the wavelength of the incoming neutrons) Inset: The vortex lattice velocity is shown as a function of the ratio E/B , obtained varying the current at a fixed magnetic induction of 0.3 T, showing the equality between v_L and E/B .

The exploration of dynamic effects in the extended time domain of $10^{-11} - 10^{-6}$ s of the SNS NSE instrument will be of decisive significance for the exploration of vortex matter in superconductors, both conventional and high temperature. The phase diagram of vortex behaviour is quite complex, including liquid and glassy phases, and it has a fundamental role in determining the conductivity losses in superconductors. Improved resolution NSE offers particularly crucial new opportunities in the investigation of the vortex liquid states and the phase transitions between vortex liquid and less mobile (glass or Bragg glass) phases. Better understanding of the vortex matter in superconductors is of primary importance for practical applications of superconductivity too.

4 Instrument description

The proposed NSE instrument is of the original generic IN11 kind, which is the technique with the largest potential to extend the resolution beyond current limits. The new instrument will possess a number of unique features:

1. Highest resolution of all neutron spectrometers: $\tau_{\max}=1\mu\text{s}$ ($\Rightarrow 0.7\text{neV}$).
2. Huge dynamical range extending up to $1:10^6$.
3. Position sensitive area detector.
4. Field compensation and magnetic shielding.
5. Optional ferromagnetic mode.
6. Optional intensity-modulated mode.

A moderator detector distance of 18m yields a frame width of $\Delta\lambda=0.366\text{nm}$. Compared to a reactor based instrument using a 10% FWHM wavelength band from a velocity selector a gain factor⁶ $g>1$ is obtained for all wavelength $\lambda<3.2\text{nm}$. In the second frame ($0.366<\lambda/\text{nm}<0.732$) the gain factor reaches $g=\ln(2)/10\%=6.9$. The resolution of $\tau_{\max}=1\mu\text{s}$ shall be obtained for $\lambda>1.8\text{nm}$ ($g=1.8$). In addition due to the TOF λ separation the wavelength dependent part of the Q-resolution is an order of magnitude better than at reactor instruments.

Exploiting that the Fourier time $\tau \sim \lambda^3$ a subsequent use of various frames covering $0.3<\lambda/\text{nm}<3.0$ and a variation of the magnetic field (integral) by a factor >1000 on extreme dynamical range is achieved. By automatic set-up procedures the change of wavelength frames will be a routine operation with negligible time delay. The inherent change of $Q(\lambda)\sim 1/\lambda$ fortunately complies with the usual dispersion of relaxation rates $\Gamma\sim Q^2\dots Q^4$.

An area-sensitive fast detector of 30cm diameter covers a solid angle of $\Delta\Omega>2.5^\circ\times 2.5^\circ$ and assures efficient data collection rate.

The magnetic stray field of the main coils is compensated down to $1..1.5\times 10^{-4}\text{T}$ in 1.5m distance. Thereby it becomes possible to enclose the instrument area by a magnetic shielding which ensures a stable and reliable operation. The latter also depends on a rigid mechanical design. The thus achieved signal stability is an utterly important but often overlooked quality.

Additional flippers (ferromagnetic mode) and polarizer/analysers (intensity modulated mode) will offer the unique opportunity to perform a polarization analysis of the scattering from magnetic samples, to deal with depolarising samples, or separate coherent and spin-incoherent scattering.

4.1 Introduction

The placement of neutron optical elements and spectrometer components along the beam is indicated in Fig. 16. After a collimator insert that between moderator and shutter restricts the cross section to the used width in the target block area, the neutron guide section starts with the shutter insert. Guides shall be Ni-coated and have a cross section of 4cm (width) x 8cm (height). A first chopper is located in the cavity at 5.5m distance from the moderator. Between this first chopper and the following at 6.36m a short polarizing bender is located that introduces a bend of 3.5° out of the beam direction. For different wavelength ranges –each covering several frames- different solid state benders are required. For that purpose 2-3 benders are situated in a revolver. A fourth position of the revolver (length $\sim 0.5\text{m}$) serves as secondary beam stop. By the

⁶ The gain factor g is the factor in time needed at a continuous reactor source to perform a series of experiments covering exactly the same range as covered by the considered frame with the same statistics, provided that the average flux of the pulsed and the continuous source are the same.

deviation of 3.5° a direct sight from the neutron guide end to the moderator is safely avoided. After the deviators a guide field in the neutron guide is needed to preserve the polarization. Between the last (3^{rd}) chopper at 8.06m the guide field is rotated from vertical to longitudinal direction.

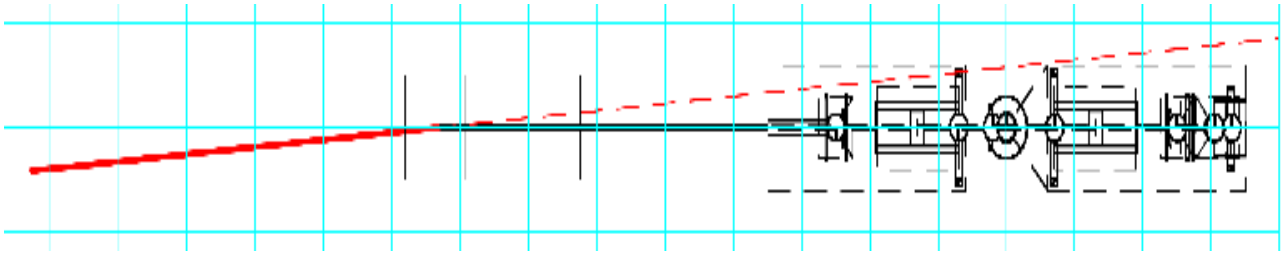


Fig. 16: Schematic layout of neutron guides, choppers and magnetic spectrometer components.

The last neutron guide section is tapered and slightly increases the cross section towards the end, in order to reduce the divergence. Since the neutron guide ends about 3m before the sample at highest achievable wavelengths this measure increases the available flux at the sample.

The “primary” shielding sector around the neutron guide ends at about 10.0m. The following NSE area is enclosed by a combined magnetic and radiation shielding. The functional components are located on three separate mechanical carriers: first arm, sample stage and second arm, see Fig.17. The carriers move on air pads on a special floor (tanzboden). The main solenoids -one on each arm- are compensated for lowest stray field. Flippers limit the precession paths. They are operated with current ramps that are adapted to the time varying wavelength within the selected frame.

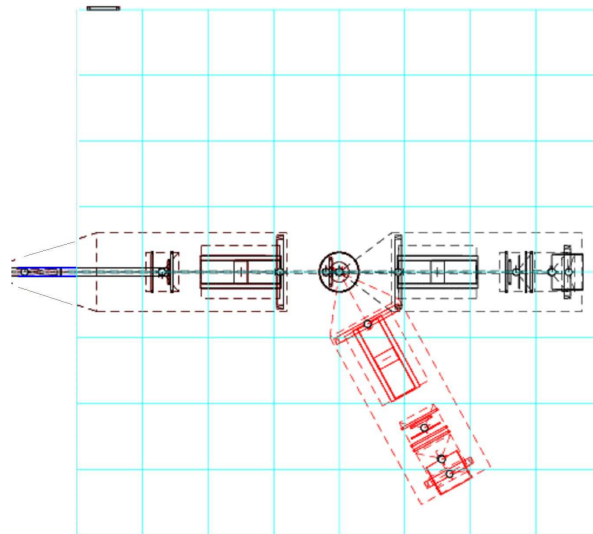


Fig. 17: Placement of solenoids on carriers in the experimental enclosure. The red sketch indicates the position of the second arm at $Q=8\text{nm}^{-1}$ with $\lambda=0.8\text{nm}$. The sign of the scattering angle may be chosen according to an optimisation of available space.

After traversing the last $\pi/2$ -flipper the neutrons enter a combination of background suppression collimator and analyser, before those with the right final spin polarization hit the detector. The scattering arm has to be rotated around the sample position in order to realize a reasonable momentum transfer (Q) range. This determines the lateral space requirement of the instrument. A full 90° scattering angle requires the (partial) use of one of the neighbouring sectors. Otherwise the instrument use has to be restricted to the SANS region and the dynamics therein.

The principle layout looks as follows. The high resolution, i.e. long Fourier-times, requires the exploitation of long wavelength neutrons up to 2nm or beyond. On the other hand the neutron pulse length is of minor importance. These facts leave a cold coupled moderator as optimal choice. Neutrons emitted from the cold coupled moderator are fed into a neutron guide system. The neutron optical system consists of a massive iron background reduction “collimator” respectively beam cross section limiter, followed by a Ni coated neutron guide starting with the shutter insert section. After the necessary windows and gaps for a first chopper it contains a 3.5° bend outside the target block at about 6m. The bend is effected by one of (2 or 3) polarizing microbenders, it moves the beampath out of direct moderator sight within the next meter. After the bend a guide field is needed to preserve the polarisation. At the end a tapered section with increasing cross section (!) is foreseen to reduce the divergence of the emitted neutrons - especially for long wavelength - and thereby receive a higher flux at the sample in about 3m distance. A system of a total of 3 disc choppers is used to select neutrons from one frame at a time only.

Further optical elements are the main collimator/analyser combination and optional analyser/ polarizer to be placed in the sample region in case that the optional intensity modulation mode is selected. For low Q-SANS an optional converging collimator in front of the sample is foreseen.

4.2 Beam transport

4.2.1 Guide system and polarizers

Overall Description

Figure 18 shows schematically the placement of guides and choppers in a very schematic way, it also illustrates the input for the MC simulations that were performed to estimate the flux at the sample position.

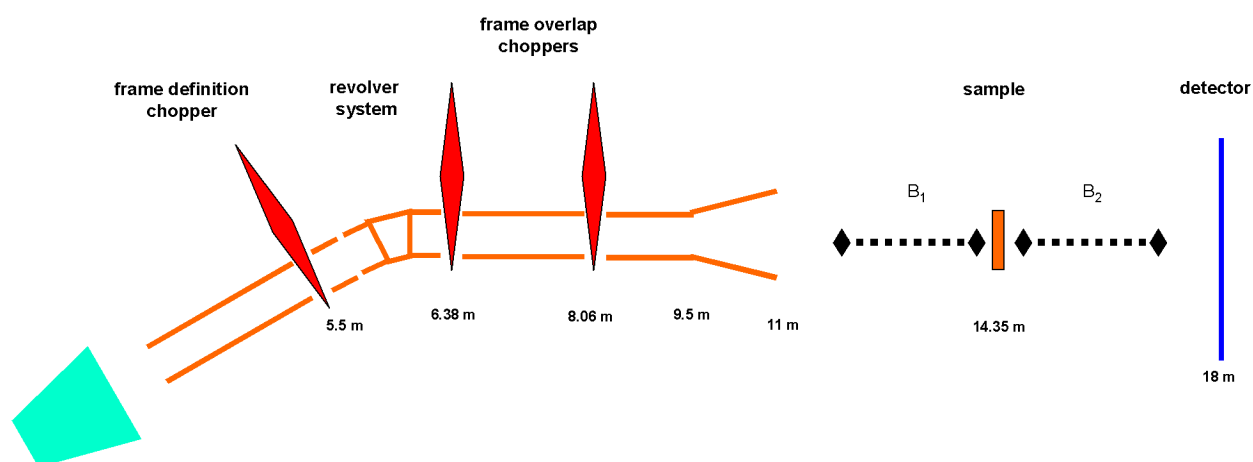


Fig. 18: The principle layout of the guide system. Starting with the moderator; at a distance of 2.5m the guide starts; three choppers are foreseen at 5.5m, 6.38m and 8.06m. The revolversystem with SM polarizers is positioned at 6.38m.

The neutron guide will consist of Ni on boron rich glass and has an inner cross section of 4cm width and 8cm height. The first section is located in the shutter insert and starts at 2.5m distance from the moderator.

Neutron guides outside the target block are contained in a vacuum housing. After the interfacing window at the exit from the target block a short guide section leads to the first chopper at 5.5m moderator distance. In the 0.86m gap between the first and second chopper the bend of the beam direction and the beam polarisation is performed. For that purpose a revolver containing different microbenders for different wavelength ranges with feeding neutron guide pieces is planned, see Figs. 20 and 19.

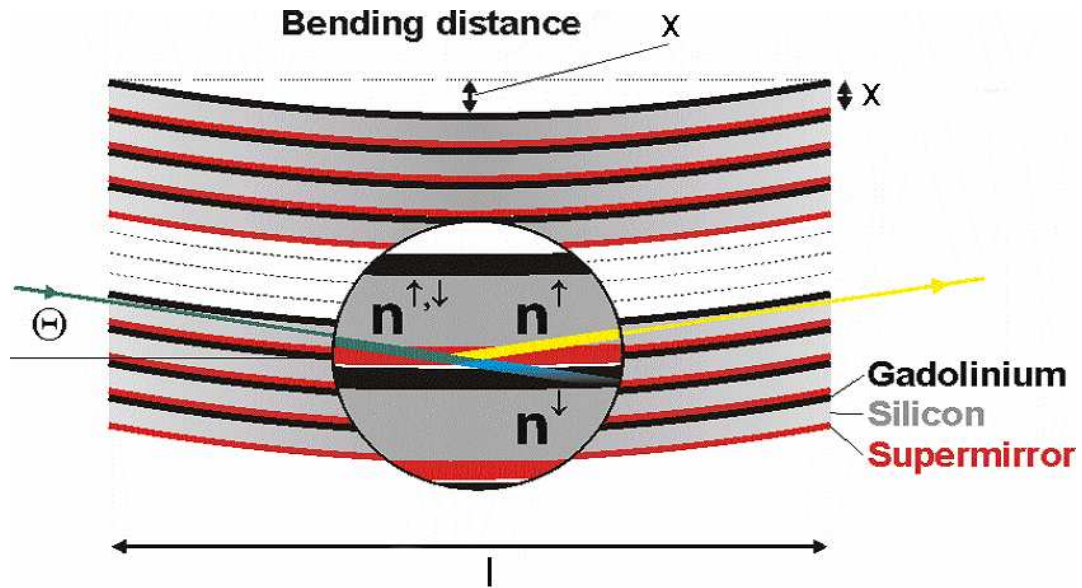


Fig. 19: Schematic display of the bender principle. An unpolarized beam is transmitted through the silicon layer. One spin direction (n^\uparrow) is reflected at the supermirror. The other spin direction (n^\downarrow) is absorbed in the Gadolinium layer.

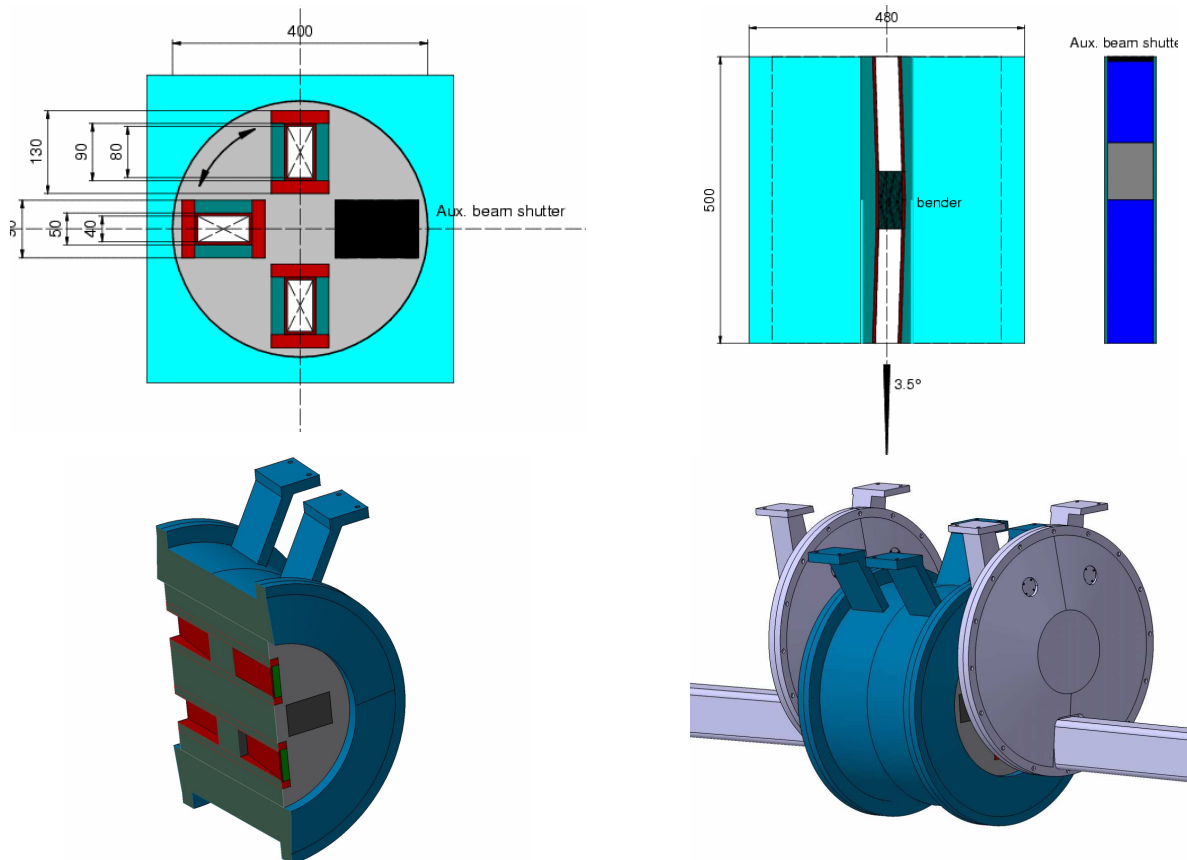


Fig. 20: Revolver system with the supermirror bender providing an inclination angle of 3.5° .

One position of the revolver may serve as auxiliary beam shutter. At and after the polarizing benders a guide field of several mT is needed to keep the polarization. Until close to the end of the guide section this is a

vertical transversal field generated by permanent magnets. Special attention is required to extend the guide fields across the chopper gaps.

The layout for the “revolversystem” looks as follows. It should be equipped with 3 short bend supermirror polarizers to cover the wavelengths range from 0.3(0.2)nm up to 3nm and an auxiliary shutter. 3 polarizers are designed for a deflection angle of 3.5° , their lengths range from 18cm to 3cm while the revolver drum has an overall length of 0.5m, the residual gaps are equipped with guide sections.

To get maximum transmission also for large wavelength the number of windows and air gaps in the guide system shall be kept as low as possible. In particular we aim for a construction that has a common vacuum in the guide, revolver and choppers.

The guide field is rotated to longitudinal direction and then generated by a wire wound around the guide (2 turns/cm, 10..20A).

Optimization by MC simulation – neutron guide

In Monte Carlo simulations the beginning of the guide was varied from 1 m from the moderator to 2.5 m. No significant change of the flux at the sample was found. Thus, the beginning was set to 2.5 m.

The guide after the last chopper – from 9.5 to 11 m from the moderator - was varied to increase the flux at the sample. It was divided into 3 pieces of 50 cm length. The sizes of these pieces were optimized to give the highest flux at the sample. A diverging exit as well as a converging exit was allowed and various shapes were tested.

The optimization was performed with a simulation of a band from 18.3 to 22Å. 29 Mio. trajectories were started and the simulation interrupted after the last chopper, where more than 0.5 Mio. trajectories were still in the simulation. The rest of the simulation was then performed several times with the varied parameters. This was done with different random seeds and different starting values.

The result was that the flux at the sample could be risen significantly – up to 16% especially at high wavelengths compared to a guide of constant size. The shapes are significantly different in both directions due to the larger height compared to the width. A similar gain is also found for other wavelength bands above 10 Å, because the divergence is similar. But for shorter wavelengths (with a smaller divergence), the diverging guide exit causes a decrease in the flux, especially in the range 5 – 9 Å. This loss could be diminished by using a guide of constant size for the third piece (10.5 – 11 m). Table 1 shows the results.

The optimal shape finally turns out to be a tapered guide section that approximates a parabolic/elliptic mirror which focuses a virtual source from inside the guide onto the sample position. That yields a gain –compared to a plain straight guide- of about 16% especially for long wavelengths (see table 1). The exit cross section of the neutron guide thereby increases slightly to 4.9cm x 8.5cm.

Since the 16% gain at large λ comes with a corresponding loss at medium wavelength a discussion is still needed to decide between a simple straight guide or the diverging variety, or whether a revolver option could be a solution.

Similar examinations for the first part of the guide gave no significant improvements by a converging or diverging entrance compared to a straight guide.

Instrument description

design: 3. piece constant	B x H [cm ²]			
	9.5 m	10 m	10.5 m	11 m
constant	4 x 8	4 x 8	4 x 8	4 x 8
weak div.	4 x 8	4.323 x 8.112	4.646 x 8.224	4.646 x 8.224
optim. div.	4 x 8	4.536 x 8.324	4.898 x 8.478	4.898 x 8.478

design: 3. piece constant	flux at sample [n/(cm ² s)]	rel. diff. to constant shape	flux at sample [n/(cm ² s)]	relative diff. to constant shape	flux at sample [n/(cm ² s)]	rel. diff. to constant shape	flux at sample [n/(cm ² s)]	rel. diff. to constant shape	flux at sample [n/(cm ² s)]	rel. diff. to constant shape
	2.0 -	5.7 Ang	5.0 -	8.7 Ang	11.0 -	14.7 Ang	18.3 -	22.0 Ang	29.3 -	33.0 Ang
constant	7.180e7	+/- 0 %	3.284e7	+/- 0 %	2.288e6	+/- 0 %	2.329e5	+/- 0 %	1.8464e4	+/- 0 %
weak div.	6.289e7	-12 %	2.823e7	-14 %	2.522e6	+10 %	2.630e5	+13 %	2.644e4	+12 %
optim. div.	6.039e7	-16 %	2.496e7	-24 %	2.656e6	+16 %	2.746e5	+18 %	2.745e4	+17 %

Tab. 1: Flux changes by a diverging exit of the neutron guide. Upper part: neutron guide cross sections at different distances of the source; lower part: resulting neutron fluxes in the different wavelength bands.

Optimization by MC simulation – bender

Polarizing benders as designed before were inserted into the simulation. The first effect is that the flux of the fast neutrons ($\lambda < 1\text{\AA}$) decreases. A few neutrons per second for the 2° benders and a few neutrons per minute for the 3° benders were found at the sample in the simulations. That corresponds to portions of about 2ppm (2° bender) and 0.01ppm (3° bender) for 20Å. For 30Å, it is one order of magnitude higher.

With the 3.5° and 4° benders, practically no hot neutrons were found at the sample.

The second effect is that the neutrons are polarized. In all cases, the polarization is already practically perfect behind the bender. All neutrons have an up-polarization except for the hot neutrons. Compact polarizing benders have a good transmission. Fig .21 shows the measured transmission for such a bender system.

For wavelengths below about 10Å, the beam divergence at the end of the guide is determined by the maximal angle that can be reflected at the guide, i.e. $0.1^\circ \cdot \lambda/\text{\AA}$. For higher wavelengths this is not true any more. Firstly the divergence is limited by the sizes of guide and moderator and their distances, giving a maximal value of 1.6° in horizontal direction. Secondly the bender restricts the divergence. Analyzing the horizontal flux distribution at the sample position gives divergences of 0.90° (2° bender), 1.43° (3° bender), 1.65° (3.5° bender) and 1.89° (4° bender), which corresponds to the typical reflection angles (cf. Table 2). This results in a decreasing ratio of neutrons hitting the sample to neutrons leaving the guide with increasing bender angle (and with increasing wavelength). This effect decreases the flux at the sample compared to the flux at the guide exit.

curvature of bender	int. flux at sample in band 2.0 - 5.7 Ang [n/(cm ² s)]	int. flux at sample in band 5.0 - 8.7 Ang [n/(cm ² s)]	int. flux at sample in band 11.0 - 14.7 Ang [n/(cm ² s)]	int. flux at sample in band 18.3 - 22.0 Ang [n/(cm ² s)]	int. flux at sample in band 29.3 - 33.0 Ang [n/(cm ² s)]
2°	9.643e07	3.815e07	2.248e06	2.119e05	1.957e04
3°	8.000e07	3.408e07	2.376e06	2.366e05	2.330e04
3.5°	7.180e07	3.284e07	2.288e06	2.329e05	2.355e04
4°	6.410e07	2.967e07	2.109e06	2.243e05	2.276e04

Tab. 2: Flux at the sample for different bender angles and different wavelength bands.

On the other hand, the transmission of the long wavelength benders increases with increasing bender angle, because the length and therefore the absorption decreases. This will increase the flux at the sample. So one expects an optimal bender angle, which is wavelength dependent. This is indeed found in the simulations

(see Table 2). For wavelengths below 10 Å the 2° bender gives the highest flux. Between 10 and 20 Å, it is the 3° bender and for even higher wavelengths, the 3.5° bender yields the highest flux. As it is our aim to render possible measurements with long wavelengths, the 2° bender seems not favorable. Additional disadvantages are the less effective suppression of fast neutrons and the deviation from the direct view.

On the other hand the angle should not be too large, because the flux below 5 Å is substantially less. So a bender of 3° or 3.5° seems to be a good compromise. For space requirements an angle of 3.5° is chosen, which is used in the following simulations.

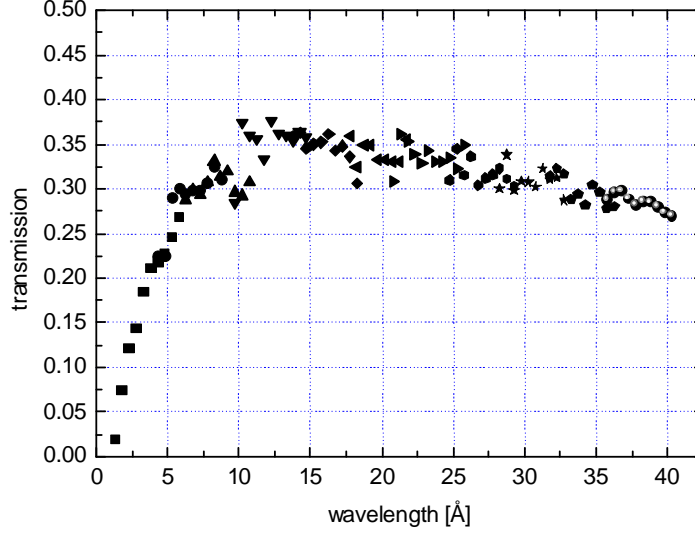


Fig. 21: Transmission measurement at a bender with an inclination angle of 3.5°. The transmission was calculated in terms of the flux ratio at the sample with bender to the flux at sample without bender. (An ideal bender would have a transmission of 0.5, as all spin down neutrons are absorbed.)

4.2.2 Chopper system

The shortest feasible moderator-detector distance is about $L=18\text{m}$, which has been chosen for the design of the proposed NSE instrument. Therefore the width of one usable wavelength frame is:

$$\Delta\lambda = \frac{h}{m_n v L} = \frac{65.93 \cdot 10^{-10} \text{ m}^2}{L} = 0.36610 \text{ nm} \quad (3)$$

I.e. independent of selected wavelength λ_0 the wavelength band is $\Delta\lambda=0.366\text{nm}$ (see Fig. 3). The simulated pulse width is $180\mu\text{s}/\text{nm}$ resulting in a wavelength resolution of $\Delta\lambda/\lambda \cong 0.5\%$. The resulting Q-resolution is much better than at reactor based instruments. In order to avoid T_0 pulse contamination effects within one wavelength band the default choice of the wavelength bands –as selected by chopper phasing- will be $n\Delta\lambda < \lambda < (n+1)\Delta\lambda$ for $n=0,1,2,3, \dots$

The chopper system consists of 3 disc choppers for the selection of a wavelength frame. A T_0 -chopper is not foreseen because the 3.5° bend in the guide system at 6m (i.e. in the chopper archway) leads to a blocking of the direct sight within the following meter.

The number and positions of the disc-choppers have been optimised in order to obtain a frame with minimal contamination by neutrons of undesired velocities. Particular emphasis has been put to the property that no wavelength **shorter** than those of the selected frame is transmitted. This is important since the long wavelength bands up to $\lambda=2\text{nm}$ (and more) are important to reach the highest possible Fourier times and at

the same time –unfortunately– have orders of magnitude lower flux than neutrons from the spectral maximum at 0.2-0.3nm. With the simple model that assume infinitely short neutron pulses a solution for the position could be found that only exhibits contaminations with $\lambda > 7\text{nm}$.

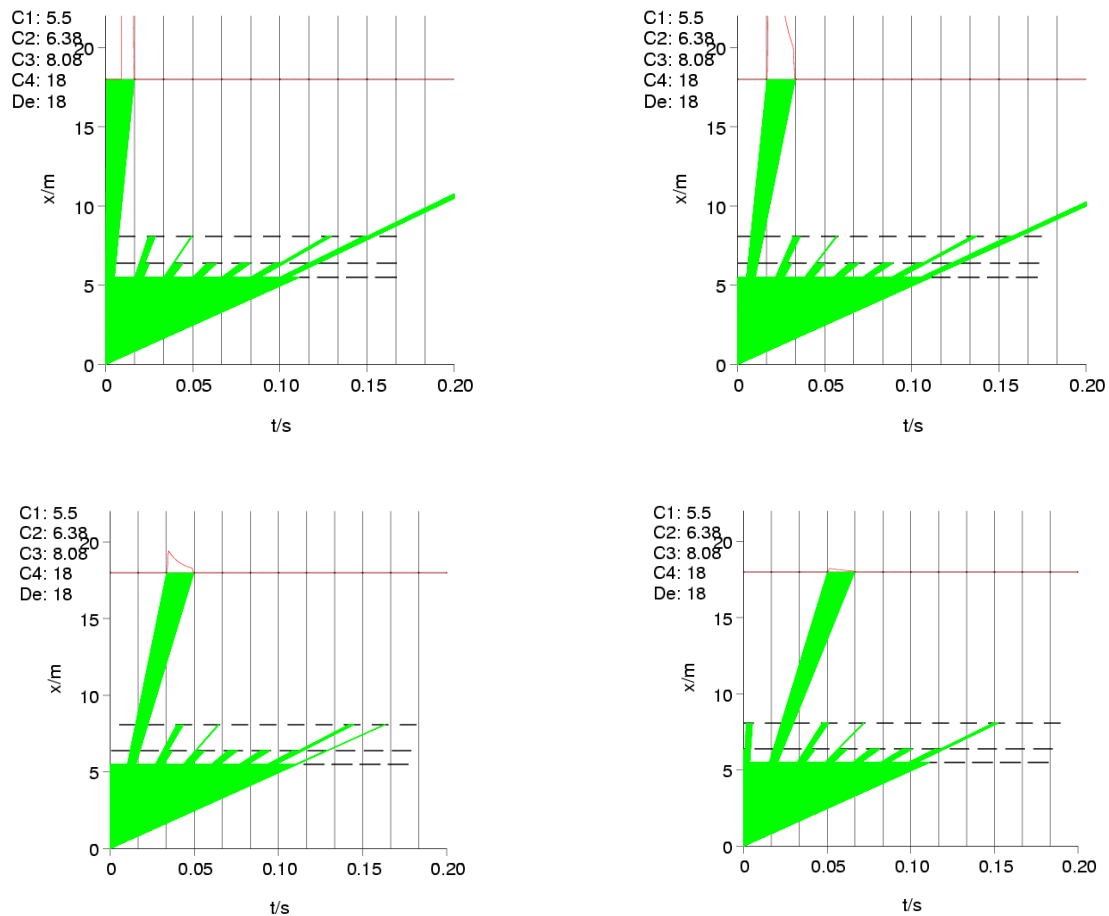


Fig. 22: Transmission patterns of the 3-chopper system for the first 4 frames. Note that a contamination only occurs with wavelength of 7nm and more. The positions of the choppers have been refined to distances of 5.5m, 6.38m and 8.08m from the moderator.

The resulting chopper - moderator distances are 5.5m, 6.38m and 8.06m. The exact moderator position may vary by 10cm without loosing the above property. These optimisation results have also been corroborated by Monte Carlo simulations (see Fig. 22) with realistic pulse shape.

MC Simulation on the chopper system

Further MC simulations have been performed on the comparison between a three and a four chopper system. The simulations were performed to check, if only neutrons of the desired wavelengths reach the detector. At first, an ideal absorption of the choppers was assumed. Chopper systems consisting of 3 and 4 choppers were examined.⁷ For the proposed instrument a three chopper system was selected. The 4th chopper would be located at 9.5 m from the source. A maximal evaluation time (of 13.08 ms) at the detector (without using the half shadow region) is reached for frame definition choppers between 165° and 190°. We used an aperture of 172° in the simulations. Depending on the performance costs optimization 4th chopper may be included to improve the frame definition. Openings and phases of the frame overlap choppers were chosen in a way that

⁷ The position of the fourth chopper also results from the optimization procedure for the chopper positions. For the ideal pulse case, however, it turns out that the 4th chopper will not catch any neutron. For a check of higher order effects it was included into the MC sequences to enable a comparison in a more realistic case.

they do not stop any neutron with a desired wavelength of the main part of the pulse ($t_{\text{start}} < 0.8$ ms) that is able to pass the frame definition chopper. In the simulations, the choppers have a radius of 35 cm, the beam passes 30 cm from the center of rotation. A realistic absorption inside the chopper material is assumed. The guides have a usual Nickel coating. A waviness of 0.005° and abutment losses at the ends of guide segments are included in the simulation.

The MC result with the Software Vites [40] corroborates that the 4 choppers would prevent frame overlap perfectly. No neutron with a wavelength different to the selected frame reach the sample. With three choppers, a small contamination (with wavelengths about 9 Å above the desired band) was found (see Fig. 23). The portion of wrong wavelengths was between 1.4 ppm (9.2 Å) and 12.3 ppm (34.8 Å). This contamination is negligible for spin echo experiments. Therefore we decided for a system with 3 choppers placed at 5.50m, 6.38m, and 8.06m with apertures of 107° , 121° and 148.5° is a good solution.

If the same simulations are performed with non-ideal absorption in the choppers and with a straight instrument, one gets neutrons from the band $\lambda < 0.1$ nm that pass all choppers. However because of the cut-off of the benders these neutrons are efficiently removed.

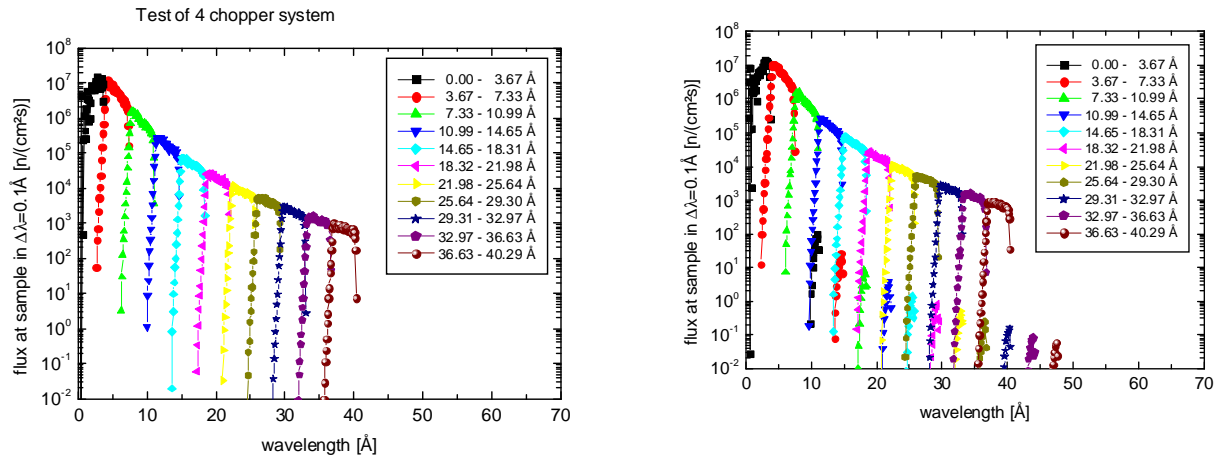


Fig. 23: Left side: the transmitted intensity for the 4 chopper system. Right side: the corresponding data of the selected 3 chopper system.

The beam-line of the instrument was simulated using the Monte Carlo package Vites [40]. These simulations include the source, the guide system, a polarizing bender, and disk choppers. The input parameters are displayed in Tab. 3.

The aim of most of the simulations was to determine the flux at the sample as a function of wavelength. Instrument parameters were varied to achieve a highest flux at the sample. But we also paid attention to the polarization and the fraction of not desired wavelengths (see above). Fig. 18 shows a schematic drawing of the instrument as used in this simulation. Usually $5 \cdot 10^8$ trajectories are started in a run, of which typically 50000 reach the sample. Gravity is included in the simulations.

As has been pointed out a three chopper system is sufficient for operation of the NSE spectrometer with any wavelength frame. Nevertheless all following simulations were performed with the additional 4th chopper added to the system in order to be able to detect further small effects without being influenced by the small chopper leaking.

Instrument description

	Position [m]	simulation of short wavelengths example: 2.0 - 5.7 Ang	simulation of long wavelengths example: 14.7 - 18.3 Ang
Source Moderator	0.0	SPSS 60 Hz Hydrogen, coupled, 10x12 cm ²	SPSS 60 Hz Hydrogen, coupled, 10x12 cm ²
Wavelength [Ang]		0.0 - 44.0; div. 4.671.1°	0.0 - 44.0; div. 4.671.1 °
Pulse Lengths [ms] (end/max)		0.8 / 3.3	0.8 / 3.3
Guide	2.50 - 5.50	straight, m=1, 4 x 8 cm ²	straight, m=1, 4 x 8 cm ²
Chopper 1	5.50	single disc, 107° 3600 rpm, -123.51°	single disc, 107° 3600 rpm, -143.54° 1R
Guide	5.50 - 5.88	straight, m=1, 4 x 8 cm ²	straight, m=1, 4 x 8 cm ²
Guide	5.88 - 6.xx	straight, m=1, 4 x 8 cm ²	straight, m=1, 4 x 8 cm ²
Bender	6.xx - 6.yy	2°; 0.15 mm wavers R=256 cm, L= 8.94 cm FeCo, m=2.0; 600 nm Gd	2°; 0.15 mm wavers R=100.5 cm, L= 3.51 cm FeCo, m=2.0; 600 nm Gd
Guide	6.yy - 6.38	straight, m=1, 4 x 8 cm ²	straight, m=1, 4 x 8 cm ²
Chopper 2	6.38	single disc, 121° 3600 rpm, -141.88°	single disc, 121° 3600 rpm, -222.72°- 1R
Guide	6.38 - 8.06	straight, m=1, 4 x 8 cm ²	straight, m=1, 4 x 8 cm ²
Chopper 3	8.06	single disc, 148.5° 3600 rpm, -176.97°	single disc, 148.5° 3600 rpm, -13.89°- 2R
Guide	8.06 - 9.50	straight, m=1, 4 x 8 cm ²	straight, m=1, 4 x 8 cm ²
Chopper 4	9.50	single disc, 172° 3600 rpm, -207,04°	single disc, 172° 3600 rpm, -143,46°- 2R
Guide	9.50 - 11.00	straight, m=1 4 x 8 cm ²	straight, m=1 4 x 8 cm ²
Sample	14.35	2.8 x 2.8 x 0.2 cm ³	2.8 x 2.8 x 0.2 cm ³
Detector	18.0	30 x 30 cm ² eval.: 10.93 - 24.02 ms	30 x 30 cm ² eval.: 68.52- 81.60 ms

Tab. 3: Data input for the MC instrument simulation.

4.3 Magnetic Layout

The magnetic layout basically consists in determining the positions and parameters of a number of solenoids and other functional magnetic devices such that proper NSE operation of the instrument is ensured for all wavelength and all optional modes. The required properties as highest resolution, $\Delta\Omega=2.5^\circ \times 2.5^\circ$ detection solid angle and a short moderator detector distance (here $L=18\text{m}$) imposes conditions on the length of solenoids and distances between elements as well as on the magnetic field. In particular a field integral of at least of 1Tm has to be achieved. At the same time the field at the flipper positions and at the sample has to stay around a few times 0.1mT . The resulting magnetic landscape may not contain points of rapid field direction changes along the neutron path (zero crossings) in order not to depolarise the beam.

Flippers are the only elements where so-called non-adiabatic spin rotations are desired, they form the start and stop position for precession angle accumulation on the respective parts of the neutron paths. The standard configuration has a $\pi/2$ -flipper (start) at the entrance into the proper NSE spectrometer and one (stop) at the exit in front of the analyser detector combination. A π -flipper close to the sample effectively reverses the precession angle. The optional modes require additional $\pi/2$ -flippers in the sample gap, which has to enlarge to $2 \times 0.9\text{-}1\text{m}$ to enable this compared with the absolute minimum of $2 \times 0.7\text{m}$.

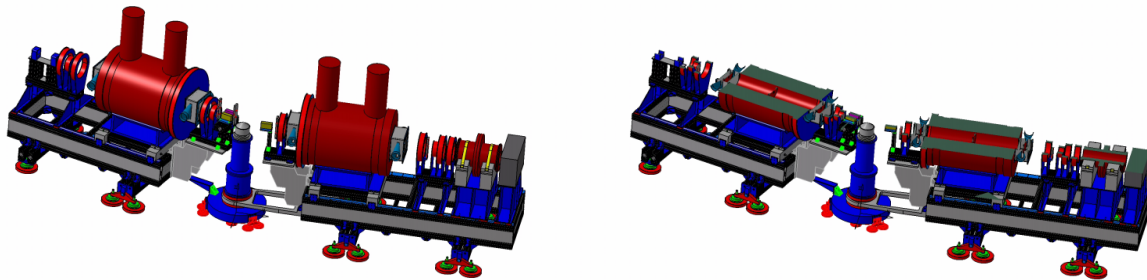


Fig. 24: Left side: the instrumental magnetic part. Right side: horizontal cut through the scattering plane.

It is not sufficient to supply a field integral of $J=1\text{Tm}$ but the variation of J , ΔJ between different paths in the neutron beam must stay below 10^{-6}Tm , i.e. $(\Delta J^2)^{1/2} < 10^{-6}\text{Tm}$ [17]. This may only be achieved by the insertion of correction elements (“Fresnel”-coils [3,11,12]) into the beam path. The mechanical design may not contain ferromagnetic parts and must ensure high position stability, in particular with respect to the relative positions of the “Fresnel”-coils and the associated main precession solenoid.

For longer wavelength a correction of the distortion due to gravity induced parabolic neutron paths is provided by current sheets in the beam path. Only flippers and these current sheets will be operated with time varying currents appropriate to $\lambda(t-t_0)$ at the respective positions. For flippers this operation mode has been experimentally verified at the IN15 (ILL,HMI,FZJ) [137].

4.3.1 Solenoids and Fields

The basic scheme of the proposed instrument is displayed in Fig. 24. The set up is closely related to the design of the Jülich NSE instrument [12] with two important changes and a number of changes to cope with the pulsed source and improvements to enhance resolution. The most important change is the use of fully compensated and shorter main precession coils that are able to provide a larger field integral (up to 1.5Tm). This is only feasible if the main coils are superconducting. The other prominent change is the inclusion of several options, in particular ferromagnetic and intensity modulated that pose additional constraints on the sample gap and the magnetic field therein. To realize the high resolution newly optimized “Fresnel”-coils with improved mechanical accuracy and stability will be installed on very precise positioning devices.

Even with the chosen type of compensation there must be room where the large inner field ($\sim 1\text{T}$) decays to the mT level which is compatible with flipper operations. This limits the closest distances to $0.7\text{-}0.8\text{m}$ on both sides of the main precession coils. To gain space for the optional modes a distance of 0.9m is chosen in the sample region. The length of the main solenoids is chosen as 1.2m . The active length from $\pi/2$ -flipper to $\pi/2$ -flipper of the spectrometer therefore is $2 \times (2.8\text{-}3.0\text{m})$. The arrangement of collimator analyzer and detector needs about 1m . The active detector plane will have a [nominal] distance of 4m from the sample, i.e. the sample-moderator distance is 14m . The feeding neutron guide ends a few cm in front of the first $\pi/2$ -flipper, i.e. at 11m .

Besides its influence on the total length of the spectrometer, the strong compensation of the main coils has other important advantages:

1. Reduction of the field at the walls of the spectrometer enclosure down to a value that allows for a closed magnetic shielding to be combined with the enclosure.
2. Decoupling of the spectrometer arms such that the mutual asymmetric influence stays low even at higher scattering angles.
3. Ease of operation due to the fact that currents of many other coils depend only weakly on the main solenoid settings.
4. Robustness of the signal against relative mechanical movements of the main solenoid sets and external coils and flippers. A property that contributes much to the final quality in terms of stability and reproducibility of echo-amplitudes.

The correction coils, however, must be very accurately (within $30\mu\text{m}$) and stable positioned in the directions perpendicular to the main magnetic axis. They will be fixed on the end plates of the main solenoid cryostat that serve as mechanical reference with respect to the coil set inside. The (outer) ‘‘Fresnel’’-coils are equipped with a positioning device with μm precision.

Fig. 25 displays the placement of solenoids and other magnetic elements.

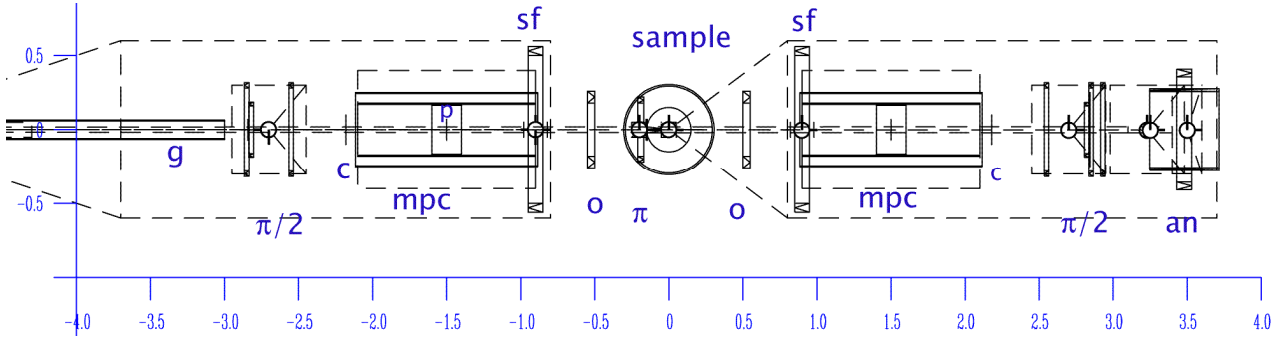


Fig.25: Layout of the solenoid positions and sizes (scattering angle= 0°), g: guide field coil, $\pi/2$: $\pi/2$ -flipper and ring coils for longitudinal field component, c: main correction (‘‘Fresnel’’) coil, mpc: compensated set of main precession coils (note: only windings are shown, i.e. not cryostat), p: phase coil winding, o: compensation for optional modes+optional $\pi/2$ -flipper, sf: sample space field coils, an: analyzer field coils. The scale shows the distances from the sample position in meters.

The axial field for a low and the highest Fourier time along the instrument is shown in Fig. 26 note that the low field section around flippers and the sample are obtained for both (and all intermediate settings) without the occurrence of field zeroes.

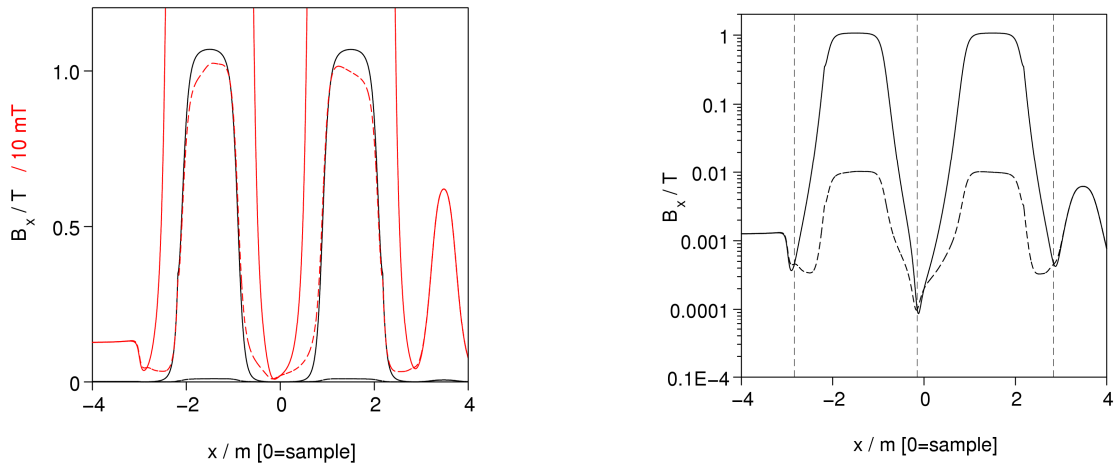


Fig. 26: Axial field component along the instrument axis (scattering angle= 0°) in the standard configuration, the dashed curves correspond to 1% of the highest Fourier time (solid lines). The red lines in the left part are multiplied by 100, the right part displays the same data on a logarithmic scale. The vertical dashed lines indicate the flipper positions. The constant level at $x=-4\text{m}$ represents the neutron guide field, the hump at $+3.5\text{m}$ stems from the analyser.

For the optional modes an extended zero field region in the sample gap is required, which may be obtained by additional current loops at $\pm 0.545\text{m}$ distance from the sample, as can be seen in Fig. 27. an extended flat low field region may be obtained.

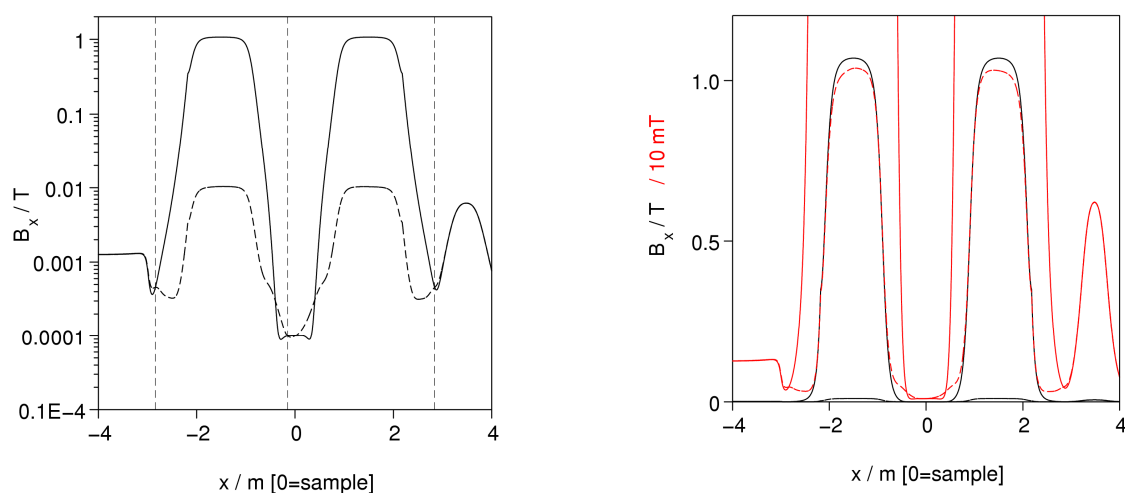


Fig.27: Axial field pattern as in Fig.26 but with additional current loops to enable the optional modes.

The resulting flipping efficiencies (at the highest resolution=most difficult situation) for the two configurations are illustrated in Fig. 28. In terms of the development of the spin projections on the magnetic field as obtained from a simulation using the Bloch/Larmor equation for the spin rotations. Results are given as red lines, optimal operation shows as transition from +1 to -1 at the π -flipper position for the longitudinal projection and 0-0 for the transversal projection.

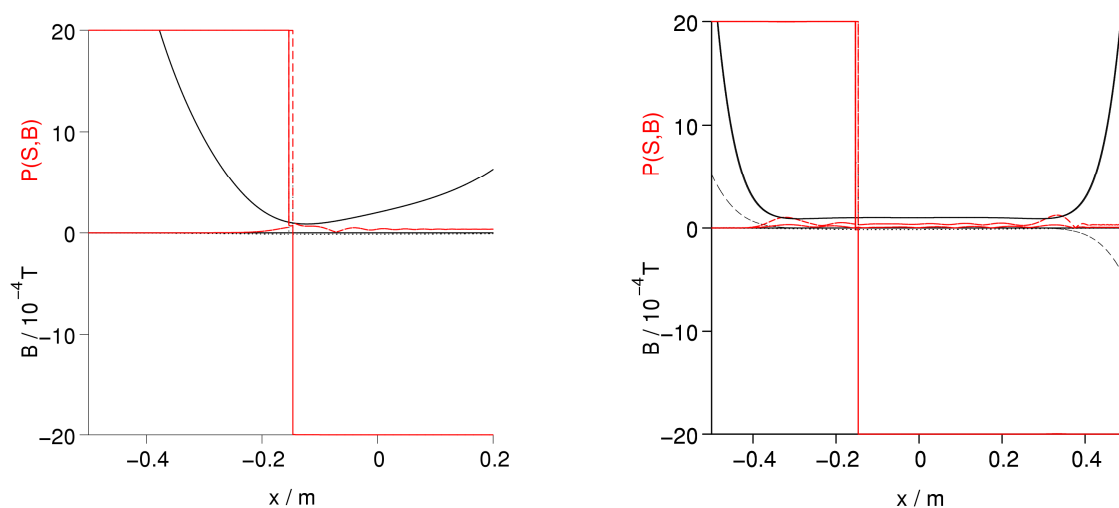


Fig. 28: π -Flipper operation in the low field region around the sample, left side: standard configuration, right side: with additional compensation loops as needed for the optional modes. The transition (red solid line) from +1 to -1 at the flipper is nearly perfect. The transversal projections which are more sensitive show marginal depolarisation effects (wiggles around zero, ideal would be zero).

Details of the coil arrangement and the resulting field patterns are shown in Fig. 29, the situation with extra compensation for the optional modes is displayed. The “normal” configuration is obtained by just omitting (disconnecting) the extra loops. Note that large scattering angles do not lead to any problematic field situations the flipping efficiency (due to transport through the low field region) is still better than 0.999.

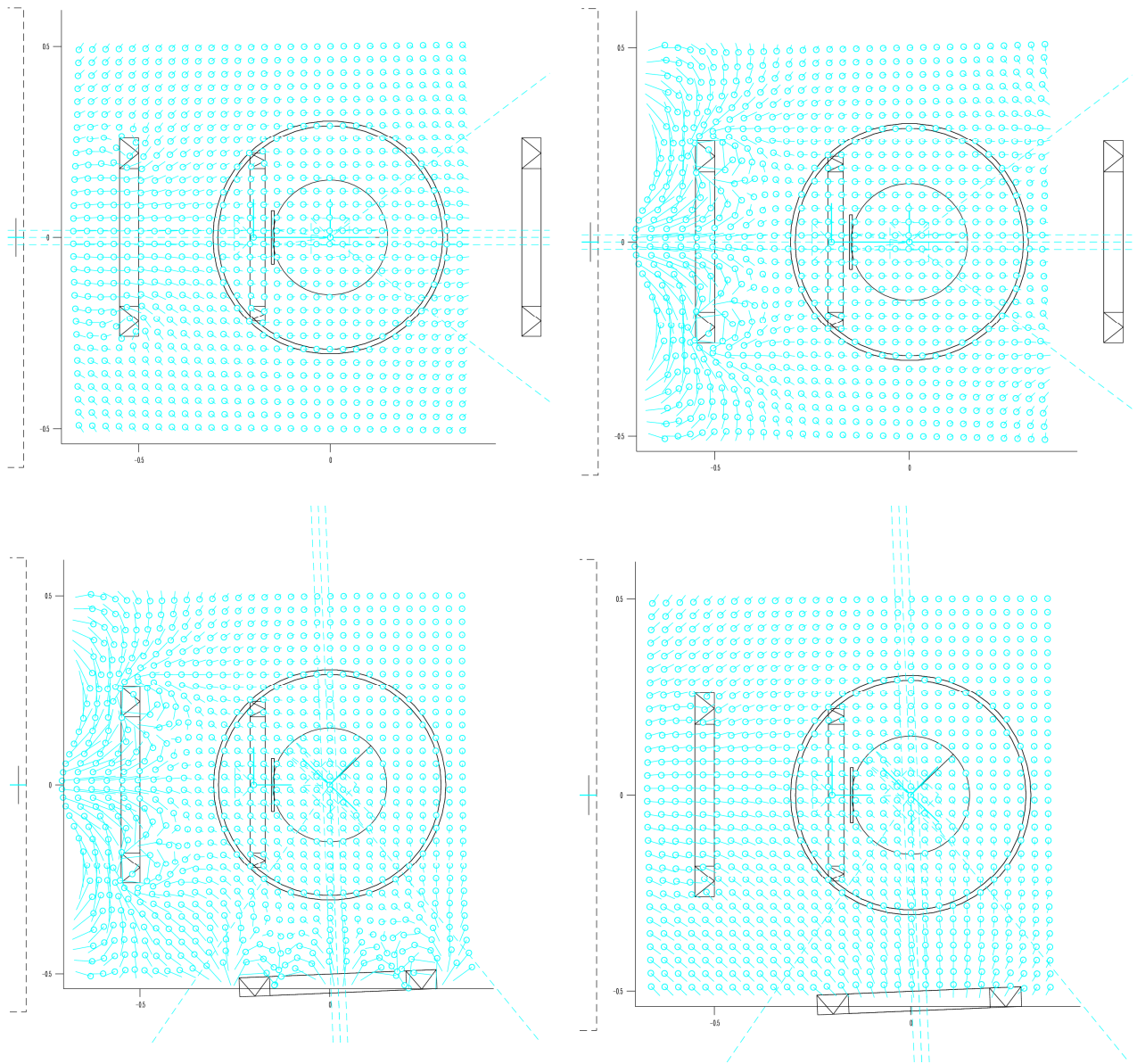


Fig.29: Field patterns in the sample region around the π -flipper position ($x=-0.15\text{m}$). The field vectors are shown in cyan with a circle indicating the base point. The values correspond to the length. It is 10^{-4}T at $x=(0,0)$. The left part shows the situation for low main solenoid field and the right part for maximum main field, the upper two parts are for 0° scattering angle, the lower parts for 88° .

4.3.2 Superconducting Main Solenoids

The superconducting magnet system is the heart piece of the instrument. Except for a few experiments with a three – axis spectrometer add – on [21] the experience with a NSE set-up using SC solenoids to boost magnetic field integrals is limited [22].

NSE requires the magnetic field integral over flipper - flipper paths in each of the spectrometer arms to be the same for all neutron trajectories. For a straight beam the highest possible field symmetry is cylindrical which imposes the use of solenoids as magnets.

A major novel design goal for a next generation spin – echo spectrometer is the use of SC main solenoids providing a field integral $J \geq 1 \text{ Tm}$ (IN15: $J_{\text{max}}=0.27\text{Tm}$). In a compensated set – up of the precession coils two outer additional compensation coils surround the inner ones and generate an opposite field to avoid magnetic stray field of the precession coils. Due to the much smaller space filling of the windings, SC coils allow for a coil geometry that enables optimal compensation of stray fields. Consistently low stray fields enable the use of a magnetic shielding enclosure of reasonable size that decouples from external field disturbances and thereby provide stable operation of the instrument.

At pulsed spallation sources (especially with higher repetition rates) the moderator-detector distance, i.e. the total length of the instrument, must be kept short to keep a large useable wavelength bandwidth. Therefore shorter precession coils with the same magnetic field integrals yielding a shorter length of the whole instrument are of advantage.

Also the superconducting magnet system allows for optimal compensation. Fig. 30 shows the magnet system simulated with and without compensation. The compensation is required for highest scattering angles (see also Fig. 50) and to avoid cross talk between the two precession coils.

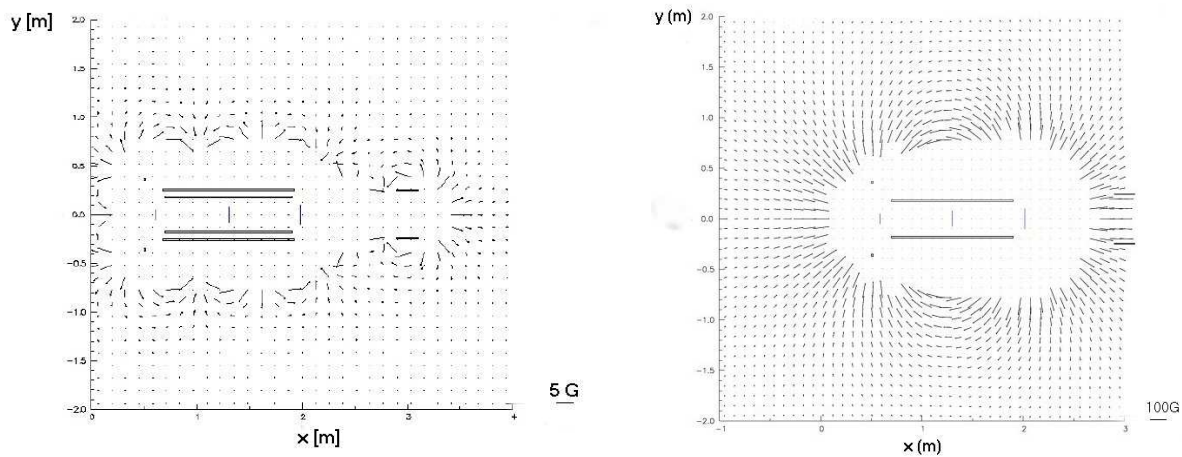


Fig. 30: On the left side the simulation of the magnetic landscape has been plotted with compensation. The right plot shows the same configuration without any compensation. Obviously at a certain distance to the superconducting magnets the compensated set – up shows a much smaller stray field at the same field integral. Note the different scales of the field vector length.

4.3.3 Effect of hysteresis fields

To estimate the effect of hysteresis fields due to flux pinning in the superconducting coils the following procedure has been used. First the magnitude and general shape of the hysteresis fields have been inferred from the measurement of the field left in a small test system (3 ring coils of about 10cm diameter) after going to high field and then to zero current. The result is shown in Figure 31, the field amplitude close to the windings reaches about 6 to 8 Gauss. It can be modelled by antiparallel coil-like extra currents within the winding volume. The net current around the axis must be zero.

Instrument description

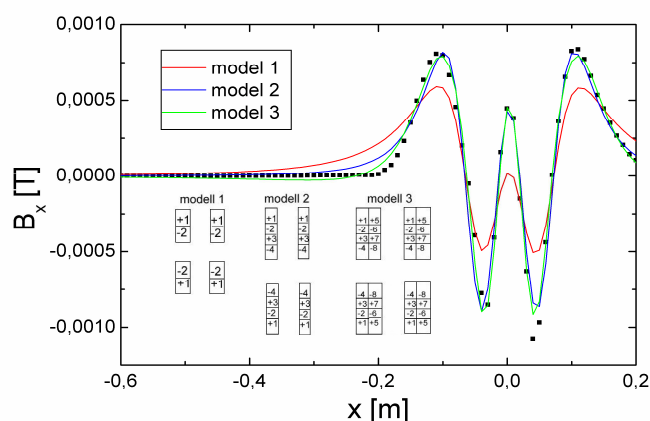


Fig. 31: Hysteresis field and model fittings; x is the axial direction.

To estimate the role of this effect on the final solenoid settings needs some modelling of an extra field of corresponding topology and magnitude added to the standard solenoid field. Since the winding thickness is small this has to come from closely counter rotating extra currents. A simple model that reproduces the expected topology of the extra field is a sequence of parallel and anti-parallel ring coils within the volume of the main coils. For the present test they were concentrated at the ends. The resulting field traces of the resulting extra field components is shown in Figure 32. The general topology of the field is analogous to the hysteresis field of the small test system.

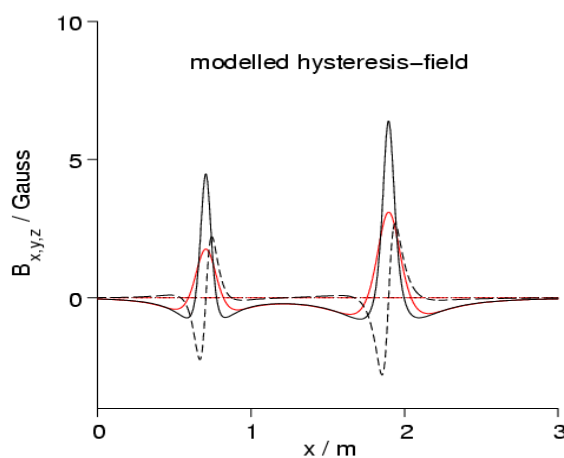


Fig. 32: Modelled “hysteresis” field for the main coil settings, red central path, black path 10cm off center, solid lines: axial components.

To check now the influence of field components of this type on the field integral homogeneity and the field integral a simulation for a situation with field integral $J=1\text{Tm}$ has been performed and correction elements have been optimised and included. In the next step the above hysteresis field multiplied by a **factor 10** (1) has been added and the field integral homogeneity has been computed with unchanged correction coils. This leads to reduction of homogeneity down to 10^{-5} . However, readjusting the currents through the correction elements by a few 10^{-3} can restore the homogeneity. Since we increased the expected fields by a factor of 10 to make the effects better visible, this is a reassuring result.

The field integral itself is changed by 0.7Gm ($\sim 10^{-4}$) for the 10 fold magnified field. However, only the difference between both main coils is important here, as soon as both coil settings are reproducible and equal only a small fraction of the above value may remain and cause some phase shift, which would be dealt with by the evaluation procedure.

The reproducibility of field values after corresponding histories (in one coil) have been checked and found to be better than the accuracy of the magnet and current sensors. These results indicate that effects of hysteresis fields on the field integrals are considerably lower than the possible field value differences at specific points (see figs.31, 32). With a careful symmetric design of the main solenoid their effect is compatible with NSE operation.

4.3.4 Correction Elements

Field integral inhomogeneities in a standard solenoid are dominated by path differences between the central path of the neutron and divergent paths especially those that hit the periphery of an area detector. For those configurations the field integral homogeneity is hardly better than 10^{-3} . Fortunately the inventor of the NSE – method already invented the so-called Fresnel coils, which will correct the magnetic landscape for each neutron trajectory also hitting the periphery of the 2D - detector.

Different designs exist to realize such Fresnel coils. The ILL spectrometers IN11 as well as IN15 use printed circuit type spirals of copper foil on kapton at the beginning and at the end of each main precession coil. Unfortunately this technique is limited by the current carrying capability of the copper foils. The FZJ-NSE spectrometer uses three aluminium Fresnel coils with a parabolic thickness modulation as could be seen in Fig. 33. Currently these are limited by finite manufacturing accuracy. A complete description of the theory and the use of the Fresnel coils can be found in references [12, 11]. The value of the average relative spread (ARS) $\delta = \sqrt{\sum_i (J_i - J_0)^2} / J_0$ is a measure for the quality of correction, where J_i denotes the field integrals for different neutron trajectories and J_0 the field integral of the symmetry axis of the precession coil.

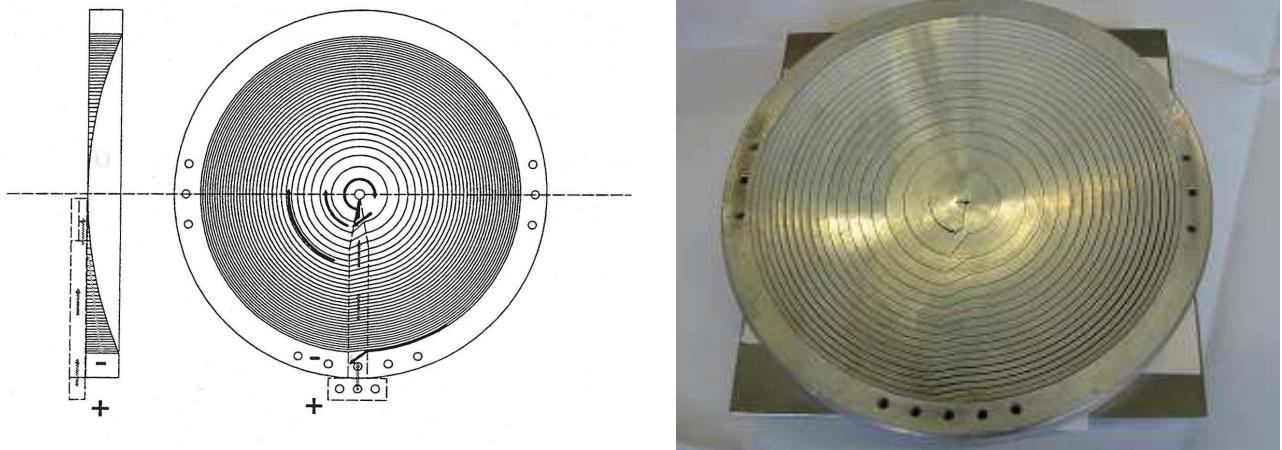


Fig. 33: Correction coil made of aluminium to improve the homogeneity of the field integral J . Left frame shows a schematic picture of the Fresnel coil which also shows the so called contact finger to provide the coil with an inlet and outlet of the current. The shape of the coil strictly must follow predetermined values. The right frame shows a prototype of such Fresnel coils.

The limit for the acceptable variation of J can be inferred from the drop of the echo signal due to the corresponding dephasing amounts to not more than $1/e$. For a maximal wavelength $\lambda \leq 2.5\text{nm}$ and field integral $J_0 = 1\text{Tm}$ this requires an ARS $\delta_{\text{max}} < 8 \times 10^{-7}$. Thus highly precise correction elements have to be developed. In addition, correct and stable positioning with respect to the windings of the main solenoid set

has to be provided. Displacements might appear due to thermal drift during normal operation. Also the effect of tilts has been studied and results are shown in Table 4 below.

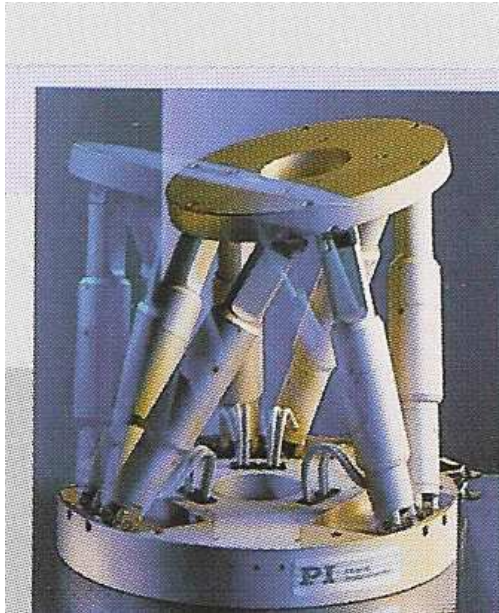
F. coil 1: d=0.05m $\varphi_1=\varphi_2$ [°]	F. coil 2: d=0.075m $\varphi_1=\varphi_2$ [°]	F. coil 3: d=0.01m $\varphi_1=\varphi_2$ [°]	δ
0.1	0	0	$1.07 \cdot 10^{-7}$
0	0	0.1	$9.7 \cdot 10^{-7}$
0.5	0	0	$4.9 \cdot 10^{-7}$
0	0.5	0	$3.14 \cdot 10^{-7}$
0	0	0.5	$4.9 \cdot 10^{-6}$

Tab. 4: Increase of the average relative spread (ARS) of the field integral in dependence of tilts φ of the Fresnel – coils. d: denotes the diameter of the Fresnel - coils.

A method to calculate Fresnel coils has been described in [11, 12] where the Fresnel coils have been modelled in terms of a thin radial current distribution function

$$\mu_0 j_{CCx}(r) = 2A_{CCx}^2 r + 4A_{CCx}^4 r^3 + 6A_{CCx}^6 r^5 \quad (4)$$

with A_{CCx}^2 , A_{CCx}^4 and A_{CCx}^6 as coefficients of this current density distribution. Whereas previous optimisation assumed infinitely this radial current distribution while a full optimisation including the thickness modulation is possible. In the optimisation of the homogeneity of the field integral, the field of the Fresnel coils are included in the field integral computations using the polynomial coefficients from each previous iteration step. In each iteration step the coefficients are refined according to the method described in [12]. Subsequently the ARS has been calculated while tilting the Fresnel coils.



Technical specifications:

20kg maximum weight mountable perpendicular

Positioning:

Travel x,y,z [mm]: $\pm 50, \pm 50, \pm 25$

Repeatability x,y,z [μm]: $\pm 2, \pm 2, \pm 1$

Travel $\theta_x, \theta_y, \theta_z$ [deg]: $\pm 15, \pm 15, \pm 30$

Repeatability $\theta_x, \theta_y, \theta_z$ [μrad]: ± 20 each

Fig. 34: Hexapod arrangement for accurate positioning of the Fresnel coils relative to the beam and the windings of the superconducting main solenoid. (from the Physics instruments catalogue).

It has been shown that tiny changes of the correct positioning and the tilts (see Table 4) are responsible for the non – existing homogeneity of the field integral J. For example a positioning $30\mu\text{m}$ perpendicular to

the symmetry – axis of the Fresnel coil also delivers an ARS of about $\delta=2 \cdot 10^{-6}$. These results show that a highly precise positioning of these coils especially at highest field integrals J_{\max} . For those reasons the final NSE spectrometer has to be equipped with a highly accurate positioning device. In first considerations a so called Hexapod from Physics Instruments might be a proper solution (see Fig. 34). However, as those hexapods are not amagnetic but can be improved to these features by further invested development work.

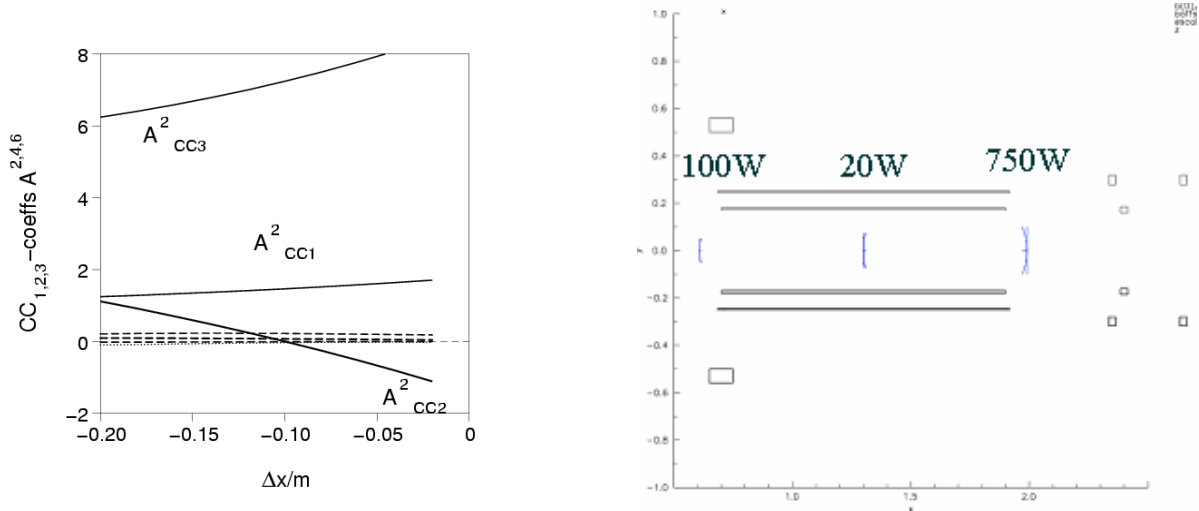


Fig. 35: Left side: example how the most important coefficient of the current distribution function varies while depositing both outer coils simultaneously to the outer part of the main precession coils (Δx). Right side: energy consumption of the three Fresnel coils in one arm of the instrument. The set up was optimized to low energy consumption of the central Fresnel coil.

The correction coil positions of the final instruments will be determined such that significant currents in the central Fresnel coil are avoided. For this purpose the outer Fresnel coils can be drawn simultaneously outside the inner bore and gain in current to correct the field integral. While calculating the energy consumption of the set – up one recognizes a significant power consumption in the third Fresnel coil (see left plot in Fig. 35: 750W). The condition of correct positioning still holds and one has to care about the thermal drift of these systems especially for the third Fresnel coil. Thus both outer coils will be equipped with a cooling mechanism (see Fig. 36).

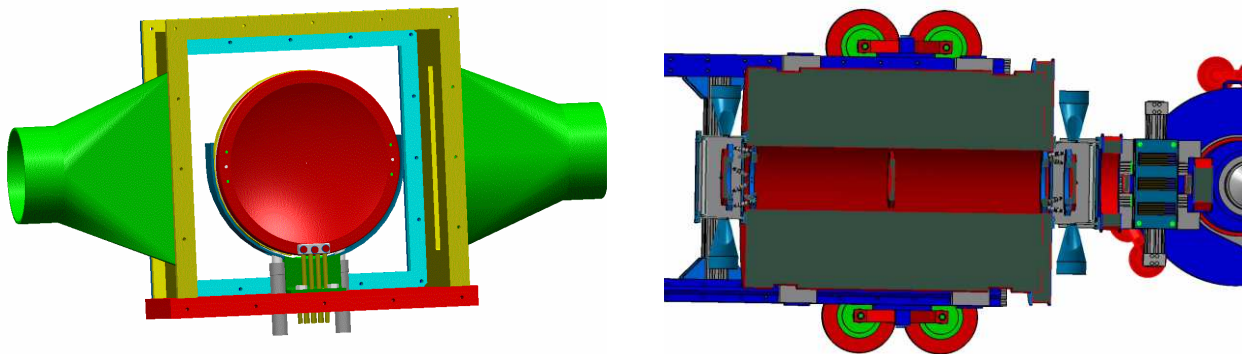


Fig. 36: The left design shows the principle layout for the cooling concept of the correction elements. The right drawing shows the correction coils at positions inside and outside the inner bore of the superconducting magnet. The cooling concept involves a gas air blower (cooling gas) which circulates gas through the correction coil box with a high volume stream.

Additionally, to correct these highest fields imposes a variety of tasks to be considered. Thus the development of correction elements is currently object of the European FP5 and will be included in the European FP6 program. Our interest is to develop and improve correction elements for the correction of magnetic fields of the order of $J=1\text{Tm}$ to achieve a field homogeneity of the field integral J for different neutron paths of about $\Delta J/J < 10^{-6}$.

To improve the manufacturing accuracy and stability the coils will be fixed on a Al groundplate.

4.3.5 Flippers

To cope with the varying $\lambda=\lambda(t)$ the Flipper fields have to vary synchronously. To avoid high inductancies and mutual inductive coupling only flippers and no longitudinal field coils can be ramped. Fig. 37 shows the spin precession in dependence of the internal magnetic field vector B_{int} to simplify the function principle of this device.

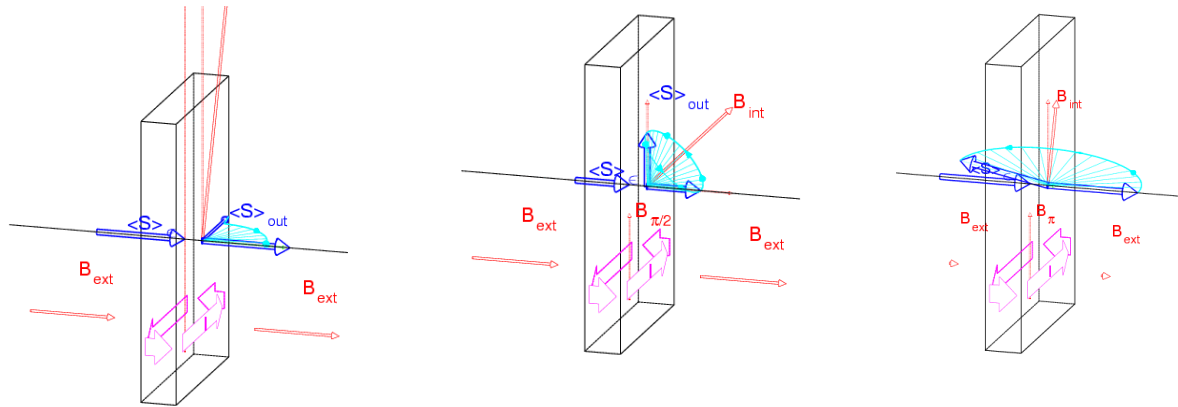


Fig. 37: The spin precession in dependence of the direction of the magnetic field vector. The left plot shows the neutron spin propagating through the in beam device performing a $\pi/2$ flip for shortest wavelengths of the selected frame using a high internal field. The middle plot shows the function principle for a $\pi/2$ - flipper in which the spin turns perpendicular to the propagation direction for the longest wavelengths of the selected frame. The right plot displays a π - flipper which turns the spin against the propagation direction.

First experiments have been performed to show that a TOF operational mode is possible [18]. The flipper operation for varying $\lambda(t)$ is shown in Fig. 38. Once the flippers are - set up, we can test whether we have an echo. On one of the precession solenoids we have a small number (N) of extra turns wound around, in which we can scan the current (phase current). This changes the symmetry of the field integrals, thus we can scan around the exact echo condition and measure the familiar echo group.

In different time channels of the detector we will have different wavelengths. On Fig. 38 the 2D - image shows the echo oscillations normalized to the beam polarization. Two cuts at 9\AA and 15\AA are shown as well. The longer the wavelength, the faster it oscillates, as a given step in phase current (ΔI) changes the field integral by $2\pi N/I$ and the change in precession phase is proportional to the wavelength. The spin precession angle is directly proportional to the wavelength, the number of turns and the current. At lower wavelength we have also more oscillations reflecting a better monochromatization. The periodicity of the echo group depends on the mean wavelength, the envelope is the Fourier Transform of the wavelength distribution. The information we are interested in $S(Q,\tau)$ (the intermediate scattering function), is given by the *echo amplitude*. Within the measurement of the beam polarization by counting for a certain time the spin up and spin down component. The difference is the maximum echo amplitude we can recover. Once the periodicity of the “phase current” has been measured the measurement of four points around the centre of the echo with 90° steps will deliver the average amplitude, the echo amplitude and the phase. However, this measurement procedure can be further optimised in terms of better determination of the final $S(Q,\tau)$.

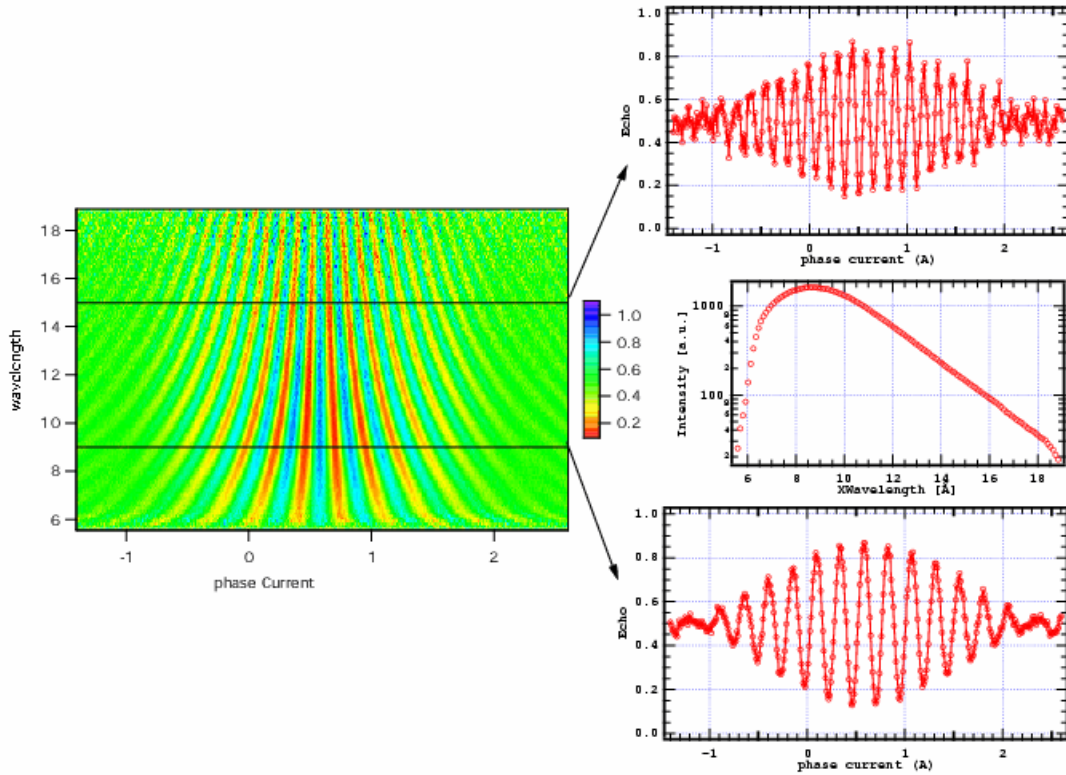


Fig. 38: On the left side the TOF echo group normalized to the beam polarization is shown. Right side, upper and lower plot: two cuts of the echo groups at 5Å and 9Å; middle plot: wavelengths dependence of the incoming intensity [18, 137].

This method can be easily translated to a TOF - NSE. The echo amplitude has to be extracted from:

$$I(n) = Aver(\lambda) + E_{Ampl}(\lambda) \cos(\varphi + n\varphi_{step}(\lambda)) Envelope(n, \lambda) \quad (5)$$

so many echo points we now certainly have to take into account the echo group $Envelope(n, \lambda)$ function, and the echo step size, $\varphi_{step}(\lambda) \propto I_{step} \lambda$, is also a function of wavelength. Fortunately both of them can be measured on the straight beam and used as known in the treatment.

Fig. 38 shows on the right side two cuttings of echo groups measured in TOF operation and the feasibility for the usage of the so called flippers with a ramped current has already been shown [137]. Alternative methods for these flippers also exist [99] but the feasibility has to be checked so far.

4.3.6 Analyzer

The analyzer in front of the detector has to provide a polarization dependent transmission close to 1 for “up” neutrons and close to zero for neutrons with the opposite longitudinal polarization. It covers the total detector area of 30×30 cm². In order to utilize all available neutrons it should fully accept the divergence that corresponds to the size of the sample, i.e. $\delta = w/D \approx 0.5^\circ$, where ($w \approx 20$ -30mm is the sample width and $D \approx 3200$ mm is the sample-analyzer distance). The analyzer will have the shape of a radial collimator with a channel length of 500mm and a distance between adjacent lamellae of 4mm, each lamella having a thickness of 0.5mm. The lamellae consist of thin boron glass sheets covered by supermirrors layers on both sides. The accepted divergence is limited by the outer reflection θ_u edge for the “up”-polarization on the one side and by either the increase of reflectivity for the “down”-polarization edge θ_d or by the direct line of sight angle θ_g as illustrated in Fig. 39.

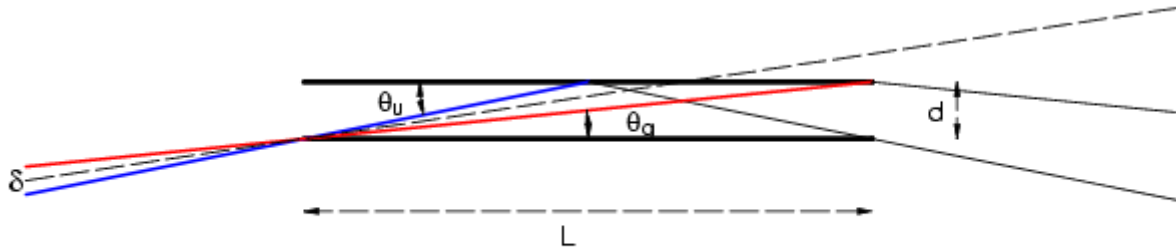


Fig. 39: One collimator channel covered with multilayer mirrors on both sides. δ illustrates the polarizing acceptance range between the direct line-of-sight (red) and the outer edge of the reflectivity band (blue). This range increases with increasing wavelength. The dashed line points to the sample position.

For the given dimension the direct line of sight inclination is $\theta_g=4/500\approx 0.45^\circ$ whereas θ_u and θ_d depend on the wavelength and the supermirror quality, i.e. the multiplier value m that relates the critical angle of Ni, $\theta_c=1^\circ/\text{nm}$ to $\theta_u=m\times\theta_c$, typically $\theta_d\approx 0.2\times\theta_u$. The current technological limit for m is $m=4$ [19], however, the effort (900 layers) to achieve this is large and too costly for the large area of about 20m^2 . A value of $m=3$ which needs only 300 single layers is foreseen for the analyzer mirrors of the FeCo/Ti-type. For $\lambda=0.3\text{nm}$ this yields $\theta_u=0.9^\circ$ ($\theta_d\approx 0.2^\circ$) which allows for an accepted divergence of $\delta=\theta_u-\theta_g=0.45^\circ$ which increases rapidly with increasing wavelength. With the inclination to the beam the polarization obtained in a single reflection starts to get worse as soon as $\theta_d(\lambda)>0.45^\circ$, i.e. $\lambda>0.75\text{nm}$, however, the polarization efficiency is lost gradually and only partially and can be restored by a slight rotation of the analyzer. For larger wavelength, e.g. $\lambda=2\text{nm}$, the condition $\delta>0.5^\circ$ is easily fulfilled and requires an inclination of the “collimating channel” to the line-of-sight to the sample between about 1.7° - 5.5° within this window the optimum combination of transmission and polarization may be selected, which probably is close to 1.7° .

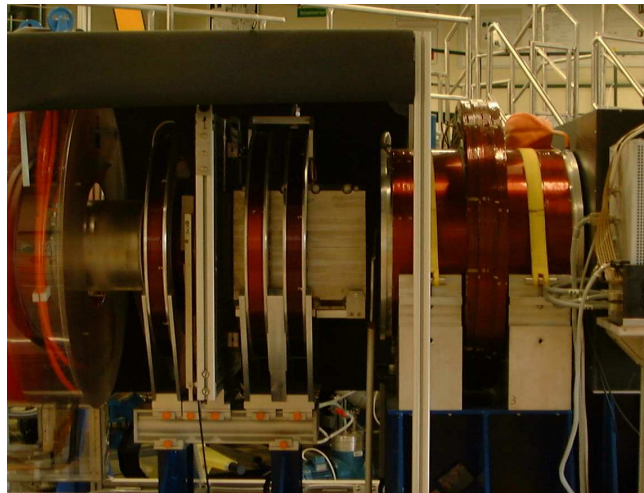


Fig 40: Soller collimator and analyzer system of the NSE spectrometer in Jülich.

This means that some adjustment of the inclination angle of the analyzer in the range between 0° and $\approx 6^\circ$ depending on the selected wavelength frame is required, therefore a computer controlled rotation mechanism is foreseen.

To reduce neutron background that may result from directions of the direct line-of-sight of the analyzer channels a radial collimator in front of the analyzer restricts the free pathways to those pointing to the sample. This is a measure that significantly improves the background ratio at small scattering angles. A

feature that has been experimentally shown at the Jülich NSE instrument (see Fig. 40) and at the first time allowed for the measurement of inelastic incoherent scattering in the SANS regime. At larger scattering angles the usual beam path limiters (diaphragms, etc.) sufficiently reduce the background such that the collimator might be removed to avoid the associated transmission loss (0.6).

4.3.7 Add - on : Ferromagnetic and Intensity Modulated NSE

Flexibility and reliability will be the keys for the success of the proposed spectrometer. The design will allow for routine operation in optional configurations, which have been tested but were never used on a permanent basis because of complicated installation procedures and inherent intensity losses. This is the case of the Intensity Modulated NSE, an extremely powerful technique, if the losses in neutron intensity are acceptable. Neutron spin echo spectroscopy inherently involves polarization analysis features. In its actual form, however, NSE does not allow to investigate spin-flip and non-spin-flip scattering channels independently from each other. At the expense of some loss of signal it is, however, possible to generalize the NSE technique for the study of spin-dependent scattering processes in the most general sense of neutron polarimetry. This means to perform inelastic NSE analysis on the partial scattering cross-section corresponding to the transition from any incoming spin direction P to any outgoing spin direction P' . The first successful realization is described in [130], where the magnon dynamics was investigated in the ferromagnetic phase of Fe, where the sample completely depolarizes the beam and all information contained in the neutron spin polarization is lost.

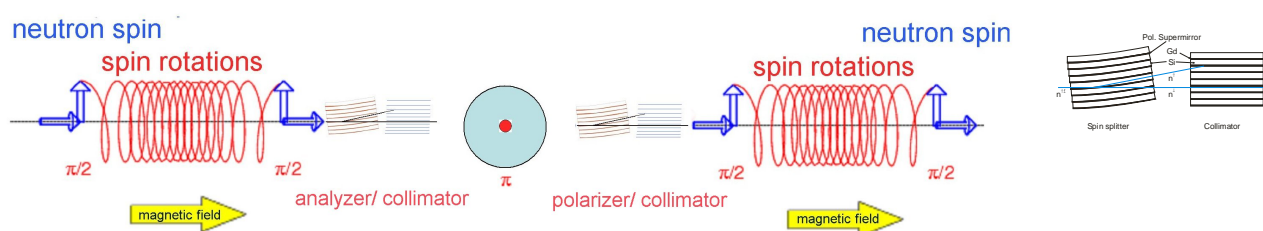


Fig. 41: Left side: schematic view of the intensity modulated NSE principle. Right side: operation principle of the transmission polarizer or analyzer in combination with a collimator .

A modified NSE set-up may be used in order to prepare a delicately intensity modulated (in contrast to the usual spin direction modulated) incoming beam, which is then analyzed by an identical Larmor-precession-based intensity modulator. This so-called Intensity Modulated NSE set-up corresponds to the following spin manipulation sequence: Polarizer - $\pi/2$ flip-Precession- $\pi/2$ flip-Analyzer-Sample-Polarizer- $\pi/2$ flip-Precession- $\pi/2$ flip - Analyzer (see Fig. 41) to compare with the usual NSE set-up: Polarizer - $\pi/2$ flip-Precession-Sample Precession- $\pi/2$ flip -Analyzer. The intensity modulation transforms the ordinary NSE spin direction modulation into intensity modulation by using a polarizer- $\pi/2$ flip-precession- $\pi/2$ flip-polarizer sequence, which leads to a conventionally, uniformly “up” polarized and intensity modulated beam shown in Fig. 42. The first element of the outgoing beam manipulation is spin analysis. So one can apply all the polarization analysis schemes around the sample and perform a polarization analysis selection of a neutron scattering channel between any two spin vector states “up” and “down” simultaneously with the NSE inelastic analysis, the latter being independently carried out by the intensity modulation. This technique opens up the possibility to use NSE with samples, which depolarize the beam, like ferromagnetic systems, as in its very first realization, where it was used to measure in Fe just below T_c the smallest energy magnons probably ever observed (Fig. 43). Furthermore, Intensity Modulation NSE allows for separate determination of the nuclear spin coherent and incoherent channels, a feature of fundamental importance in understanding polymers and biological substances.

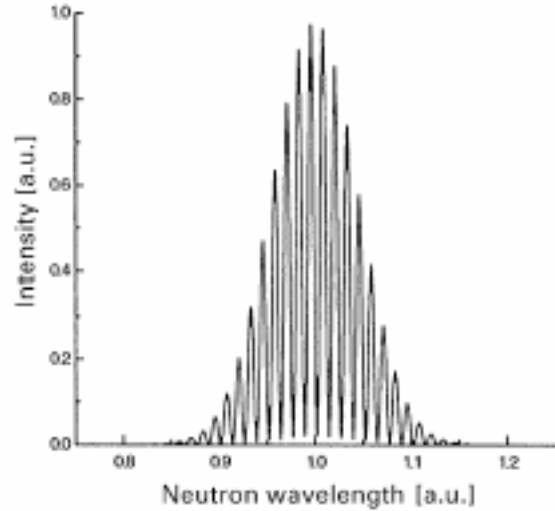


Fig. 42: Example for the neutron wavelength distribution in the incoming beam at the sample using the intensity modulated NSE set-up.

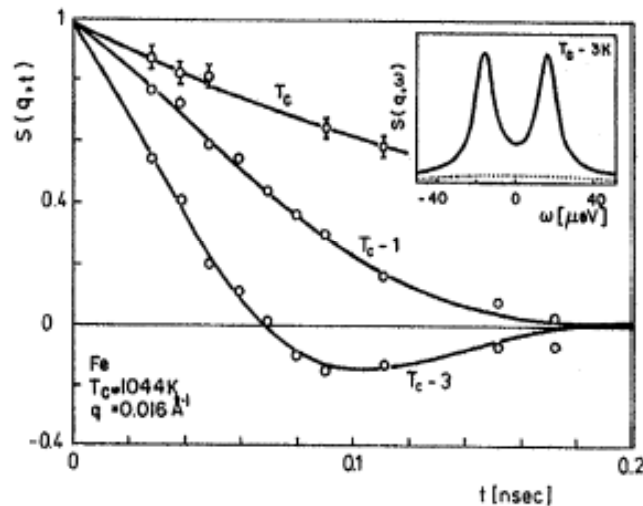


Fig. 43: Critical scattering spectra from Fe as directly measured by intensity-modulated NSE. The inset shows the $S(Q,\omega)$ spectrum corresponding to the T_c -3K curve (after Ref. [130]).

The price for this powerful technique is, besides the complexity of the set-up, the losses in neutron intensity due to the polarizer-analyzer pairs next to the sample. These losses were up to now prohibitive for most experimental realizations. We propose to fully take advantage of the recent progress in neutron optics and polarizing supermirrors, and foresee routine operation of the proposed spectrometer also in the Intensity Modulation NSE modus. This will be a worldwide unique feature, which will open up new experimental possibilities in soft matter research and in particular in the field of magnetism. In order to cope with the compact design requirements of the spectrometer and also for reducing the intensity losses, we propose to use compact “solid state” polarizer and analyzer components with remanent layers, developed at the HMI [118, 119, 120].

These elements must be performing in the low magnetic field of the sample area and would not require any additional magnetic field. Therefore any cross talk with the magnetic field configuration of the spectrometer will be avoided.

The compact design of the analyzer-polarizer reduces the length requirement of the Intensity Modulated NSE option considerably and no more than 20 cm additional length on either sides of the sample would be required. Three pairs of analysers-polarisers will be needed to cover the whole wavelength range of the spectrometer and their change and positioning will be done fully automatically with stepping motors (see Fig. 44).

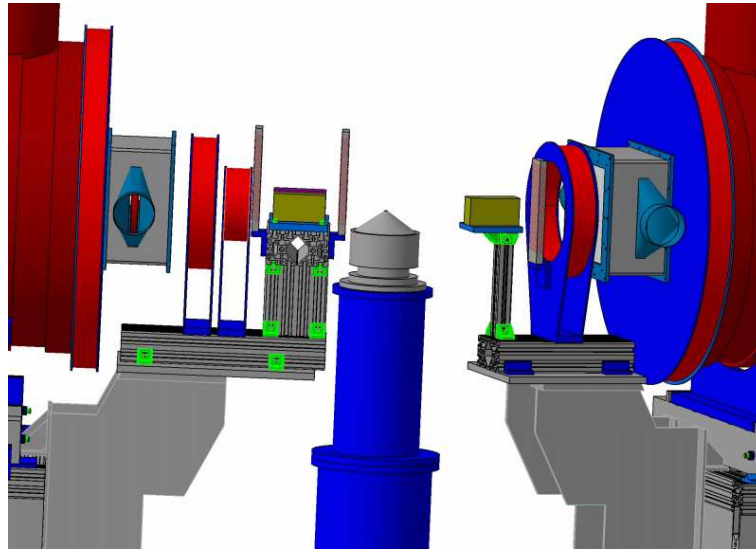


Fig. 44: Set-up for the intensity modulated NSE spectrometer.

The ferromagnetic NSE add – on offers new possibilities for modern, new physics. However, the flux is strongly decreased especially at high wavelengths due to the “in beam devices” and the reduced usable area at the 2D - detector. The “in beam devices” are polarizer, analyzer, collimators and two additional $\pi/2$ flippers. We expect a factor of about 100 reduced intensity in comparison to the normal operation mode of the NSE spectrometer. The highest wavelengths are not achievable and it delivers a reduced maximum Fourier time τ .

4.3.8 Add – on: “small - echo”

The dynamic range $1:10^6$ is easily accessible due to the inherent pulsed operation. For a typical NSE spectrometer at the reactor source the dynamical range is in the order of $\tau_{\max}/\tau_{\min} = 100$. There is however a possibility to gain another order of magnitude. If the magnetic field can not be lowered than the length has to be shortened. Thus one places two additional $\pi/2$ flippers at the end of the first and beginning of the second main precession coil and puts two additional coils between them as new precession coils. This set – up is a so-called double echo layout. Whereas the outer coils produce the normal “big echo” and the inner coils a so-called “small echo”. The active coil pair produces the echo while the other are inactive, or serve as guide field only respectively. This will extend the dynamic range by a factor 10 to three decades. Taking the $\approx \lambda^3$ dependence of the Fourier time τ into account one realizes that a dynamic range of $\approx 1:10^6$ will be accessible.

For a so-called “small - echo” additional coils will be required with power supplies and in beam devices like two $\pi/2$ flippers (see Fig. 45).

Instrument description

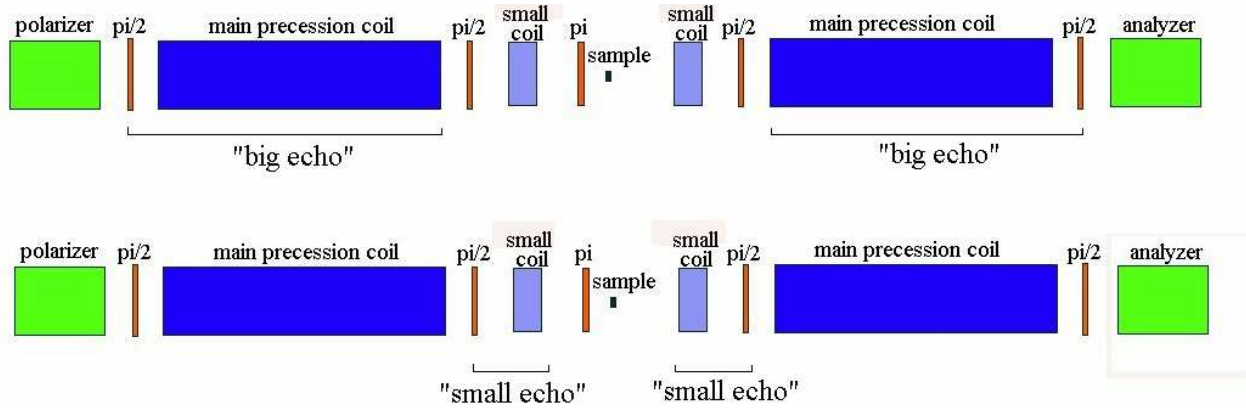


Fig. 45: The upper plot shows the “big – echo” operation mode in which the precession of the neutron spin is generated by the main precession coils, while the inner coils are inactive. The lower plot displays the inner coils as neutron precession generating sources. The main precession coils are used to produce the guide field..

4.3.9 Magnetic shielding

This type of neutron spectrometer utilizes static magnetic fields to code minute velocity differences into a neutron spin precession angle. This implies that the spins in a neutron beam precess in a preparation field by a solenoid over a path of about 3m length and are analyzed after scattering at the sample and back precession through a second symmetric solenoid. The fields are produced by symmetric solenoids before and after the sample at B with an active shielding and of about 1T. However, the symmetry requirement is such that disturbing varying external fields shall not introduce additional differences between the field integrals of the two arms exceeding $\Delta J=0.1\mu\text{Tm}$. The instrument itself is constructed in a way that its own stray field does not exceed 100 μT in 1.5m distance from the solenoid axis.

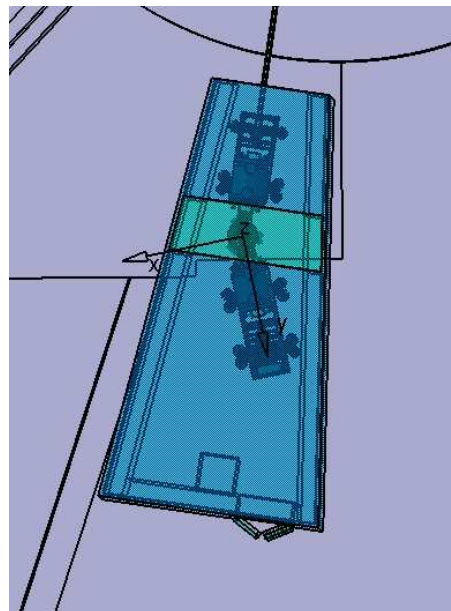


Fig. 46: The plot shows the instrument with the surrounding magnetic shielding housing and side walls of about 0.5m to protect neighbours from the radiation originating within the segment.

We plan to ensure the required stability of the magnetic field landscape by isolating the instrument area from field changes due to motion of large iron parts in the neighbourhood (e.g. crane movements) or fringe fields of instruments at other beam ports (10^{-3}T at the outer boundary of the shielding?). For that purpose we plan

to install a magnetic shielding enclosure. Both fields inside the shielding housing as well as outside the housing should be “compensated” simultaneously. The tentative ground plan of the shielded room is shown in Fig. 46.

The magnetic shielding must be installed in combination with a concrete radiation shield. In particular the requirement holds that (large parts of) the ceiling may easily be removed and reinstalled (up to 2-3 times per year) from above without performance loss.

4.4 Miscellaneous

4.4.1 Radiation Shielding

Due to the high power and high primary energy of the SNS source, especially for fast neutrons, massive shielding will be required for all instruments. At the same time the shielding design must allow access to all beamline components. The main radiation shielding splits into several parts. One part is the main shielding covering the whole radial segment up to 10m distance from the moderator and the second part comprises the walls around the magnetic part of the instrument at a distance from 11m to 22m from the moderator. This second part should consist of walls between each radial segment associated with each instrument to separate neighbour instruments from each other and minimize the influences of the neighbouring instruments. These walls will have a thickness of about 0.5m. Their detailed layout will depend on the actual neighbours.

To avoid significant influence of the fastest neutrons a shell made of steel including moderators and absorbers will envelop the guide system. In particular in the region, where the direct beam hits, the guide walls need additional steel and possibly Boron PE- layers.

As the geometric design of the NSE spectrometer is similar to the EQSANS we expect to benefit from the layout work there.

4.4.2 Detector

Due to the used polarizer elements, the NSE spectrometer will have a short wavelength cut off at $\lambda \cong 3\text{\AA}$. For the distance to the detector this reveals a flight time of about 14ms (see Eq. 6). To resolve the best, 0.5% monochromatization with a factor 10 oversampling, the electronics needs only a time resolution of a few hundred microseconds which is very easy to achieve.

$$t(\lambda) = L_D m \lambda / h \quad (6)$$

On the other side a detector has to be used which is able to handle the high count rates. Between the highest ($\cong 25\text{\AA}$) and lowest ($\cong 3\text{\AA}$) wavelengths there will be easily a factor 10^3 in the flux. The detector should cover a solid angle $\Omega=4^\circ \times 4^\circ$. This requires a sensitive area of about $300 \times 300 \text{mm}^2$ at a distance 18m from the moderator. Detector electronics and detector should deliver reliable operation for reliable data acquisition for years.

For the design of the 2D - detector two practical possibilities exist:

- The detector could either be build from an 20 array of single detector tubes.
- The detector is a gemmine 2D – detector device.

A detector with single tubes offers the advantage to be modular. This is of benefit in order e.g. to single out Bragg spots. Also defect single detectors can be easily replaced. The window thickness of those detectors is of about 10 mm. The useful area (no distortion) will be 300 mm x 300 mm and assuming a spatial resolution: 2 cm (X and Y) => 15 x 15 detectors with a count rate better than $> 2 \text{kHz/cm}^2$ per detector and 1MHz integrated over the whole area of the detector would be a good solution. For this solution 225 single detector tubes were required.

The second possibility is a 2D - ^3He - detector with an active area of $300 \times 300 \text{mm}^2$. Here the physical resolution often is better than $5 \times 5 \text{mm}^2$ but for the most physical problems this is not required. The maximal count rate limits could be a problem. Finally, a solution in between the two could be an array at linear position sensitive detectors.

We understand, that most of the experiments commercially available detectors will serve most the needs. For experiments with strongly scattering samples, detectors with higher counting rate are desirable. There are many competing detector technologies currently in development. Some of these efforts are directed at high counting rate detectors that will be suitable for our needs. We will consider these new detector technologies as they come along. The detector needs a surrounding shielding box of PE-B4C composite. The necessary thickness has yet to be determined.

4.4.3 Mechanical Layout – Structural Support

Figure 47 shows the mechanical layout of the carrier system for the superconducting coils and partly the instrument sample environment.

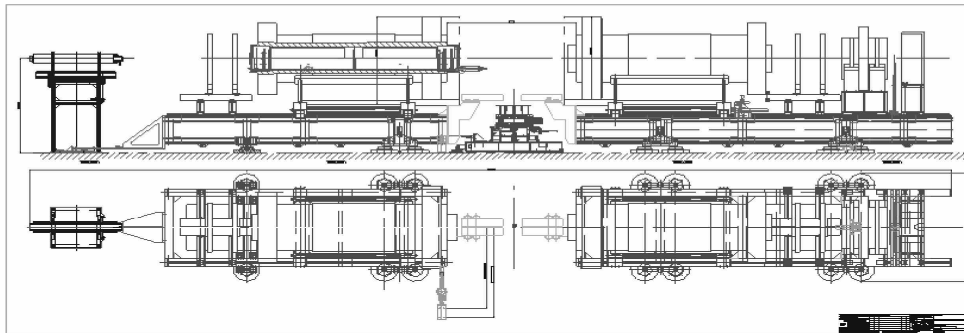


Fig. 47: The support structure elements for the magnetic part (11.5m – 18m) of the spectrometer at NIST. The final system will be similar to the presented one.

Most of the structural elements will be bought from external companies and the rest will be supplied from the FZ Jülich. The support structure mainly will be developed by the engineers in the technical department of the FZJ and manufactured there.

The mechanical parts and components which have to be implemented in the system are summarized as follows: two carriersystems for the main precession coils, spectrometer axis, friction wheel, polarizer in the revolversystem, carrier for the analyser with in/out mechanism, solenoid inserts, mechanical structure for $\pi/2$ and π flippers, sample table with controlling unit, parts to integrate all components with each other, construction of the whole system, manufacturing of all solenoids.

4.5 Automatic Controlling

To control a NSE spectrometer is challenging, since it possesses a large number of degrees of freedoms. For example IN15 and IN11 have to be “tuned” for each set point using the neutron signal. In this way the correct currents and associated fields are set. As long as the configuration and the desired settings stay the same the current values can be restored from tables.

The proposed instrument will be equipped with control software that will minimize the need of neutron assisted tuning. This property is supported by the low stray field, from the actively shielded, design of the main precession coils. This design avoids cross talk and thereby strongly reduces mutual influences on the optimal current setting. During normal operation mainly wavelength and scattering angle have to be changed. Also the optional modes for the short, ferromagnetic and intensity option are to be served.

The control software for the instrument will be based on the experience acquired during the creation of the existing program running the NSE spectrometers in Jülich and at NIST. This program will have to be extended for TOF-operation. The core module will contain a virtual image of the spectrometer that enables the computed set-up of magnetic fields, thereby enabling easy and efficient use of the instrument. The highest abstraction level will allow the user to just specify Q-value, Fourier time, wavelength frame sample parameters like T and the selected operation mode. The software will set currents, angles, chopper phases etc.

Parameters that e.g. control the exact positioning of correction elements have to be determined after assembly using measuring techniques including neutron signals. They will be stored as physical parameters, e.g. deviations from ideal positions: Δx , Δy ... and fed into the physical model of the whole instrument to yield computed geometrical actuator values (e.g. for the Hexapods).

4.5.1 Hardware Interfacing

General notes

For instruments on the Jülich research reactor and the Munich FRM-II the electronics department of the FZ-Jülich has standardized a control system framework and a choice of front-end hardware to support. This is the so-called "Jülich-Munich-Standard". This concept was proven on a number of experiments in various states of construction and operation. For the proposed NSE instrument we would like to keep close to these technologies, in order to benefit from existing developments and to economical use manpower resources. Adaptation to local circumstances, like technical support facilities at SNS and interfacing to SNS services (e.g. timing and choppers, detectors, networking and data archiving) should be possible with moderate effort.

Hardware

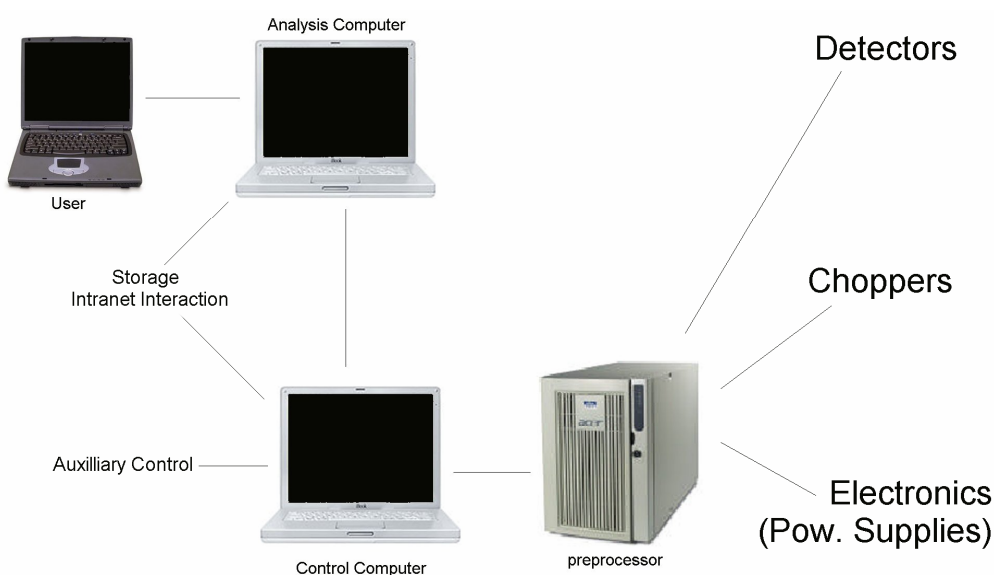


Fig. 48: Scenario for the foreseen control hardware connected with the instruments components.

For control of the movable parts (in a wider sense, i.e. including electrical currents) of the instrument we are generally using three layers (see Fig. 48):

- A "control computer" (PC) running user control programs and the engine for automatic measurement runs.
- "Front-end computers" (rackmount, CompactPCI), connected to the control computer by Ethernet/IP. These computers run programs ("TACO device servers", see below) for low-level hardware access

- "Process periphery". We are preferring Siemens S7 series PLCs and associated input/output modules, coupled to the front end computer by Profibus/DP (a popular fieldbus).

There is a number of choices how the Profibus I/O modules are connected to the system:

- Directly to the Profibus at the front end computer: For non-critical input/output modules.
- Attached to the PLC bus: I/O which is critical for safety or machine integrity, needing real-time response or other PLC features (e.g. logical abstraction, persistence).
- Attached to the PLC through a secondary Profibus: Same as before, if the capacity of the PLC bus is exceeded or if a different location is preferred for space reasons or for simplification of cabling.

As I/O modules generally the Siemens ET-200 series equipment is preferred, for good integration with the PLC system. Other Profibus-DP products can be integrated if the logical interface to the Profibus is reasonably specified, usually by a "GSD" (device description) file.

Other (non-Profibus) front end devices to consider are:

- Detector: At SNS, a Fibre Channel connection to the detector subsystem will be necessary.
- Devices (as lab measurement equipment, power supplies etc.) connected to serial lines (RS232, RS485) or GPIB, if not handled by SNS supplied front end computers: Interface cards in CompactPCI formfactor can be used.

Software

The TACO package, developed at ESRF, is used as communication system between application programs (running on the "control computer" as introduced above, or on possible additional computers, e.g. status display panels or handheld appliances) and hardware. TACO is a client-server framework based on Sun RPC with a name service and a simple database for configuration information. Programs interacting directly with the hardware (running on the "front end computers") are "device servers"; higher-level programs act as "clients. TACO is available as source code and is potentially usable on all major computing platforms. Graphical "Qt" applications will serve as comfortable display and configuration tools, while Python scripting provides low-level control and individual methods for experienced users. Since SNS has chosen LabView "Data sockets" as software interconnects between instrument specific applications and central services, a gateway to TACO/RPC will be needed. It should be possible to implement a LabView application which also implements a TACO server by linking in TACO Windows libraries. It might also be possible to create a standalone gateway application using an Active-X control provided by National Instruments.

4.5.2 Data (pre-) treatment and User Interface

The first step of data treatment requires the extraction of normalized echo amplitudes with respect to those of a resolution sample, eventually scattering from a background sample has also to be included. Once these data are available the user will get a table of $S(Q,\tau)/S(Q)$ over the covered (Q,τ) -space. It is intended to provide software with the ability to automatically select the optimal control parameters for this evaluation and yield an unbiased result.

4.6 Sample Environment

All sample environments have to be **amagnetic** this requires the exclusive use of amagnetic construction materials as well as resistive heaters -if used- that do not create magnetic fields in the beam region on current flow.

The outer diameter of the sample environment in and below the beam region may not exceed 170mm in order to allow an outside placement of the π -flipper.

The **standard NSE sample environments** will be:

1. Thermostated enclosure $T=250K$ to $350K$ with the sample in gas at ambient pressure for work with ordinary solutions, microemulsions, biological samples ...

2. Cryofour: Cryostat with extended high temperature range, $T=3\text{K}$ to 500K , sample in vacuum.
3. Furnace: $T=300\text{K}$ to 800K , sample in vacuum.
4. Pressure cell: $T=280\text{K}$ to 370K , $p=1\text{-}1000\text{bar}$ (eventually 3000bar with reduced cross section).

4.7 Further Requirements

4.7.1 Space

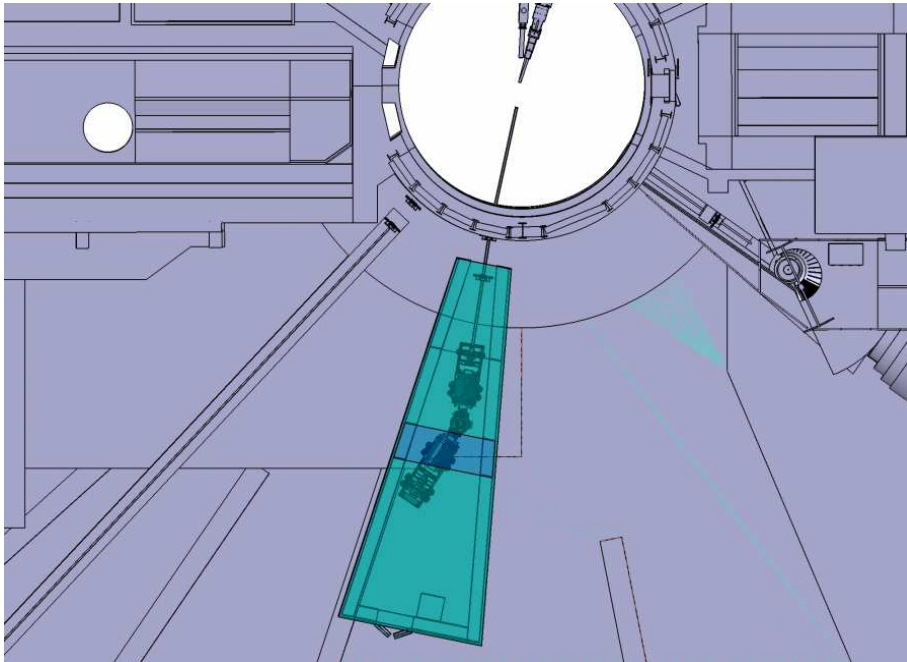
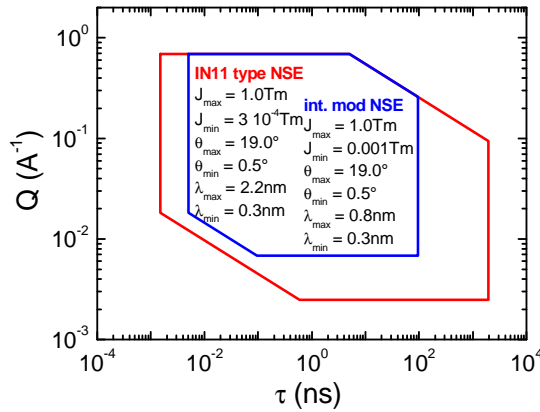


Fig. 49: The instrument within its radial segment of 13.75° width. The instrument is placed in its magnetic shielding with 2 walls (0.5m thick) of radiation shielding on both sides.

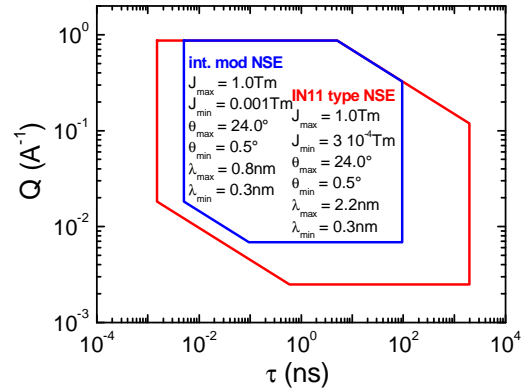
The standard radial segment which is offered delivers an aperture angle of 13.75° . According to the interface control document 1.6 and 1.7 of the SNS, beamlines 13, 14 and 15 are connected to the coupled cold moderator (Rep. Rate: 60 Hz, Power 2 MW (4MW), Location: Top down stream, Type: Coupled LH2, Pulse width: $\sim 18 \mu\text{s}$ FWHM per \AA). However, from the SNS Interface Control document regarding target systems and neutron scattering systems it became obvious that beamline 14BD has two beamlines separated by 2.4° each from the symmetry axis of the radial segment. The other two beamlines 13 and 15 have just one beam dividing the 13.75° into two radial segments of 6.875° each.

It became clear that a inclination angle of 3.5° at the exit of target shielding is optimized in order to avoid the direct view and to use appropriate polarizer elements for highest flux. Figure 49 displays the instrument within its magnetic shielding restricted to the 13.75° radial segment at BL14.

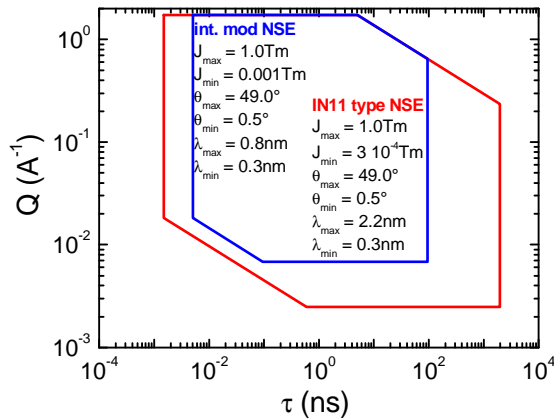
Assuming a width of 0.8m of the instrument arms and a radiation shielding with sidewalls of 0.5m thickness we determined the appropriate Q and τ range for the normal operation and the intensity modulated NSE. The criterion to include a certain Q, τ point is that the average flux at the sample is not less than 10^5 n/cm^2 . Due to additional in beam devices the intensity modulated NSE is only at a 1% intensity level. Therefore its range of operation is limited additionally. Furthermore with the intensity modulated NSE add-on the “small echo” cannot be used and the Q, τ space is further limited. The results are plotted in Fig. 50.



(a)



(b)



(c)

Fig. 50: The accessible Q - τ dynamic ranges for 3 different maximum scattering angles.

(a): instrument at BL13 or BL15; $\Theta_{\max}=19^\circ$,

(b): instrument in BL14; $\Theta_{\max}=24^\circ$,

(c): instrument at either BL13 or BL15 with only a shielded guide in BL14; $\Theta_{\max}=49^\circ$

a) Instrument at BL13 or BL15, b) instrument in BL14, c) instrument at either BL13 or BL15 with only a shielded guide in BL14.

To turn the second arm perpendicular to the floor is not a possible solution. At highest magnetic fields the main precession coils produce about 10^5 precessions which have to be analyzed with an accuracy of about $1/10$ of 2π . Assuming a 1% monochromatization of the wavelength at the entrance of the second precession coil. It turns out that at highest magnet fields because of gravity the spin in the shortest and longest wavelength within the beam at any time will perform a number of precession that spreads over of 80 different turns. Possible modifications of the inclination angle or off symmetric guides will have to be explored.

4.7.2 Media

The instrument needs pressurized air for the air pads, about 25kW electrical power for the power supplies and 25kW electrical power for the He compressor and cooling water.

Media like air conditioning in offices and separate rooms for electronics, water supply for cooling etc. has to be specified in more detail by the IDT and will be discussed with the SNS once the instrument has been funded.

4.7.3 Magnetic and Radiation Shielding Interface

Due to their similar geometry, the shielding requirements are similar to the shielding requirements of the EQSANS. Difference are visible due to the chopper positions foreseen at 5.5, 6.38m and 8.06m from the moderator and the revolver system, which are for the polarizing benders and the auxiliary beam shutter.

The layout of the interface between the radiation and the magnetic shielding will strictly follow practical considerations. The magnetic shielding will be at the interior of the radiation shielding especially at the sidewalls. The radiation shielding itself will provide the support structure for the magnetic shielding.

4.8 Summary

Flexibility, reliability in combination with huge dynamic ranges and highest resolution in space and time are the remarkable features of this highest - resolution spin - echo spectrometer ever build. The dynamic range will cover more than 6 decades in time $1\text{ps} < \tau < 1\mu\text{s}$ with the maximal resolution at about $\tau > 1\mu\text{s}$. As a fringe benefit of the pulsed source a monochromatization of at least 1% of the wavelength will deliver highest Q – resolution also.

The beam transport will be performed by a Ni coated guide system with $m=1..1.5$. This guide system mainly will start 2.5m from the moderator and lead to the spectrometer entrance at 11m from the source. At the end of the guide a “diverging exit” will be placed in order to optimize the flux at high wavelengths. At 6.36m from the source a neutron bender will deviate the beam by 3.5° , in order to come out of direct sight. At the same time the bender will polarize the beam by a revolver system of three supermirror polarizer elements each working in a certain wavelength band between $3\text{\AA} < \lambda < 22\text{\AA}$. A chopper system of three choppers has to be installed delivering wavelength bands of 3.6\AA taking the instruments length of about 18m into account. The band width relates to an instrument length of 18m. As the three chopper system involves a few ppm a contamination of neutrons a fourths chopper could be installed dependent on cost/performance optimisation.

To achieve highest resolution the spectrometer will be equipped with superconducting precession coils as heart components which will deliver highest current carrying capabilities with a precession field integral of more than $J > 1\text{Tm}$ at an optimization geometry. In this spectrometer component secondary windings will be installed for full compensation of stray fields and a reliable, environment independent operation. The instrument will be housed in a magnetic shielding for independent operation from other magnetic field sources in the experimental hall. The high magnetic fields have to be corrected such that different neutron trajectories receive the same field integral in passing. For that purpose the instrument will be equipped with correction elements with optimised current carrying capability, cooling mechanism, low background scattering and highest positioning accuracy. Also in beam devices like flippers etc. are object of a research program as they produce background contributions to the small angle scattering signal. The correction elements as well as in beam devices will be finalized at the time when the instrument will be installed at the SNS.

The detector will be a 2D - Detector covering an area of about $30 \times 30\text{cm}^2$. As those detectors are always under development, a Detector will be chosen and acquired at the latest possible stage.

The spectrometer will be equipped with several add ons, a small echo option in order to gain an additional order of magnitude in dynamic range, a ferromagnetic spin echo set up or an intensity modulated NSE option.

Around the sample in the magnetic part at about 14m from the moderator the spectrometer should be operational either with the add-on of a so called small - echo option for an additional decade of time to lower values or with an intensity modulated NSE option. While the first add-on is necessary in order to establish the huge dynamic range, the second option offers the possibility to separate intensity and spin polarization from each other allowing to address new classes of scientific problems especially in the field of magnetism.

The presented highest resolution neutron spin - echo spectrometer will be equipped with the best and so far newest neutron scattering components and technologies for such a spectrometer - type and will deliver the highest resolution in time $\tau > 1\mu\text{s}$ and the largest dynamic range worldwide.

5 Estimated costs (unburdened)

6 IDT Organization

7 References

- [1] D. Richter, T. Springer, *A twenty years forward look at neutron scattering facilities in the OECD countries and Russia*, OECD and ESF technical report (1998), ISBN 2-912049-03-2
- [2] Final Report OECD Megascience Forum Working Group on Neutron Sources (1997), www.OECD.ORG//dsti/sti/s_t/ms/prod/online.htm
- [3] Ed. F. Mezei, Neutron Spin Echo Proceedings, *Lecture Notes in Physics V 128*, Springer, Berlin (1979)
- [4] C. Pappas, F. Mezei, *J. Neutron Res.* **5**, 35 (1996)
- [5] R. Papoular, MESS NSE-spectrometer at the LLB, Saclay, France; These Universite de Paris-sud, Centre d'Orsay (1992): "*La spectrometrie par echos de spin de neutrons. Application a l'etude de la dynamique des polymeres en solution*".
- [6] R. Golub and R. Gähler, "A Neutron Resonance Spin-Echo Spectrometer for Quasi-Elastic and Inelastic-Scattering", *Phys. Lett. V A123*, 43 (1987)
- [7] D. Richter, J.B. Hayter, F. Mezei, B. Ewen, "Dynamical Scaling in Polymer-Solutions Investigated by Neutron Spin-Echo Technique", *Phys. Rev. Lett.* **41**, 1484 (1978)
- [8] D. Richter, B. Farago, L.J. Fetters, J.S. Huang, B. Ewen, C. Lartigue, "Direct Microscopic Observation of the Entanglement Distance in a Polymer Melt", *Phys. Rev. Lett.* **64**, 1389 (1990)
- [9] D. Richter, B. Farago, R. Butera, L.J. Fetters, J.S. Huang, B. Ewen, "On The Origins of Entanglement Constraints Macromolecules", *Macromolecules* **26**, 795 (1993)
- [10] A. Arbe, J. Colmenero, M. Monkenbusch, "Dynamics of glass-forming polymers: "Homogeneous" versus "heterogeneous", D. Richter, *Phys. Rev. Lett.* **81**, 590 (1998)
- [11] M. Monkenbusch, "On Solenoid Design for Neutron Spin-Echo Spectrometers", *Nucl. Inst. and Methods in Phys. Research V A287*, 465 (1990)
- [12] M. Monkenbusch, R. Schaetzler, D. Richter, "The Julich neutron spin-echo spectrometer - Design and performance", *Nucl. Inst. and Methods in Phys. Research V A399*, 301 (1997)
- [13] D. Dubbers, R. Vlaming, E. Klemt, "Bistable Neutron Spin Flippers", *Nucl. Inst. Meth.* **A270**, 95 (1988)
- [14] C.M.E. Zeyen, P.C. Rem, R.A. Hartmann, L.J.M. Vandeklundert, "Optimal Neutron Larmor Precession Magnets", *IEEE Transactions on Magnetics V 24*, 1540 (1988)
- [15] F. Mezei, in *Thin Film neutron optical Devices*, C. Majkrzak ed. (SPIE 1989) p.10
- [16] M. Russina and F. Mezei, in *Neutrons and Numerical Methods*, M.R. Johnson et al. editors, AIP Conference Proc. 479 (New York 1999)
- [17] M. Monkenbusch, "Neutron Spin Echo Spectrometers of the Next Generation – Where are the Limits" in "Neutron Spin Echo Spectroscopy", Eds. F. Mezei, C. Pappas, T. Gutberlet, *Lecture Notes in Physics*, 601, Springer-Verlag Heidelberg (2003)
- [18] B. Farago, "Time-of-Flight Neutron Spin Echo: present status" in "Neutron Spin Echo Spectroscopy", Eds. F. Mezei, C. Pappas, T. Gutberlet, *Lecture Notes in Physics*, 601, Springer-

References

- Verlag Heidelberg (2003) [19] P. Böni, *Physica*, “*Supermirror-based beam devices*”, **B234-236**, 1038 (1997)
- [20] Homepage of the HRNSE spectrometer for the SNS, (available soon under) www.fz-juelich.de/iff.
- [21] J. Kulda, E. Farhi, C.M.E. Zeyen, “*Thermal variation of phonon frequency and line width in Ge studied*”, *Phys.* **B 297**, 37 (2001)
- [22] S. Komura, T. Takeda, T. Miyazaki, M. Saga, S. Ueno, “*A Neutron Spin-Echo Spectrometer Using Superconducting Magnets*”, *Nucl. Instr. Meth. Phys. Res.* **A 267**, 425 (1988)
- [23] A. Schebetov, B. Peskov, N. Pleshanov, V. Pusenkov, V. Syromyatnikov, V. Ul'yanov, “*Neutron optical devices of PNPP*”, see <http://nrd.pnpi.spb.ru/pdf/ulyanov.pdf> and references therein.
- [24] M. Ohl, M. Monkenbusch, D. Richter, “*Neutron spin - echo spectrometer development for spallation sources*” *Physica B* (2003), accepted for publication
- [25] G.D. Wignall, “*Neutron scattering studies of polymers in supercritical carbon dioxide*”, *J. Phys. Cond. Matt.* **11**, R157 (1999) .
- [26] A. Arbe, F. Boué, J. Colmenero, S. Janssen, F. Mezei, K. Mortensen, D. Richter, J. Rieger, P. Schurtenberger, R.K. Thomas, “*Soft Condensed Matter*”, in “*New Science and Technology for the 21st Century*”, The ESS Project **II**, 4-43 (2002), ISBN 3-89336-302-5
- [27] D. Horn, J. Rieger, “*Organic nanoparticles in the aqueous phase - theory, experiment*”, *Angew. Chem. Int. Ed.* **40**, 4330 (2001)
- [28] P.F.W. Simon, R. Ulrich, H.W. Spiess, U. Wiesner, “*Block copolymer-ceramic hybrid materials from organically modified ceramic precursors*”, *Chem. Mater.* **13**, 3464 (2001)
- [29] DOE - Nanotechnology report, www.er.doe.gov/bes/nanoscale.pdf
- [30] B. Loppinet, R. Sigel, A. Larsen, G. Fytas, D. Vlassopoulos, G. Liu, “*Structure and dynamics in dense suspensions of micellar*”, *Langmuir* **16**, 6480-4 (2000)
- [31] A. Caneschi, D. Gatteschi, C. Sangregorio, R. Sessoli, L. Sorace, A. Cornia, M.A. Novak, C. Paulsen, W.S.O Wernsdorfer, “*The molecular approach to nanoscale magnetism*”, *J. Magnetism and Magnetic Materials* **200** (1-3), 182 (1999)
- [32] R.H. Kodama, “*Magnetic nanoparticles*”, *J. of Magnetism and Magnetic Materials* **200** (1-3), 359 (1999)
- [33] F. Gazeau, E. Dubois, M. Hennion, R. Perzynski, Yu. Raikher, “*Quasi-elastic neutron scattering on gamma-Fe₂O₃ nanoparticles*”, *Europhys. Lett.* **40** (5), 575 (1997)
- [34] H. Casalta, P. Schleger, C. Bellouard, M. Hennion, I. Mirebeau, G. Ehlers, B. Farago, J.-L. Dormann, M. Kelsch, M. Linde, F. Phillipp, “*Direct measurement of superparamagnetic fluctuations in monodomain Fe particles via neutron spin-echo spectroscopy*”, *Phys. Rev. Lett.* **82** (6), 301-4 (1999)
- [35] V.T. Lebedev, G. Torok, G. Kali, L. Cser, D.N. Orlova, A.I. Sibilev, “*Dynamics of concentrated ferrofluid with labelled particle*”, *J. Magnetism and Magnetic Materials* **201**, 133-5 (1999)
- [36] F. Aliotta, B. Fazio, “*Percolative phenomena in branched reverse micelles*”, *Physica A* **304** (1-2), 111-18 (2002)

References

- [37] C. Gutierrez-Wing, P. Santiago, J.A. Ascencio, A. Camacho, M.José-Yacamán, "Self-assembling of gold nanoparticles in one, two, and three dimensions", *Appl. Phys. A* **71**, 237 (2000)
- [38] J.-C. Li, D.K. Ross, C. Lartigue, "Neutron Spin-Echo Measurements of the Diffusion of Water in Porous Solids", *J. of Physics: Condensed Matter* **5** (41) 7529-36 (1993)
- [39] C. Martin, J.P. Coulomb, M. Ferrand, "Direct measurement of the translational mobility of deuterium hydride molecules confined in a model microporous material: AlPO₄-5 zeolite", *Europhys. Lett.* **36** (7), 503-8 (1996)
- [40] G. Zsigmond, K. Lieutenant, F. Mezei, "Monte Carlo Simulations of Neutron Scattering Instruments by VITESS: Virtual Instrumentation Toll for ESS", *Neutron News* **13.4**, 11 (2002)
- [41] T.C.B. McLeish, "Tube theory of entangled polymer dynamics", *Advances in Physics* **51**, 1379 (2002)
- [42] H. Watanabe, "Viscoelasticity and Dynamics of Entangled Polymers", *Prog. Polym. Sci.* **24**, 1253 (1999)
- [43] M. Doi, D.M. Edwards, "Dynamics of Concentrated Polymer Systems", *J. Chem. Soc. Faraday Trans.* **74** (2), 1789 (1978)
- [44] P. Schleger, B. Farago, and C. Lartigue, A. Kollmar and D. Richter, "Clear Evidence of Reptation in Polyethylene from Neutron Spin-Echo Spectroscopy", *Phys. Rev. Lett.* **81**, 127 (1998)
- [45] A. Wischnewski, M. Monkenbusch, L. Willner, D. Richter, "Direct observation of the transition from free to constraint single - segment motions in entangled polymer melts " *Phys. Rev. Lett.* **90**, 058302 (2003)
- [46] P.G. De Gennes, "Coherent Scattering By One Reptating Chain", *J. de Physique* **42**, 735 (1981)
- [47] D. Richter, R. Butera, L.J. Fetters, J.S. Huang, B. Farago, B. Ewen, "Entanglement Constraints in Polymer Melts - A Neutron Spin-Echo Study", *Macromolecules* **25**, 6156 (1992) ; D. Richter, B. Farago, L.J. Fetters, J.S. Huang, B. Ewen, C. Lartigue, "Direct Microscopic Observation of the Entanglement Distance in a Polymer Melt", *Phys. Rev. Lett.* **64**, 1389 (1990); D. Richter, B. Farago, R. Butera, L.J. Fetters, J.S. Huang, B. Ewen, "On the Origins of Entanglement Constraints", *Macromolecules* **26**, 795 (1993); D. Richter, L. Willner, A. Zirkel, B. Farago, L.J. Fetters, J.S. Huang, "Onset of Topological Constraints in Polymer Melts - A Mode Analysis by Neutron Spin-Echo Spectroscopy", *Phys. Rev. Lett.* **71**, 4158 (1993); D. Richter, L. Willner, A. Zirkel, B. Farago, L.J. Fetters, J.S. Huang, "Polymer Motion at the Crossover from Rouse to Reptation Dynamics", *Macromolecules* **27**, 7437 (1994); B. Ewen and D. Richter, "Neutron spin echo investigations on the segmental dynamics of polymers in melts, networks and solutions", *Adv. Polym. Sci.* **27** (1) (1997).
- [48] A. Wischnewski, M. Monkenbusch, L. Willner, D. Richter, A.E. Likhtman, T.C.B. McLeish, B. Farago, "Molecular observation of contour-length fluctuations limiting topological confinement in polymer melts", *Phys. Rev. Lett.* **88**, 058301 (2002)
- [49] H. Montes, M. Monkenbusch, L. Willner, S. Rathgeber, L.J. Fetters, D. Richter, "Neutron spin echo investigation of the concentration fluctuation dynamics in melts of diblock copolymers", *J. Chem. Phys.* **110** (20), 10188 (1999)
- [50] H. Montes, M. Monkenbusch, L. Willner, S. Rathgeber, D. Richter, L.J. Fetters, B. Farago, "Direct observation of domain wall excitations in symmetric diblock copolymer melts at and above the order-disorder transition", *Europhys. Lett.* **58** (3), 389 (2002)
- [51] A. Arbe, M. Monkenbusch, J. Stellbrink, D. Richter, B. Farago, K. Almdal, R. Faust, "Origin of internal viscosity effects in flexible polymers: A comparative neutron spin-echo and light scattering

References

- study on poly(dimethylsiloxane) and polyisobutylene*”, *Macromolecules* **34** (5), 1281 (2001); D. Richter, M. Monkenbusch, J. Allgeier, A. Arbe, J. Colmenero, B. Farago, Y.C. Bae, R. Faust, “*From Rouse dynamics to local relaxation: A neutron spin echo study on polyisobutylene melts*”, *J. Chem. Phys.* **111** (13), 6107 (1999)
- [52] T. Hellweg, , “*Phase structures of microemulsions*“, *Current Opinion in Colloid & Interface Science* **7**, 50 (2002)
- [53] T. Takeda, Y. Kawabata, H. Seto, S. Komura, S.K. Ghosh, M. Nagao, D. Okuhara, “*Neutron spin-echo investigations of membrane undulations in complex fluids involving amphiphiles*”, *J. Physics and Chemistry of Solids* **60** (8-9), 1375 (1999)
- [54] H. Endo, M. Mihailescu, M. Monkenbusch, J. Allgaier, G. Gompper, D. Richter, B. Jakobs, T. Sottmann, R. Strey, I. Grillo, , “*Effect of amphiphilic block copolymers on the structure and phase behavior of oil-water-surfactant mixtures*”, *J. Chem. Phys.* **115** (1), 580 (2001)
- [55] M. Mihailescu, M. Monkenbusch, H. Endo, J. Allgaier, G. Gompper, J. Stellbrink, D. Richter, B. Jakobs, T. Sottmann, B. Farago, “*Dynamics of bicontinuous microemulsion phases with and without amphiphilic block-copolymers*”, *J. Chem. Phys.* **115** (20), 9563 (2001)
- [56] M. Mihailescu, M. Monkenbusch, J. Allgaier, H. Frielinghaus, D. Richter, B. Jakobs, T. Sottmann, “*Neutron scattering study on the structure and dynamics of oriented lamellar phase microemulsions*”, *Phys. Rev. E* **66** (4), 041504 (2002)
- [57] B.-S. Yang, J. Lal, M. Mihailescu, M. Monkenbusch, D. Richter, J.S. Huang, J. Kohn, W.B. Russel, R.K. Prud’homme, “*Neutron spin-echo study of dynamics of hydrophobically modified polymer-doped surfactant bilayers*”, *Langmuir* **18** (1), 6 (2002)
- [58] S. Komura, T. Takeda, Y. Kawabata, S.K. Ghosh, H. Seto, M. Nagao, “*Hydrodynamic interactions in the structural fluctuation of a ternary amphiphilic system C12E5/water/n-octane*”, *European Physical Journal E* **5** (3), 329 (2001)
- [59] S. Komura, T. Takeda, Y. Kawabata, S.K. Ghosh, H. Seto, M. Nagao, “*Dynamical fluctuation of the mesoscopic structure in ternary C12E5-water-n-octane amphiphile system*”, *Phys. Rev. E* **63** (4), 041402 (2001)
- [60] B. Farago, M. Gradzielski, “*The effect of the charge density of microemulsion droplets on the bending elasticity of their amphiphilic film*”, *J. Chem. Phys.* **114** (22), 10105 (2001)
- [61] J.S. Huang, S.T. Milner, B. Farago, D. Richter, “*Study Of Dynamics Of Microemulsion Droplets By Neutron Spin-Echo Spectroscopy*”, *Phys. Rev. Lett.* **59** (22), 2600 (1987)
- [62] T. Hellweg, D. Langevin, “*Bending Elasticity Of The Surfactant Monolayer In Droplet Microemulsions: Determination By A Combination Of Dynamic Light Scattering And Neutron Spin-Echo Spectroscopy*”, *Phys. Rev. E* **57** (6), 6825 (1998)
- [63] B. Farago, D Richter, J.S. Huang, S.A. Safran, S.T. Milner, “*Shape And Size Fluctuations Of Microemulsion Droplets - The Role Of Cosurfactant*”, *Phys. Rev. Lett.* **65** (26), 3348 (1990)
- [64] B. Farago, “*Static And Dynamic Neutron X-Ray Scattering*”, *Current Opinion in Colloid & Interface Science* **1** (1), 17 (1996)
- [65] B. Farago, M. Monkenbusch, K.D. Göcking, D. Richter, J.S. Huang, “*Dynamics Of Microemulsions As Seen By Neutron Spin-Echo*”, *Physica B* **213**, 712 (1995)
- [66] G.C. Maitland, “*Oil and gas production*”, *Current Opinion in Colloid & Interface Science* **5**, 301 (2000)

References

- [67] R.M. Hill, “*Silicone surfactants--new developments*”, *Current Opinion in Colloid & Interface Science* **7**, 255 (2002)
- [68] M. Adam, B. Farago, P. Schleger, E. Raspaud, D. Lairez, “*Binary Contacts In Semidilute Solution: Good And Theta Solvents*”, *Macromolecules* **31** (26), 9213 (1998)
- [69] J. Texter, T.A. Hatton, “*Colloid and interface science applications*”, *Current Opinion in Colloid & Interface Science* **7**, 253 (2003)
- [70] S. Rathgeber, M. Monkenbusch, M. Kreitschmann, V. Urban, A. Brulet, “*Dynamics of star-burst dendrimers in solution in relation to their structural properties*”, *J. Chem. Phys.* **117** (8), 4047 (2002)
- [71] D. Richter, B. Farago, J.S. Huang, L.J. Fetters, B. Ewen, “*A Study Of Single-Arm Relaxation In A Polystyrene Star Polymer By Neutron Spin-Echo Spectroscopy*”, *Macromolecules* **22** (1), 468 (1989)
- [72] J. Stellbrink, J. Allgaier, M. Monkenbusch, D. Richter, A. Lang, C.N. Likos, M. Watzlawek, H. Löwen, G. Ehlers, P. Schleger, “*Neither Gaussian chains nor hard spheres –star polymers seen as ultrasoft solids*”, *Prog. Colloid Polym. Sci.* **115**, 88 (2000)
- [73] B. Loppinet, R. Sigel, A. Larsen, G. Fytas, D. Vlassopoulos, G. Liu, “*Structure and dynamics in dense suspensions of micellar nanocolloids*”, *Langmuir* **16** (16), 6480 (2000)
- [74] T. Kanaya, H. Watanabe, Y. Matsushita, T. Takeda, H. Seto, M. Nagao, Y. Fujii, K. Kaji K, “*Neutron spin echo studies on dynamics of polymeric micelles*”, *J. Phys. and Chemistry of Solids* **60** (8-9), 1367 (1999)
- [75] M. Monkenbusch, D. Schneiders, D. Richter, B. Farago, L.J. Fetters, J. Huang, “*Dynamics Of Polymer Brushes - What Can Neutron Spin-Echo Spectroscopy Contribute*”, *Physica B* **213**, 707 (1995); M. Monkenbusch, D. Schneiders, D. Richter, B. Farago, L.J. Fetters, J.S. Huang, “*Aggregating Block-Copolymers As Model Systems To Study Polymer Brush Dynamics*”, *Nuovo Cimento D* **16** (7), 747 (1994); B. Farago, M. Monkenbusch, D. Richter, J.S. Huang, L.J. Fetters, A.P. Gast, “*Collective Dynamics Of Tethered Chains - Breathing Modes*”, *Phys. Rev. Lett.* **71** (7), 1015 (1993)
- [76] H. Matsuoka, Y. Yamamoto, M. Nakano, H. Endo, H. Yamaoka, R. Zorn, M. Monkenbusch, D. Richter, H. Seto, Y. Kawabata, M. Nagao, “*Neutron spin-echo study of the dynamic behavior of amphiphilic diblock copolymer micelles in aqueous solution*”, *Langmuir* **16** (24), 9177 (2000)
- [77] B. Ewen, D. Richter, “*Diffusional Processes on Polymer Networks as studied by Neutron Spin Echo Spectroscopy*”, p.82-98, *Proceedings of the 5th IFF-ILL Workshop Jülich 1988*, Springer Proceedings in Physics **42**, Molecular Basis of Polymer Networks, Eds. Baumgärtner A, Picot C.E., Springer Berlin-Heidelberg (1989)
- [78] T.A. Waigh, A. Papagiannopoulos, A. Voice, R. Bansil, A.P. Unwin, C.D. Dewhurst, B. Turner, N. Afdhal, “*Entanglement coupling in porcine stomach mucin*”, *Langmuir* **18** (19), 7188 (2002)
- [79] A. Prokop, E. Kozlov, G. Carlesso, J.M. Davidson, “*Hydrogel-Based Colloidal Polymeric System For Protein And Drug Delivery: Physical And Chemical Characterization, Permeability Control And Applications*”, *Adv. in Polymer Science* **160**, 119 (2002)
- [80] B. Kim, J.P. Gong, Y. Osada, “*Surfactant binding by polyelectrolyte gels and its application to electro-driven chemomechanics*”, *Polymer International* **48** (8), 691 (1999)
- [81] N.S. Cameron, A. Eisenberg, G.R. Brown, “*Amphiphilic block copolymers as bile acid sorbents: 2. Polystyrene-*b*-poly(*N,N,N*-trimethylammoniummethylene acrylamide chloride): Self-assembly and application to serum cholesterol reduction*”, *Biomacromolecules* **3** (1), 124 (2002)

References

- [82] M.A. Hubbe, “*Reversibility of polymer-induced fiber flocculation by shear. 2. Multi-component chemical treatments*”, Nordic Pulp & Paper Research Journal **16** (4), 369 (2001)
- [83] Y. Watanabe, K. Kubo, S. Sato, “*Application of amphoteric polyelectrolytes for sludge dewatering*”, Langmuir **15** (12), 4157 (1999)
- [84] S. Forster, N. Hermsdorf, C. Bottcher, P. Lindner, “*Structure of polyelectrolyte block copolymer micelles*”, Macromolecules **35** (10), 4096 (2002)
- [85] J. Travas-Sejdic, R. Steiner, J. Desilvestro, P. Pickering, , “*Ion conductivity of novel polyelectrolyte gels for secondary lithium-ion polymer batteries*”, Electrochimica Acta **46** (10-11), 1461 (2001)
- [86] W. Zajac, B.J. Gabrys, O. Scharpf, K.H. Andersen, E.E. Parsonage, “*Structure of poly(ethylene oxide) (PEO and PEO-LiSO₃CF₃) studied with spin polarised neutrons*”, Solid State Ionics **147** (3-4), 213 (2002)
- [87] M.L. Saboungi, D.L. Price, G.M. Mao, R. Fernandez-Perea, O. Borodin, G.D. Smith, M. Armand, W.S. Howells, “*Coherent neutron scattering from PEO and a PEO-based polymer electrolyte*”, Solid State Ionics **147** (3-4), 225 (2002)
- [88] P. Carlsson, R. Zorn, D. Andersson, B. Farago, W.S. Howells, L. Borjesson, “*The segmental dynamics of a polymer electrolyte investigated by coherent quasielastic neutron scattering*”, J. Chem. Phys. **114** (21), 9645 (2001)
- [89] A.M. Hecht, F. Horkay, P. Schleger, E. Geissler, “*Thermal fluctuations in polymer gels investigated by neutron spin echo and dynamic light scattering*”, Macromolecules **35** (22), 8552 (2002)
- [90] S. Westermann, Thesis
- [91] J. Kotz, S. Kosmella, “*Polymers in lyotropic liquid crystals*”, Current Opinion in Colloid & Interface Science **4** (5), 348 (1999)
- [92] K. Avramova, A. Milchev, “*Drift of a polymer chain in a porous medium –A Monte Carlo study*”, Eur. Phys. J. E **7**, 65 (2002)
- [93] H. Jobic, “*Neutron scattering methods for the study of zeolites*”, Current Opinion in Solid State & Materials Science **6** (5): 415 (2002)
- [94] H. Jobic, A. Methivier, G. Ehlers, “*Different diffusivities of xylene isomers in BaX zeolite measured by the neutron spin echo technique*”, Microporous and Mesoporous Materials **56** (1), 27 (2002)
- [95] W. Paul, G.D. Smith, D.Y. Yoon, B. Farago, S. Rathgeber, A. Zirkel, L. Willner, D. Richter, “*Chain motion in an unentangled polyethylene melt: A critical test of the rouse model by molecular dynamics simulations and neutron spin echo spectroscopy*”, Phys. Rev. Lett. **80** (11), 2346 (1998)
- [96] A. Arbe, J. Colmenero, F. Alvarez, M. Monkenbusch, D. Richter, B. Farago, B. Frick, “*Non-Gaussian nature of the alpha relaxation of glass-forming polyisoprene*”, Phys. Rev. Lett. **89** (24), 245701 (2002)
- [97] D. Richter, M. Monkenbusch, A. Arbe, J. Colmenero, “*Neutron scattering and the glass transition in polymers - present status and future opportunities*”, Journal of Non-Crystalline Solids **287** (1-3), 286 (2001)
- [98] G. Zsigmond, D. Wechsler, F. Mezei, “*Monte Carlo simulation of NSE at reactor and spallation sources*”, Publication: Proceedings of the Fifteenth Meeting of the International Collaboration on Advanced Neutron Sources. ICANS-XV. Advanced Neutron Sources towards the Next Century-(JAERI-Conf 2001-002).

References

- [99] V.T. Lebedev, G. Torok, “*Broadband neutron spin-flippers on magnetized foils*”, Nuclear Instruments & Methods in Physics Research B **195**, 449 (2002)
- [100] R. H. Austin, K.W. Beeson, L. Eisenstein, H. Frauenfelder, I.C. Gunsales, “*Dynamics of Ligand-Binding to Myoglobin*”, Biochemistry **14**, 5355 (1975)
- [101] W. Doster, S. Cusack, W. Petry, “*Dynamical Transition of Myoglobin Revealed by Inelastic Neutron-Scattering*” (1989) Nature **337**, 754 (1989)
- [102] J. Fitter, R.E. Lechner, N.A. Dencher, “*Picosecond molecular motions in bacteriorhodopsin from neutron scattering*”, Biophys. J. **73**, 2126 (1997)
- [103] F. Parak, E.W. Knapp, “*A Consistent Picture of Protein Dynamics*”, Proc. Natl. Acad. Sci. USA **81**, 7088 (1984)
- [104] M. Kurzynski, “*A synthetic picture of intramolecular dynamics of proteins. Towards a contemporary statistical theory of biochemical processes*”, Prog. Biophys. & Mol. Biol. **69**, 23 (1998)
- [105] Y. Alpert, “*Neutron Spin Echo: Proc. of a Laue-Langevin Workshop*”, Editor F. Mezei, Springer Verlag Berlin, 87 (1980)
- [106] Y. Alpert, L. Cser, B. Farago, F. Franek, F. Mezei, Y.M. Ostanevich, (KFKI-1982-106), (Hung. Acad. Sci., Budapest, 1982)
- [107] S. Dellerue, A. Petrescu, J.C. Smith, S. Longeville, M.-C. Bellissent-Funel, “*Collective dynamics of a photosynthetic protein probed by neutron spin-echo spectroscopy and molecular dynamics simulation*”, Physica **B 276**, 514, (2000)
- [108] A. Gall, J. Seguin, B. Robert, M.-C. Bellissent-Funel, “*Membrane proteins in bulk solution can be used for quasi-elastic neutron scattering studies: The case for the photochemical reaction center*”, J. Phys. Chem. B **106**, 6303 (2002)
- [109] K. Hinszen, A.J. Petrescu, S. Dellerue, M.-C. Bellissent-Funel, G.R. Kneller, “*Liquid-like and solid-like motions in proteins*” J. Mol. Liquids **98-99**, 381 (2002)
- [110] M. Tarek, D.J. Tobias, “*The dynamics of protein hydration water: A quantitative comparison of molecular dynamics simulations and neutron-scattering experiments*” Biophys. J. **79**, 3244, (2000) ;
ibid, “*Role of protein-water hydrogen bond dynamics in the protein dynamical transition*”, Phys Rev Lett **88** (13): art. no. 138101 (2002)
- [111] E. Sackmann, H.P. Duwe, W. Pfeiffer, “*On The Biomembranes As Composite Lamellae of Smectic-A Liquid-Crystal And Macromolecular Network - Elastic Properties, Local and Collective Dynamics*”, Physica Scripta Vol. T25, 107 (1989)
- [112] V.I. Gordeliy, V.G. Cherezov, J. Teixeira, “*Evidence of entropic contribution to "hydration" forces between membranes .2. Temperature dependence of the "hydration" force: A small angle neutron scattering study*”, J. Mol. Struct. **383**, 117 (1996)
- [113] W. Pfeiffer, G. Schlossbauer, W. Knoll, B. Farago, A. Steyer, E. Sackmann, “*Ultracold Neutron-Scattering Study of Local Lipid Mobility in Bilayer-Membranes*”, J. Physique **49**, 1077 (1988)
- [114] W. Pfeiffer, S. Konig, J.F. Legrand, T. Bayerl, D. Richter, E. Sackmann, “*Neutron Spin-Echo Study of Membrane Undulations in Lipid Multibilayers*”, Europhys. Lett. **23**, 457 (1993)
- [115] J. Ostermann, L. Orci, K. Tani, M. Amherdt, M. Ravazzola, J.E. Rothman, “*Stepwise Assembly Of Functionally Active-Transport Vesicles*”, Cell **75**, 1015 (1993)

References

- [116] G. Schiavo, F. Benfenati, B. Poulain, O. Rossetto, P. Polverino de Laureto, B.R. DasGupta, C. Montecucco, "*Tetanus and Botulinum-B Neurotoxins Block Neurotransmitter Release by Proteolytic Cleavage of Synaptobrevin*", Nature 359, 832 (1992)
- [117] J.E. Rothman, L. Orci, "*Budding vesicles in living cells*", Scient. American 274, No. 3, 50 (1996)
- [118] Th. Krist, C. Pappas, Th. Keller, F. Mezei, "*FeCo-Si Superspiegel*", Physica B **213 & 214**, 939 (1995)
- [119] Th. Krist, S. J. Kennedy, T. J. Hicks, F. Mezei, "*Polarizing bender*", Physica B **241-243**, 82 (1998)
- [120] Th. Krist and F. Mezei, "*Compact Neutron Optical Elements*", Physica B **276-278**, 208 (2000)
- [121] Th. Krist and F. Mezei, "*High performance, short solid state collimators with reflecting walls*", Nucl. Instr. and Methods in Phys. Res. A **450**, 389 (2000)
- [122] C. Pappas, F. Mezei, G. Ehlers, I.A. Campbell, "*Experimental Evidence for Dynamic Scaling in Spin Glasses*", Appl. Phys. **A74**, 907 (2002)
- [123] F. Mezei, "*The Dynamical Behavior Associated With The Spin-Glass Transition*", Journal Of Magnetism And Magnetic Materials **31&34**, 1327 (1983)
- [124] H. Casalta, P. Schleger, C. Bellouard, M. Hennion, I. Mirebeau, G. Ehlers, B. Farago, J.-L. Dormann, M. Kelsch, M. Linde, and F. Phillipp, "*Direct measurement of superparamagnetic fluctuations in monodomain Fe particles via neutron spin-echo spectroscopy*", Phys. Rev. Lett. **82**, 1301 (1999) [125] H. Casalta, P. Schleger, C. Bellouard, M. Hennion, I. Mirebeau, G. Ehlers, and B. Farago, "*Low Q measurement of super-paramagnetic fluctuations in monodomain Fe particles*", Physica **B 276-278**, 664 (2000)
- [126] E.M. Forgan, P.G. Kealey, S.T. Johnson, A. Pautrat, Ch. Simon, S.L. Lee, C.M. Aegerter, R. Cubitt, B. Farago, P. Schleger, "*Measurement of vortex motion in a type-II superconductor: A novel use of the neutron spin-echo technique*", Phys. Rev. Lett. **85**, 3490 (2000)
- [127] G. Ehlers, A.L. Cornelius, M. Orendác, M. Kajnaková, T. Fennell, S.T. Bramwell, J.S. Gardner, J. Phys.: Condens. Matter **15**, n.a. (2003)
- [128] A. P. Ramirez, in Handbook of Magnetic Materials, ed. by K. H. J. Buschow, Vol. **13**, Chapter 4 (Elsevier, Amsterdam, 2001)
- [129] S.T. Bramwell, M.J.P. Gingras, "*Spin ice state in frustrated magnetic pyrochlore materials*", Science **294**, 1495 (2001)
- [130] B. Farago, F. Mezei, "*Study of Magnon Dynamics in Fe near T_c by Modified Neutron Spin-Echo Techniques*", Physica B **136**, 627 (1986)
- [131] S.F. Edwards and D. G. Grinev. in "*Jamming and Rheology: Constraint Dynamics on Microscopic and Macroscopic Scales*", (eds A. J. Liu & S. R. Nagel) 80 – 93 (Taylor and Francis, New York, 2001)
- [132] V. Trappe, V. Prasad, L. Cipeletti, P. N. Segre, D. A. Wetzl, "*Jamming phase diagram for attractive particles*", Nature **411**, 772 2001
- [133] A.J. Liu, S.R. Nagel, "*Nonlinear dynamics - Jamming is not just cool any more*", Nature **396**, 21 (1998)
- [134] P.N. Pusey, W. van Megen, "*Observation of a Glass-Transition in Suspensions of Spherical Colloidal Particles*", Phys. Rev. Lett. **59**, 2083 (1987)

References

- [135] M.C. Grant, W.B. Russel, “*Volume-Fraction Dependence of Elastic-Moduli and Transition-Temperatures for Colloidal Silica-Gels*”, Phys. Rev. E **47**, 2606 (1993)
- [136] D.A. Weitz, M. Oliveria, “*Fractal Structures Formed by Kinetic Aggregation of Aqueous Gold Colloids*”, Phys. Rev. Lett. **52**, 1432 (1984)
- [137] B. Farago, *private communication* (2003)
- [138] K. N. Pham, A. M. Puertas, J. Bergenholtz, S. U. Egelhaaf, A. Moussaid, P. N. Pusey, A. B. Schofield, M. E. Cates, M. Fuchs, W. C. K. Poon, “*Multiple Glassy States in a Simple Model System*”, Science, **296**, 104 (2002)
- [139] K.A.. Dawson, “*The glass paradigm for colloidal glasses, gels, and other arrested states driven by attractive interactions*”, Curr. Opin. Coll. Interf. Sci., **7**, 218 (2002)
- [140] W. van Meegen and S.M. Underwood, “*Glass transition in colloidal hard spheres: measurement and mode coupling theory analysis of the coherent intermediate scattering function*”, Phys. Rev. E, **49**, 4206 (1994)
- [141] L. B. Lurio, D. Lumma, A. R. Sandy, M. A. Borthwick, P. Falus, and S. G. J. Mochrie, J. F. Pelletier and M. Sutton, A. Malik and G. B. Stephenson, “*Absence of Scaling for the Intermediate Scattering Function of a Hard-Sphere Suspension: Static and Dynamic X-Ray Scattering from Concentrated Polystyrene Latex Spheres*”, Phys. Rev. Letters, **84**, 785 (2000)
- [142] V.T. Lebedev, Gy. Török, *private communication*
- [143] L.M. Walker, “*Rheology and structure of worm-like micelles*”, Current Opinion in Colloid & Interface Science **6**, 451 (2001)
- [144] R.D. Koehler, S.R. Raghavan, E.W. Kaler, “*Microstructure and dynamics of worm-like micellar solutions formed by mixing cationic and anionic surfactants*”, J. Phys. Chem. **B104**, 11035 (2000)
- [145] A. Mukhopadhyay, S. Granick, “*Micro- and nanorheology*”, Current Opinion in Colloid & Interface Science **6**, 423 (2001)
- [146] W. Götze, “*Aspects of Structural Glass Transition*”, In: Liquids, Freezing and the Glass Transition, ed. By J.P. Hansen, D. Levesque, J. Zinn-Justin (North – Holland, Amsterdam 1991)
- [147] W. Götze and L. Sjörgren, “*Relaxation Processes in Supercooled Liquids*”, Rep. Prog. Phys. **55**, 241 (1992).
- [148] A. Arbe, D. Richter, J. Colmenero, B. Farago, “*Merging of the α and β relaxations in polybutadiene: A neutron spin echo study*”, Phys. Rev. E, **54** (4), 3853 (1996)
- [149] M. Koppe, M. Bleuel, R. Gähler, R. Golub, P. Hank, T. Keller, S. Longeville, U. Rauch, J. Wuttke, “*Prospects of Resonance Spin Echo*”, Physica **B 266**, 75 (1999)
- [150] A. Tölle, H. Schober, J. Wuttke, and F. Fujara, “*Coherent dynamic structure factor of orthoterphenyl around the mode coupling crossover temperature T_c* ”, Phys. Rev. E **56**, 809 (1997)
- [151] A. Alegria, J. Colmenero, P. Mari, and I. Campbell, “*Dielectric investigation of the temperature dependence of the non-exponentiality of the dynamics of polymer melts*”, Phys. Rev. E **59**, 6888 (1999)
- [152] J. Ferry, “*Viscoelastic Properties of Polymers*” (John Wiley & Sons, New York, 1970)

References

- [153] D. Richter, A. Arbe, J. Colmenero, in C.A. Angell, T. Egami, J. Kieffer, U. Nienhaus, K. L. Ngai (Eds.), *Materials Research Society: 1996 Fall Meeting Symposium Proceeding, Glasses and Glass Formes – Current Issues*, Materials Research Society, Pittsburgh, PA, (1997) p.3.
- [154] D. Richter, A. Arbe, J. Colmenero, M. Monkenbusch, B. Farago, R. Faust, “*Molecular motions in polyisobutylene: A neutron spin-echo and dielectric investigation*”, *Macromol.* **31**, 1133 (1998)
- [155] D. Richter, M. Monkenbusch, A. Arbe, J. Colmenero, B. Farago, “*Dynamic Structure Factors due to Relaxation Processes in Glass – Forming Polymers*”, *Phys. B* **241**, 1005 (1998)
- [156] D. Richter, M. Monkenbusch, A. Arbe, J. Colmenero, B. Farago, R. Faust, “*Space time observation of the alpha-process in polymers by quasielastic neutron scattering*”, *J. Phys.: Condensed Matter* **11**, A297 (1999)
- [157] N. G. McCrum, B. E. Read and G. Williams, in “*Anelastic and Dielectric Effects in Polymer Solids*” (Wiley, London, 1967)
- [158] G. P. Johari and J. Goldstein, “*Viscous Liquids and Glass Transition .2. Secondary Relaxations in Glasses of Rigid Molecules*”, *J. Chem. Phys.* **53**, 2372 (1970)
- [159] J. Eilhard, A. Zirkel, W. Tschop, D. Hahn, K. Kremer, O. Schärpf, D. Richter, U. Buchenau, J., “*Spatial correlations in polycarbonates: Neutron scattering and simulation*”, *Chem. Phys.* **110**, 1819 (1999)
- [160] J.J. Portman, “*Non-Gaussian dynamics from a simulation of a short peptide: Loop closure rates and effective diffusion coefficients*”, *J. Chem. Phys.* **118**, 2381 (2003)
- [161] B. Frick, B. Farago, D. Richter, “*Temperature dependence parameter in polybutadiene in the neighborhood of the glass transition*”, *Phys. Rev. Lett.* **64**, 2921 (1990)
- [162] B. Farago, A. Arbe, J. Colmenero, U. Buchenau, D. Richter, “*Intermediate length scale dynamics of polyisobutylene*”, *Phys. Rev. E* **65**, 051803-1 (2002)
- [163] C. Donati, J.F. Douglas, W. Kob, S.J. Plimpton, P.H. Poole, S.C. Glotzer, “*Stringlike cooperative motion in a supercooled liquid*”, *Phys. Rev. Lett.* **80**, 2338 (1998)
- [164] S. Hoffmann, L. Willner, D. Richter, A. Arbe, J. Colmenero, B. Farago, „*Origin of dynamic heterogeneities in miscible polymer blends - a quasielastic neutron scattering study*”, *Phys. Rev. Lett.* **85**, 772 (2000)